COMPUTATIONAL INTELLIGENCE IMAGE PROCESSING FOR PRECISION FARMING ON-SITE NITROGEN ANALYSIS IN PLANTS

Susanto Budi Sulistyo

A thesis submitted for the degree of
Doctor of Philosophy

FACULTY OF SCIENCE, AGRICULTURE AND ENGINEERING
SCHOOL OF ENGINEERING

October 2017

Abstract

Nitrogen is one of the macronutrients which is essentially required by plants. To support the precision farming, it is important to analyse nitrogen status in plants in order to prevent excessive fertilisation as well as to reduce production costs. Image-based analysis has been widely utilised to estimate nitrogen content in plants. Such research, however, is commonly conducted in a controlled environment with artificial lighting systems. This thesis proposes three novel computational intelligence systems to evaluate nitrogen status in wheat plants by analysing plant images captured on field and are subject to variation in lighting conditions. In the first proposed method, a fusion of regularised neural networks (NN) has been employed to normalise plant images based on the RGB colour of the 24-patch Macbeth colour checker. The colour normalisation results are then optimised using genetic algorithm (GA). The regularised neural network has also been effectively utilised to distinguish wheat leaves from other unwanted parts. This method gives improved results compared to the Otsu algorithm. Furthermore, several neural networks with different number of hidden layer nodes are combined using committee machines and optimised by GA to estimate nitrogen content. In the second proposed method, the utilisation of regularised NN has been replaced by deep sparse extreme learning machine (DSELM). In general the utilisation of DSELM in the three research steps is as effective as that of the developed regularised NN as proposed in the first method. However, the learning speed of DSELM is extremely faster than the regularised NN and the standard backpropagation multilayer perceptron (MLP). In the third proposed method, a novel approach has been developed to fine tune the colour normalisation based on the nutrient estimation errors and analyse the effect of genetic algorithm based global optimisation on the nitrogen estimation results. In this method, an ensemble of deep learning MLP (DL-MLP) has been employed in the three research steps, i.e. colour normalisation, image segmentation and nitrogen estimation. The performance of the three proposed methods has been compared with the intrusive SPAD meter and the results show that all the proposed methods are superior to the SPAD based estimation. The nutrient estimation errors of the proposed methods are less than 3%, while the error using the renowned SPAD meter method is 8.48%. As a comparison, nitrogen prediction using other methods, i.e. Kawashima greenness index (GI_{kaw}) and PCA-based greenness index (GI_{PCA}) are also calculated. The prediction errors by means of I_{kaw} and I_{PCA} methods are 9.84% and 9.20%, respectively.

Acknowledgements

In the name of Allah, the Most Gracious, the Most Merciful. Praise and gratitude be to Allah for giving me strength and guidance, so that this thesis can be finished accordingly.

First and foremost, I would like to express my utmost gratitude to my supervisors, Dr. Wai Lok Woo and Prof. Satnam Dlay for their guidance, encouragement, and support at every stage of my graduate study. I am very appreciated all their contributions and supervisions. I am also grateful to Mrs. Gillian Webber for her kindness and administrative support during my study.

I would like to thank Prof. Zabih Ghassemlooy and Dr. Martin Johnston as my thesis examination committee members for their time, constructive criticisms, and feedback.

I would also like to thank Dr. Paul Bilsborrow for giving me opportunity to get involved in his farm experiment for field data collection. I also appreciate to Mr. Gavin Hall for his guidance during data collection at Nafferton Farm. My sincere thanks to my colleagues, especially Di Wu, for our collaborative work.

My heartfelt thanks to my parents, my beloved wife and daughters for their incredible love, prayers, patient, and encouragement.

Last, but not least, I gratefully acknowledge my sponsor and my institution, Indonesia Ministry of Research, Technology and Higher Education and Jenderal Soedirman Univeristy for the financial support throughout my study.

Table of Contents

List of Figures

List of Tables

List of Abbreviations

AET	Adjustable Exponential Transform
BPNN	Backpropagation Neural Network
CCI	Chlorophyll Content Index
CCM	Colour Co-occurrence Method
CIVE	Colour Index of Vegetation Extraction
CM	Continuity Measure
DBN	Deep Belief Network
DGCI	Dark Green Colour Index
DL-MLP	Deep Learning Multilayer Perceptron
DN	Digital Number
DSELM	Deep Sparse Extreme Learning Machine
ELM	Extreme Learning Machine
ExG	Excess Green
FFT	Fast Fourier Transform
FIP	Fast Image Processing
FISTA	Fast Iterative Shrinkage Thresholding Algorithm
GA	Genetic Algorithm
GIS	Geographic Information Systems
GLCM	Grey Level Co-occurrence Matrix
GMR	Green Minus Red

GPS	Global Positioning System
GW	Grey World
HSI	Hue Saturation Intensity
HSL	Hue Saturation Luminance
HSV	Hue Saturation Value
ISTA	Iterative Shrinkage Thresholding Algorithm
LAI	Leaf Area Index
LED	Light Emitting Diode
MAE	Mean Absolute Error
MAPE	Mean Absolute Percentage Error
MLP	Multilayer Perceptron
MSE	Mean Square Error
NIR	Near-Infrared
NN	Neural Network
PCA	Principal Component Analysis
PNN	Probabilistic Neural Network
RBM	Restricted Boltzmann Machines
RCRD	Robust Crop Row Detection
RGB	Red Green Blue
RMSE	Root Mean of Squared Error
SBM	Scale-By-Max
SELM	Sparse Extreme Learning Machine

SLFN	Single-Layer Feedforward Neural Network
SOM	Self Organising Map
SPAD	Soil Plant Analysis Development
SSE	Sum of Squared Error
SVM	Support Vector Machine
TPCA	Top Projected Canopy Area
VI	Vegetation Index

List of Symbols

$\bar{B}$	Mean value of blue colour
$\bar{G}$	Mean value of green colour
L^*	Lightness component of CIE-Lab
N_{pop}	Number of population
N_s	Number of samples
$\bar{R}$	Mean value of red colour
a^*	a-component of CIE-Lab
b^*	b-component of CIE-Lab
n_h	Number of hidden layer nodes
n_{SV}	Number of support vectors
n_i	Number of input layer nodes
n_o	Number of output layer nodes
n_p	Number of training samples
p_T	Total pixels
ΔE	Euclidean distance
B	Blue colour
G	Green colour
GI	Greenness index
H	Hue
HP	High pass filter
I	Intensity
LP	Low pass filter
Q	Number of combined neural networks
R	Red colour
S	Saturation
T	Neural network target

X	Neural network inputs
Z	Neural network final output
b	Blue colour index
bg	Background colour
fg	Foreground colour
g	Green colour index
n	Number of iteration
p	Priori probability
r	Red colour index
w	Weight
α	Weight matrix of network output for colour normalisation
β	Output weights
η	Learning rate
λ	Lagrange multiplier
ρ	Probability of mutation
σ	Standard deviation

List of Publications

Published

1. S. B. Sulistyo, W. L. Woo, and S. S. Dlay, "Regularized neural networks fusion and genetic algorithm based on-field nitrogen status estimation of wheat plants," *IEEE Transactions on Industrial Informatics*, vol. 13, no. 1, February 2017, pp. 103-114.

2. S. B. Sulistyo, W. L. Woo, and S. S. Dlay, "Computational Intelligent Color Normalization for Wheat Plant Images to Support Precision Farming," *Proceedings of 8th IEEE International Conference on Advance Computational Intelligence (ICACI)*, February 2016, Chiang Mai, pp. 130-135.

3. S. B. Sulistyo, W. L. Woo, and S. S. Dlay, "Ensemble Neural Networks and Image Analysis for On-site Estimation of Nitrogen Content in Plants," *Proceedings of SAI Intelligent Systems Conference (IntelliSys) vol. 2*, September 2016, London, pp. 103-118, Lecture Notes in Networks and Systems, vol. 16. Springer.

Accepted

1. S. B. Sulistyo, Di Wu, W. L. Woo, and S. S. Dlay, "Computational Intelligence Vision Sensing for Nutrient Content Estimation in Agricultural Automation," *IEEE Transactions on Automation Science and Engineering.*

2. S. B. Sulistyo, W. L. Woo, and S. S. Dlay, "Building A Globally Optimized Computational Intelligence Image Processing Algorithm for On-Site Inference of Nitrogen in Plants," *IEEE Intelligent Systems.*

Chapter 1

Introduction

1.1. Background

Along with the increase of number of people in the world, the need of food also increases. According to Food and Agriculture Organisation (FAO) of the United Nations (UN), by the year 2030 the world population is projected to grow to around 8.3 billion [1]. In 1988 extensification in agriculture was firstly introduced. In the extensive agriculture system, large areas of farm field is utilised, but with less inputs as well as capital and labour expenses. The intensive agriculture system, in contrast, can be defined as a process of farming which aims to enhance productivity on a given area of farm field by increasing the use of inputs, such as water, chemicals, and fertilisers, including capital and labour. Both extensification and intensification have raised issues about preservation of environment.

In the traditional agriculture, farmers usually apply very large amounts of fertilisers and chemicals in order to yield sufficient crops. This traditional technique, indeed, can boost the farm production yet it can cause several damages to the environment, such as killing of life in the topsoil and subsoil, and leaking of nitrogen to the groundwater and soil as a consequence of excessive fertilisation. Moreover, excessive fertilisation and chemicals application may poison the plant itself and harm its life.

As staple food sources, cereals (wheat, rice, maize, sorghum) and tubers (potato, cassava), are needed by most of people in the world. Rice is the most common food for people in Indonesia. According to [2], in 2014 Indonesia has about 13.8 million hectares of rice field with 70.8 million tons paddy production. The paddy yield, thus, is up to 5.13 tons/ha. In general agricultural practices in Indonesia are still conducted traditionally. For instance, farmers usually spread fertiliser over the ground without considering the nutrient amount in plants and its availability in the soil. In fact, the nutrient content in some crops may relatively differ from other crops even they are in the same field. Additionally, this condition may also happen to the soil where the plants grow. The nutrient availability in the soil of a particular area can be different from that of other specific area even in the same farming field. Such fertilisation practice, therefore, can lead to some environmental problems as previously

mentioned, such as leaking of nitrogen to the groundwater and soil due to excessive fertilisation.

In order to tackle the disadvantages of the traditional agricultural practices, a new concept of farming has been developed. This new farming technique has been known as precision farming. For the last few years, precision farming has become a topical agricultural issue. According to [3], precision farming or precision agriculture can be defined as information and technology based system in agricultural practices which aims to identify, analyse and manage variability within fields, including farm inputs, crops and soil, to obtain optimum profitability and sustainability as well as preservation of the environment and land resources. This concept utilises site-specific information to enhance crop management. The idea of precision farming comes from two principal concerns: economic and environmental issues. With regard to the economic issue, the purpose of precision farming technology is to increase crop productivity as well as to reduce production costs [4]. In the meantime, this concept also aims to minimise the negative impact of agricultural practices on the surrounding environment [5], [6]. The precision farming model, therefore, will lead to a more efficient application of farm resources, such as water, seeds, chemicals and fertilisers. Rather than applying the same amount of fertilisers over an entire farm field, precision agriculture will measure variations in conditions within a field and determine its fertilising strategy accordingly [7]. In order to support this idea, it is important to estimate the nutrient status of plants to improve the efficiency of the fertiliser application.

Nitrogen (N) is one of the macronutrients which are required in substantial amounts by plants to ensure growth given that this element is a component of chlorophyll, which has a significant role in photosynthesis. According to [8], there are four common methods utilised to assess nitrogen content in plants, i.e. chemical and combustion tests, vegetation index (VI), SPAD (soil plant analysis development) meter and leaf colour chart.

Due to the most recent developments in vision sensing and computational systems with rapidity and ease of image data collection, extensive research estimating the nitrogen status in crops has been conducted by means of image-based analysis [9]. Nevertheless, most of these nutrient estimation approaches are not practical, time-consuming and require some additional equipment in view of the fact that they are typically performed in a controlled environment, such as in a closed chamber, with artificial lighting systems, as seen in Figure 1.1 [10], [11]. Such methods cannot be applied in fields seeing as the intensity of sunlight is always changing and this will lead to inconsistent and unreliable image acquisition in addition to

incorrect nutrient estimation. There are a number of challenges in estimating the nutrient content of plants based on images captured of fields, including the effect of sunlight intensity that is varied, besides how the images are normalised, in order to reduce the colour variability of all the images captured under sunlight with an extensive range of light intensity.

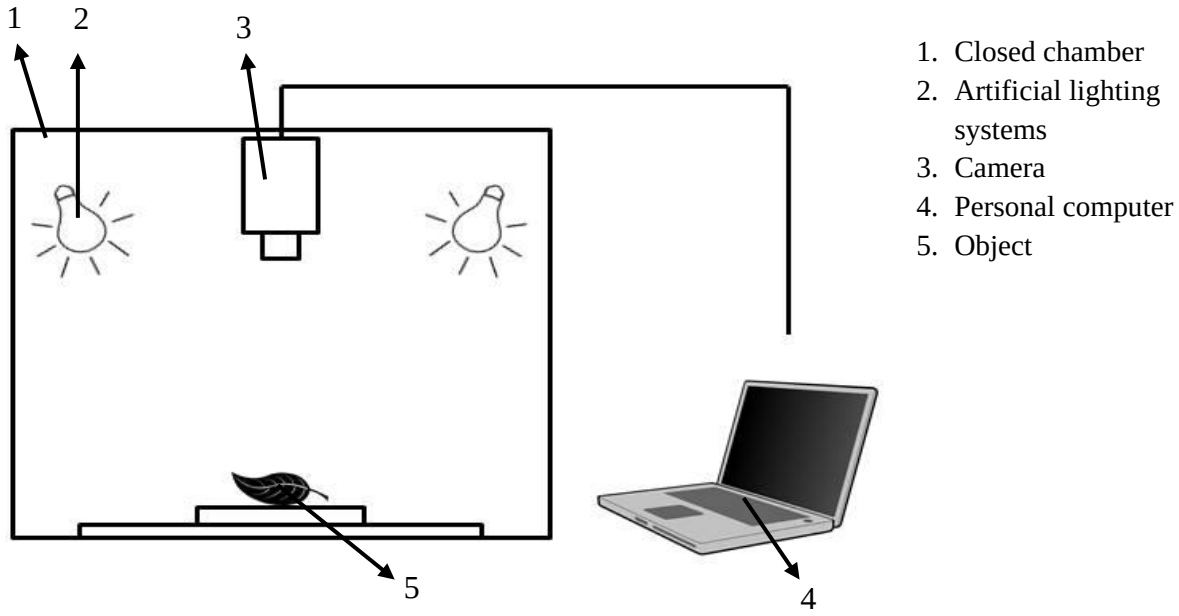

Figure 1.1. Common image acquisition in a controlled environment with artificial lighting systems.

1.2. Motivation and Challenges

Estimating nitrogen content based on plant images acquired from a field is a challenging task. Some of the challenges which need to be resolved according to this work are how to minimise the effect of sunlight of various intensities, as well as how to normalise images with the purpose of making sure that all the images obtained under a variety of light intensities comprise colour deviations that are relatively small.

The colour of images will change dynamically in conjunction with the change of light intensity. As seen in Figure 1.2, wheat plants from the same field with the same fertilising levels will appear different if the light intensity of the light source is different. Such images could not be used directly in nutrient estimation given that they are acquired under different illuminations. The images, therefore, need to be normalised prior to the advanced steps of image processing, in order to make a more reliable comparison of the images. After image normalisation, it can be assumed that the differences in colour of the wheat leaves are solely

caused by different fertilising levels. In general, if a smaller amount of nitrogen fertiliser is applied to the plants, subsequently the leaves will reveal a lighter green colour.

(a) (b) (c)

Figure 1.2. Examples of wheat plant images captured under different sunlight intensities: (a) low light intensity (8 Klux), (b) medium light intensity (50 Klux), and (c) high light intensity (80 Klux).

1.3. Aim and Objectives of the Thesis

The primary aim of this thesis is to develop new, low-cost, simple and accurate approaches to estimate nitrogen content in wheat leaves based on leaf images that are captured in fields under sunlight by using a digital still camera to support the precision farming. Three novel methods have been proposed regarding on-field nitrogen content estimation in wheat leaves. These encompass three types of neural network expert systems, i.e. regularised multilayer perceptron, deep sparse extreme learning machine (DSELM) and deep learning multilayer perceptron (DL-MLP). The proposed methods have also employed committee machines as expert system combiners and genetic algorithms (GA) as a tool for optimisation.

The objectives of this thesis are as follows:

a) To investigate the feasibility of using computational intelligence image processing in relation to on-farm nitrogen estimation in wheat leaves.
b) To develop colour normalisation algorithms by using fusions of the aforementioned three types of neural network systems based on the Macbeth colour checker as the image reference to normalise wheat plant images.
c) To generate image segmentation and features extraction algorithms to distinguish wheat leaves from other surrounding parts using the three neural network systems.

d) To develop neural network systems based nutrient estimation algorithms by means of a committee machine to combine several networks based on statistical moment features of wheat plant images.
e) To produce generic algorithms based global optimisation, so as to enhance the colour normalisation and nutrient estimation results.
f) To compare the results of the proposed methods with that of the common and renowned method using chlorophyll meter (SPAD meter) readings.

To analyse the colour normalisation results, Euclidean distance is measured to figure out the accuracy level of the proposed methods. Furthermore, several colour normalisation techniques, i.e. grey world, scale-by-max, linear model and single neural network, are also employed to normalise images as comparison. In addition, to determine the effectiveness of the proposed colour normalisation method, colour variability of the wheat plant images is measured by calculating standard deviation of RGB values of the plant images.

In order to analyse the nitrogen estimation results, several statistical features of RGB colours with various order from the plant images, i.e. mean, variance, skewness and kurtosis, are extracted and then utilised as neural network inputs to estimate nutrient content. The accuracy level of this prediction is determined by mean absolute percentage error (MAPE). In this thesis, a number of existing estimation methods are also employed as a comparison. The existing methods are green index using Kawashima and principal component analysis (PCA) method and also the most well-known technique using chlorophyll meter (Minolta SPAD-502).

1.4. Thesis Contributions

This thesis considers the problem of computational intelligence image processing for on-field nitrogen status analysis in wheat plants. The novel contributions of the thesis are concluded below:

a) As an entire system, nutrient estimation based on plant images captured on field using a digital still camera is a new technique given that up until now, it has only been conducted in a controlled environment. The utilisation of a common digital camera can reduce analysis costs compared to that of other devices, such as satellite remote sensing and thermal camera. This contribution is described in Chapter 3, 4 and 5.

b) The proposed method involves colour normalisation to reduce the colour variability due to the variation in light intensities. The problem related to high colour variability can be handled by developing fusions of three types of neural network systems, i.e. regularised MLP, DSELM and deep learning MLP, which is based on the colour of the 24-patch Macbeth colour checker. The technique to tackle colour normalisation problem using the three aforementioned methods can be found in Chapter 3, 4 and 5, respectively.
c) Four types of statistical moment features (mean, variance, skewness and kurtosis) of each RGB colour channel, which represent the distribution of the colour of the wheat leaves are introduced as the inputs of the developed neural networks using regularised MLP, DSELM and deep learning MLP, as explained in Chapter 3, 4 and 5, respectively.
d) The last contribution with regards to this thesis is to build globally optimised computational intelligence image processing to modify the colour normalisation and improve the nitrogen estimation results. This contribution can be found in Chapter 5.

1.5. Thesis Outline

This thesis focuses on the development of computational intelligent image processing for on-field nitrogen estimation in wheat leaves based on plant image analysis. The thesis comprises introductory sections, the main chapters and a conclusion. Three novel methods for nutrient estimation establish the principal part of the thesis. The outline of the thesis is organised as follows:

Chapter 2 describes extensively the concept and application of precision farming and explains a number of existing nitrogen estimation techniques comprehensively. In this chapter, several image processing applications employed in agricultural systems are also explained.

Chapter 3 proposes a novel method pertaining to nitrogen estimation using regularised MLP fusion. The regularised MLP fusion is utilised to normalise wheat plant images and reduce colour variability due to various light intensities. Genetic algorithm is applied to optimise the colour normalisation results. Moreover, the regularised MLP is also used in image segmentation to distinguish wheat leaves from other surrounding parts. The results of this image segmentation method are compared with the conventional Otsu algorithm. Four statistical moments features are subsequently extracted from the segmented images and employed as nutrient predictors. Furthermore, several regularised MLPs are combined using a

committee machine to estimate nitrogen content. The results are subsequently compared with the existing SPAD meter readings based estimation.

Chapter 4 proposes a new approach for nitrogen analysis using DSELM fusion. Basically, the algorithms developed in this chapter are similar to those in Chapter 3. The difference is with regards to the utilisation of DSELM in the colour normalisation, image segmentation and nutrient estimation steps.

In Chapter 5, an advanced method using deep learning MLP fusion for nutrient estimation is proposed. Besides that, this method introduces a global optimisation to modify the colour normalisation results and increase the accuracy of the nutrient estimation results.

This thesis is concluded with Chapter 6. The chapter presents the closing remarks and several points in connection with future works.

Chapter 2

Literature Review

2.1. Introduction

This chapter presents a review of several techniques regarding nitrogen status analysis in plants to support precision farming. The review initially provides a description in relation to precision farming, the idea behind it and the technology adopted to bolster the concept of precision farming. A number of applications in support of image processing in agriculture are also presented, so as to deliver several examples of computational intelligence image processing techniques, such as image segmentation, features extraction and artificial neural network. This chapter also discusses different techniques concerning existing nitrogen measurement, either destructive or non-destructive. Lastly, a number of image-based nitrogen estimation techniques are presented.

2.2. Precision Farming

Intensive agricultural practices which have resulted in an enormous increase in fertiliser inputs have been conducted increasingly since 1950. Despite the escalation in crop production, such methods have become a serious threat to the environment. Excessive fertilisation has led to deterioration in the quality of soil and water and recently, nitrogen (N) emissions have been considered a major environmental problem in many countries [12]. According to the European Environment Agency, more than 20% of the groundwater in European countries has been polluted by nitrates, which is generated by livestock breeding and application of fertiliser [13]. An environmental-friendly technique, therefore, should be introduced to reduce the negative effects of excessive fertilisation.

In conventional agricultural practices, farm resources, for instance fertiliser, pesticide and water are applied uniformly without deliberate spatial variability. Such practices will cause inaccurate treatments as each soil plot and plant has different conditions and input needs. In addition, according to [14], soil and crop properties may vary within fields depending on:

a) Texture (composition of sand, silt, loam or clay)
b) pH (acidity) of topsoil and subsoil
c) Soil content (organic matter, water and minerals)
d) Slope and orbital orientation of the soil
e) Density and morphology of crops
f) Water and minerals content of crops
g) Infestation of crops by different weeds and by various pests.

To alleviate these problems, the innovative concept of precision farming has been introduced. This concept delivers site-specific crop management to spatial variability in relation to farms, in order to optimise crop production that has a negligible negative impact on the environment. Precision farming, also known as precision agriculture, is an information-and-technology based advanced technique in agricultural production, which boosts efficiency and reduces damage to the environment, and helps to achieve agricultural sustainability [15].

Furthermore, as reported by [16], there are four important issues related to precision farming. The first issue is economics, such as production costs and revenues, cash flow and risk. The second issue is pertaining to management, which includes data acquisition and analysis, decision support systems and increased attention to management. Subsequent issues are related to technologies and the environment. The technologies required for precision farming are accurate global positioning system (GPS), variable rate technology, site specific management service and financing. Furthermore, reducing input losses, increasing the efficiency of water and nutrient (fertilisers) use is a significant aspect related to environmental issues. According to [17], the idea of precision farming is supported by the development of information and computer technology, remote sensing, ecophysiology, geostatistics and geo-spatial data management.

In a study reported by [18], information and computer technologies utilised in precision farming comprise three aspects regarding production:

a) Data collection or information input

   Data collection can be done both before and during crop production. This aspect may include soil sampling, yield monitoring and crop scouting. Some advanced technologies can also be employed for data collection, for instance GPS to collect precise location coordinates, soil probes to monitor electrical conductivity, soil moisture, and other soil

variables, and optical scanners to detect soil organic matter and distinguish weeds from plants.

b) Analysis or processing of the precision information

   A number of decision technologies, such as computer process models, artificial intelligence systems, and expert systems, can be used to analyse or process the precise data.

c) Recommendations or application of the information

   The aim of data collection and analysis is to manage each part of the field appropriately. The final decision of recommendations and applications of production inputs for each plant can be adjusted to optimize output according to the producer's agronomic, economic, and environmental goals.

In addition, the study tabulated the suite of technologies implemented in precision agriculture, as presented in Table 2.1.

Table 2.1. The technologies adopted in precision farming

Production aspect	**Technology**	
Data collection	*Prior to production*: Soil sampling, crop monitoring, remote sensing, plant inspection *Locations/coordinates*: GPS	*During production*: Field assessment of nutrients, pH, weeds
Data analysis/processing	Geographic information systems (GIS), process models, artificial intelligence systems, expert systems, human decision makers	
Recommendation/application	*Variable-rate application*: Fertiliser, micronutrients, pesticides, seeds, seed variety, irrigation	*Selective harvest*: Harvest timing determination

2.3. Application of Image Processing in Agriculture

Digital image processing has been extensively used in agricultural systems. A plethora of studies have been reported regarding the application of image processing techniques either in pre-harvest (crops cultivation) or post-harvest (agricultural product handlings) activities. In pre-harvest activities, image processing techniques have been applied in many subject areas, for instance the detection of weeds in crop fields, the detection and classification of plant diseases, measurement of the leaf area, and locating fruits on trees. Furthermore, a number of

researchers have investigated and estimated the nutrient deficiency and nutrient status of various plants. The next section will describe various estimation methods in more detail.

With regards to the detection of weeds, Tellaeche et al. [19] proposed computer vision based approaches regarding the detection and differential spraying of weeds in corn plants. The developed technique involves two stages: image segmentation and decision making. A basic image processing technique is utilised to extract cells from field images as low level units. Each extracted cell describes two segments which represent crop and weeds. In the decision making stage, a computational algorithm based on a Bayesian framework determines whether or not the analysed cells need to be sprayed. The results demonstrate that the combination of relative weed coverage and weed pressure, as the features used in decision making enhance the system's performance.

Research conducted by [20] has successfully distinguished weeds from maize crops under uncontrolled lighting in real-time conditions. The system combines two different techniques, a fast image processing delivering results in real-time (Fast Image Processing, FIP), and a slower and more accurate processing (Robust Crop Row Detection, RCRD) that is used to revise the mistakes produced by the first technique. The combination of these two algorithms produces extremely good results under various conditions. Additionally, the key factor regarding this study is the proposed image segmentation which it is claimed is robust to illumination changes. In the research, RGB colour indices ($r = -0.884$, $g = 1.262$, $b = -0.311$) have been used to discriminate vegetation pixels by creating grey images that can be processed easily into binary images using a threshold adjustment based on average intensity value. These colour indices were achieved by using a genetic algorithm based optimization and has been proved to give better results than Excess Green coefficients with $r = -1$, $g = 2$, $b = -1$.

Furthermore, an expert system has been developed to identify weeds automatically from maize fields [21]. The expert system can be used to detect weeds and crops contaminated with substances from soils when the farm is irrigated or after rain. This condition will cause traditional segmentation approaches based on image greenness to misidentify plant pixels given that they have lost their natural greenness. In the image segmentation step, the research applies a combination of vegetation indices and applies the Otsu threshold algorithm. Three indices are used in this combination, specifically excess green (ExG), colour index of vegetation extraction ($CIVE$) and vegetative (VEG), which can be expressed as follows:

- Excess green (ExG)

$$ExG = 2g - r - b \tag{2.1}$$

- Colour index of vegetation extraction ($CIVE$)

$$CIVE = 0.441r - 0.811g + 0.385b + 18.78745 \tag{2.2}$$

- Vegetative (VEG)

$$VEG = \frac{g}{\sqrt[3]{r^2 b}} \tag{2.3}$$

where r, g and b are colour index of red, green and blue, respectively, which can be obtained as follows:

$$r = \frac{R_n}{R_n + G_n + B_n}, \quad g = \frac{G_n}{R_n + G_n + B_n}, \quad b = \frac{B_n}{R_n + G_n + B_n}$$

R_n, G_n and B_n are the normalised red, green and blue colour, respectively, ranging from 0 to 1 and are achieved using the following formulae:

$$R_n = \frac{R}{R_{max}}, \quad G_n = \frac{G}{G_{max}}, \quad B_n = \frac{B}{B_{max}}$$

where $R_{max} = G_{max} = B_{max} = 255$ for 24-bit colour images.

The three indices mentioned above are subsequently combined to obtain the combination value (COM) as follows:

$$COM = w_1 ExG + w_2 CIVE + w_3 VEG \tag{2.4}$$

where w_1, w_2, and w_3 are the weights for each index, representing their relative contribution in the combination.

Further research with regards to weed and crop detection was conducted by [22]. In the research, a multi spectral camera was utilised to capture images of soybean crops and weeds in fields. The camera recorded images with three channels, namely green, red and infrared waveband. Three images from the all channels can be composed into one image, which contains more information than images captured by common digital cameras. The crop images are segmented from soil background using infrared channel distribution as the infrared

channel image is very clear and with high resolution. Morphological operations, i.e. dilation and erosion are then performed to remove small sized weeds and extract images of the soybean crop. A radial basis neural network is used to identify weeds based on five input parameters, principally area size, long and short axis length, eccentricity, and Euler number. The results reveal that the proposed technique can even detect and identify weeds of a similar size and colour.

Musthafa et al. [23] investigated the utilisation of an intelligent real-time automatic weed control system to identify and distinguish weeds. They used two techniques related to image processing, i.e. grey level co-occurrence matrix (GLCM) and fast Fourier transform (FFT), to achieve the best solution in connection with weed classification. Basically, GLCM is a matrix that defines how often different combinations of grey level pixels occur in a greyscale image at a given offset. In the research, two features are employed to distinguish weeds from crops, i.e. contrast and regularity. Contrast (Con) and regularity (Reg) can be expressed as a function of co-occurrence matrix as follows:

$$Con = \sum_i \sum_j (i-j)^2 p_{i,j} \tag{2.5}$$

$$Reg = \sum_i \sum_j \frac{p_{i,j}}{1+(i-j)^2} \tag{2.6}$$

where i and j are coordinates in the developed co-occurrence matrix ($p_{i,j}$). The values of i and j depend on the grey level used in the image. Typically, an image has 256 grey level. The values of i and j, thus, range from 0 to 255.

An investigation regarding the detection of weeds was also undertaken by [24] in an oil palm plantation. In this research, a low-high pass filtering technique is applied to process crop-weed images, especially for edge detection, while continuity measure (CM) based feature extraction is proposed to extract and minimise the pixels size of output filter. Low-pass filtering, also known as blurring or smoothing, averages out rapid changes in pixel intensity. A two dimensional low pass filter can be expressed as follows:

$$LP(u,v) = \begin{cases} 1 & if \quad D(u,v) \leq D_0 \\ 0 & if \quad D(u,v) > D_0 \end{cases} \tag{2.7}$$

where D_0 is a specified non-negative quantity and $D(u,v)$ is the distance from the coordinates (u,v). In the in the meantime, a high-pass filter can be applied to make an image appear

sharper. The mathematical expression related to a high-pass filter can be written as the opposite of a low-pass filter, as shown below:

$$HP(u,v) = \begin{cases} 0 & if \quad D(u,v) \leq D_0 \\ 1 & if \quad D(u,v) > D_0 \end{cases} \tag{2.8}$$

Image processing can also be used to detect diseases in plants. As reported in a literature survey by [25], a common practice conducted by plant scientists to identify plant disease symptoms, either in leaves or stems, is by a visual inspection regarding the scale of the affected area. Nevertheless, such practice results in subjectivity and low throughput. The literature study summarises 11 different methods regarding the detection of plant diseases and analysis, as follows:

1) Backpropagation neural network
2) Airborne hyperspectral imagery and red edge techniques
3) Image analysis integrated with the Central Lab. of Agricultural Expert System (CLASE) diagnostic model
4) Combination of morphological features of leaves, image processing, feed forward neural network based classifier and fuzzy surface selection techniques for feature selection
5) Support vector machines for developing weather based prediction models of plant diseases
6) Wavelet based image processing techniques and neural network
7) Image processing with PCA & Probabilistic Neural Network (PNN)
8) Combination of image growing, image segmentation, Zooming algorithm and Self Organising Map (SOM) neural network for classifying diseased rice images
9) Self-organising maps and back propagation neural networks with genetic algorithms for optimisation and support vector machines related to classification
10) Image clipping, filtering and thresholding
11) Otsu segmentation, K-means clustering and back propagation feed forward neural network

Research related to the application of a neural network for detecting diseases in a variety of orchid plants was conducted by [26]. This study employed image processing techniques, adjustable exponential transform (AET), grey level co-occurrence matrix (GLCM) and the backpropagation neural network (BPNN) classifier for the classification system. The developed AET and image processing technique can be applied to detect and segment the lesion areas. Three colour features (R_{mean}, G_{mean}, and B_{mean}) and 18 texture features (i.e.

contrast, uniformity, maximum probability, homogeneity, inverse difference, difference variance, diagonal variance, entropy and difference entropy of the green and blue colour regarding the lesion area) are utilised as the inputs for the BPNN classifier. The results confirm that the developed detection method can classify lesions in orchid plants effectively, with an accuracy level up to 89.6%.

An investigation into the detection of citrus canker from leaf images captured in a field was undertaken by [27]. In that research, a new approach based on global features and zone-based local features is presented to detect citrus canker on leaf images. In the image segmentation and features extraction, a hierarchical detection strategy is used to segment lesion leaf images from the background, while an improved AdaBoost technique is utilised to select the most significant features. A canker lesion descriptor is subsequently proposed by combining leaf image colour and texture features to classify citrus canker lesions. The experimental results explain that the proposed method offers classification accuracy, which is as satisfactory as identification by human experts.

Additional research with regards to disease detection in citrus plants was also undertaken by [28]. The colour co-occurrence method (CCM) textural features using hue, saturation and the intensity (HSI) colour model and statistical classification algorithm are used to identify diseased and normal citrus leaves in controlled laboratory conditions. Four different classes of citrus leaf are examined: melanose, greasy spot, scab and normal. In this research, 13 texture features for each HSI component (39 features for all) were developed to represent the colour distribution of the examined citrus leaves. The 13 texture features are uniformity, mean intensity, variance, correlation, product moment, inverse difference, entropy, sum entropy, difference entropy, information correlation 1, information correlation 2, contrast and modus. SAS statistical analyses are performed to reduce redundancy in the texture feature set. The research develops two sets of four data models, one set from leaf backs and one set for leaf fronts. Four data models of each set consist of different texture features. Model 1 comprises hue and saturation texture features, while model 2 includes intensity features. Model 3 contains hue, saturation and intensity features, whereas model 4 involves all 39 developed features. The experiments provide classification accuracy up to 81% on all data models using intensity features. When using hue and saturation features, the accuracy increases up to 95.8%. The highest accuracy achieved 100% when using all the HSI features.

Image processing can also be utilised to measure leaf areas in various plants. Leaf area is a key factor in crop growth and has significant influence on crop production. A study of leaf

area measurement using image processing techniques was conducted by [29]. In this study, image geometric distortions are firstly corrected using mapping function by applying Hough transformation, while threshold-based segmentation method is utilised to distinguish leaves from the background. Furthermore, to remove the noises in the segmented images, contour extraction and region filling are applied. The leaf area is subsequently measured by calculating pixel numbers.

Mora et al. [30] developed an image processing algorithm to measure leaf area index of fruit trees canopy. Two levels of image segmentation are applied to eliminate non-leaf material. The first level is automatic segmentation of blue colour channel based on the conventional Otsu algorithm. The second level is automatic detection of image pixel which are corresponded to trunks, branches, fruit and any other non-leaf materials. In the second level segmentation, the colour of plant images are transformed from RGB to CIE Lab colour model. The algorithm of the second segmentation is as follows:

$$I_{xy}^{(2)} = \begin{cases} 1 & \text{if } A_{xy} > 0 \\ 0 & \text{otherwise} \end{cases} \tag{2.9}$$

$$n_{non-leaf} = \sum_{x}\sum_{y} I_{xy}^{(2)} - \sum_{x}\sum_{y} I_{xy}^{(1)} \tag{2.10}$$

$$f_c = 1 - \frac{g_L}{p_T - n_{nonleaf}} \tag{2.11}$$

$$f_f = 1 - \frac{g_T}{p_T - n_{nonleaf}} \tag{2.12}$$

$$\phi = \frac{f_f}{f_c} \tag{2.13}$$

$$\Omega = \frac{(1-\phi)\cdot ln(1-f_f)}{ln(\phi)\cdot f_f} \tag{2.14}$$

$$LAI_e = LAI_A \cdot \Omega \tag{2.15}$$

where $I_{xy}^{(1)}$ and $I_{xy}^{(2)}$ are pixel values at coordinates (x, y) of binary images with dimension of $n \times m$ from the first and second level segmentation, respectively; A_{xy} is chromaticity-a component from CIE Lab of a pixel at coordinate (x, y), $n_{nonleaf}$ is number of pixels corresponding to non-leaf materials; f_c and f_f are the cover and crown cover fractions,

respectively; p_T is the total pixels in the images; ϕ and Ω are the crown porosity and clumping index, respectively; LAI_e and LAI_A are effective leaf area index and leaf area index measured by allometry, respectively.

In the harvesting process, image processing has also been used to provide assistance to human vision to locate fruits for robotic harvesting. As reported by [31], an image guided citrus fruit picker has been developed for recognizing and locating fruit, as well as detaching it according to prescribed criteria without causing damage to the fruit or the tree. A six-camera array is used to detect fruit in citrus trees. In the image segmentation step, the Naïve Bayesian method is applied to discriminate citrus fruit from the background. This process requires a supervised pixel classification from an image database collected prior to field trials. By applying a value π which represents priori probabilities, each image pixel is segmented using the following rules:

$$\text{pixel} = \begin{cases} 1, \text{fruit} & \text{if } (fg \times \pi) > \left(bg \times (1-\pi)\right) \\ 0, \text{background} & \text{if } (fg \times \pi) \leq \left(bg \times (1-\pi)\right) \end{cases} \tag{2.16}$$

where fg and bg are fruit (foreground) and background colour, respectively. The validation results confirm that at least 98% of the fruits on the tree are visible using the attached cameras and moreover, that the picker mechanisms can detach over 98% of the fruits observed.

Image-based detection of pomegranates on trees was investigated by [32]. In the research, a combination of colour and shape analyses is applied to detect pomegranate fruits on trees, which are red in colour and round in shape. Four common indices, i.e. difference index, hue-saturation index, ratio index, and normalisation index, in addition to a new index, specifically modified difference index, are used for fruit detection. The results reveal that the modified difference index has the highest classification rate. The modified index can be expressed as follows:

$$RR_g = \frac{3\Delta R_g}{\left(\overline{R} + \overline{G} + \overline{B}\right)} \tag{2.17}$$

$$RR_b = \frac{3\Delta R_b}{\left(\overline{R} + \overline{G} + \overline{B}\right)} \tag{2.18}$$

with

$\Delta R_g = \overline{R} - \overline{G}$ and $\Delta R_b = \overline{R} - \overline{B}$

where $\overline{R}$, $\overline{G}$, and $\overline{B}$ are mean values of R, G, and B, respectively.

Arivazhagan et al. [33] investigated the use of computer vision for fruit recognition based on colour and texture features. HSV (hue, saturation and value/intensity) colour space is used in contrast to the RGB colour model for its invariant properties. Four statistical colour features, principally mean, standard deviation, skewness, and kurtosis, are derived from H and S components. Thus, there are eight colour features extracted from each fruit image. Moreover, the V component is subjected to one level of decomposition Discrete Wavelet Transform and the co-occurrence matrix is constructed using the intensity value. Five texture features are subsequently extracted from the constructed co-occurrence matrix, i.e. contrast, energy, local homogeneity, cluster shade and cluster prominence. Therefore, 13 colour-texture features are used with regards to the recognition of various fruits. Fifteen different fruits were used in the experiment and the results prove that the recognition rates using only colour features and texture features are 45.5% and 70.8%, respectively. The recognition accuracy is improved by up to 86% using both colour and texture features simultaneously.

The applications of image processing can also be established in post-harvest activities, for instance in fruit sorting and grading. Research related to the detection of apple size and a grading system based on image processing was performed by [34] in controlled lighting conditions. In this case, the fruit area is firstly segmented from the image with an Ohta-colour-model based thresholding algorithm. Ohta colour space can be obtained by converting RGB colour as follows:

$$I_1 = \frac{(R+G+B)}{3} \quad ; \quad I_2 = \frac{(R-B)}{2} \quad ; \quad I_3 = \frac{(2G-R-B)}{4} \tag{2.19}$$

$$I_2' = R - B \quad ; \quad I_3' = \frac{(2G-R-B)}{2} \tag{2.20}$$

Blob algorithm is then used to remove image noises and a spline-interpolation based technique is applied to detect fruit contours. In the sorting process, the colour ratio of an apple is calculated by dividing the red colour value with the area of the apple image. The apples are subsequently sorted by Bayes classifier. The accuracy level of the classification is up to 90%.

A colour-based grading system was also conducted by [35] in connection with tomatoes and dates. In the study, a new colour mapping concept is presented. The colour mapping converts 3-D colour spaces to 1-D colour indices for automated grading. This technique has made the selection and adjustment of colour preferences more straightforward.

Mizushima et al. [36] developed an image segmentation method using support vector machine (SVM) and Otsu algorithm for apple sorting and grading. The developed image segmentation method can automatically adjust the classification hyperplane obtained from linear SVM with minimum training time. To achieve the best segmentation results, the minimum threshold (T_{min}) value around the fruit boundary is estimated and then applied to the SVM grayscale image. A classification hyperplane in the 3-D RGB space can be calculated as a linear combination of red, green and blue as follows:

$$Z(x,y) = w_R R(x,y) + w_G G(x,y) + w_B B(x,y) + b \tag{2.21}$$

with

$$w_R = \sum_{i=1}^{n_{sv}} \lambda_i t_i R_i \ , \quad w_G = \sum_{i=1}^{n_{sv}} \lambda_i t_i G_i \ , \quad w_B = \sum_{i=1}^{n_{sv}} \lambda_i t_i B_i$$

$$b = t_k - (w_R R_K + w_G G_K + w_B B_K) \ , \quad 1 \le k \le N_s$$

where $R(x,y)$, $G(x,y)$ and $B(x,y)$ are the red, green and blue values at pixel position (x,y), respectively; R_i, G_i and B_i are support vectors of red, green and blue obtained by training, respectively; R_K, G_K and B_K are the red, green and blue of any given support vector, respectively; λ_i and t_i are the positive Lagrange multipliers and the class label, respectively; and n_{sv} is the number of support vectors.

2.4. Nitrogen Content Measurement in Plants

In general, there are four different methods employed to assess nitrogen content in plants, i.e. (i) chemical and combustion test, (ii) vegetation index, (iii) leaf colour chart, and (iv) chlorophyll meter based measurement. Each method will be described in detail as follows:

a) Chemical analysis using the Kjeldahl method

As described by [37], the Kjeldahl method is commonly used for nitrogen analysis of leaf tissue and several fruit crops. The procedure of this method can be explained as follows:

A ground sample weighing 0.25g is digested with 5 mL of sulphuric acid (H_2SO_4) and the mixture is heated at a temperature of 380 ^oC until the sample solution is clear. Distilled water is then added to the digested sample until the solution volume reaches 50 mL. After adding

roughly 1 mL of 40% sodium hydroxide (NaOH) solution, a 10 mL volume of the sample is distilled. The distilled sample is then titrated with a standard solution of 0.02 N H_2SO_4 until the end point. The nitrogen concentration of the leaf sample can be calculated using the following equation:

$$N_{total}(\%) = \frac{(V_s - V_b) \times C_{H_2SO_4} \times 0.014 \times V_d \times 100}{W \times V_a} \quad (2.22)$$

where V_s is the volume of the standard H_2SO_4 (mL) used for titration to reach the end point, V_b is the volume of the standard H_2SO_4 (mL) used for titration of the blank, $C_{H_2SO_4}$ is the concentration of H_2SO_4, V_d is the volume of the digested sample solution, W is the weight of the sample (g) and V_a is the volume of the sample solution for the analysis.

In addition, [38] depicts the Kjeldahl procedure for nitrogen estimation of plant tissue in a simple diagram, as seen in Figure 2.1.

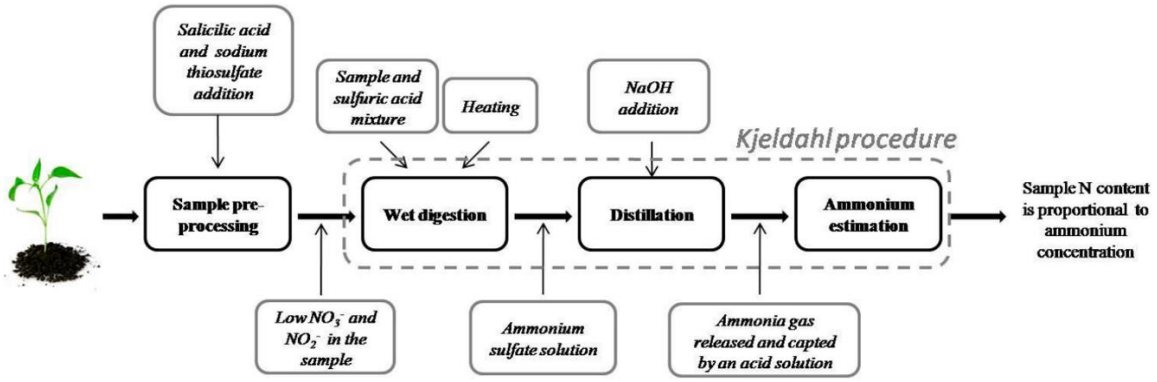

Figure 2.1. Kjeldahl method to determine nitrogen content in plant tissue.

b) Combustion method

The combustion method, also known as Dumas combustion procedure, is another destructive technique utilised to analyse nitrogen in plant leaves. Compared to the Kjeldahl method, Dumas combustion method is much quicker in application and less expensive in relation to disposing of hazardous waste [37]. In this method, dried leaf samples are burned completely in the induction furnace of the nitrogen analyser. Both organic and inorganic nitrogen are then transformed into NO_x gases, which are subsequently reduced to N_2 gas. Eventually, the amount of nitrogen is subsequently measured automatically by thermal conductivity. Munoz-Huerta et al. [38] simplifies Dumas combustion procedure in a block diagram, as depicted in Figure 2.2.

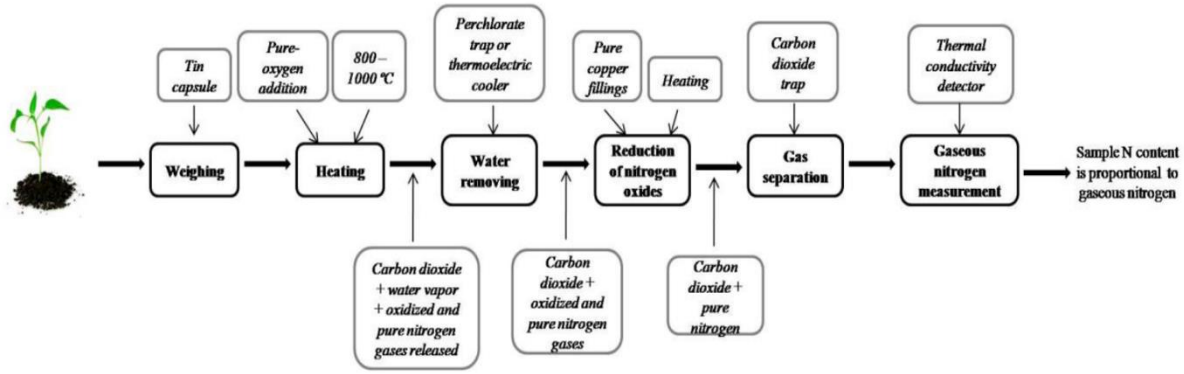

Figure 2.2. Dumas combustion method to assess nitrogen content in plant tissue.

Both the Kjeldahl and Dumas combustion methods are the most accurate techniques with respect to measuring nitrogen in leaves and the results are regularly utilised as the standard values for other techniques. Despite the accuracy of the analysis results, these methods are destructive and time-consuming and also require special expertise to operate special devices.

According to Figure 2.1 and Figure 2.2, there are several differences between Kjeldahl and Dumas method. The differences are as following:

1. There is a heating process in both methods, however, the heating temperature in Dumas method is considerably higher than that in Kjeldahl method.
2. Both methods utilise chemical substances. Dumas method uses gases, such as oxygen, nitrogen and carbon dioxide, while Kjeldahl method utilises solution (liquid), such as sulphuric acid, ammonium sulphate and sodium hydroxide.
3. The final substance, which is then used to estimate nitrogen content of the sample, obtained from the Kjeldahl method is ammonium, while that from the Dumas method is gaseous nitrogen.

c) Vegetation index (VI) method

As reported by [39], satellite remote sensing can be utilised to estimate nitrogen status with larger covered areas. Basically, this method is conducted by extracting the spectral digital number (DN) values of a remote sensing image (multispectral image) by means of commercial software, such as ENVI and ArcGIS, and subsequently calculating several vegetation indices. A multispectral image has four wavelength bands, i.e. 450-520 nm at blue light (B), 520-600 nm at green light (G), 630-690 nm at red light (R), and 760-900 nm at near-infrared (NIR). The vegetation indices are subsequently correlated with a number of plant

growth parameters, such as biomass, leaf area index, nitrogen uptake, nitrogen concentration and nitrogen nutrition index. Several VIs have been studied in relation to estimating nutrient status in plants, i.e. normalised difference vegetation index (NDVI), green normalised difference vegetation index (GNDVI), ratio vegetation index (RVI), green ratio vegetation index (GRVI), green and red ratio vegetation index (GRRVI), enhanced vegetation index (EVI), visible atmospherically resistant index (VARI), chlorophyll index (CI), structure insensitive pigment index (SIPI) and plant senescence reflectance index (PSRI).

Regardless of its large coverage area, this method is expensive pertaining to obtaining satellite images. In addition, it is not straightforward with regards to obtaining the images; thus, this technique is not appropriate for traditional farmers and agriculture practitioners.

d) Leaf colour chart

A leaf colour chart, as seen in Figure 2.3, is developed to measure the green colour intensity of crop leaves, such as rice [40]. The leaf colour chart was initially made for rice crops and it is still commonly used on rice plants. However, the symptoms of either excess or deficient nitrogen in leaves are similar to all other crops. The leaf colour chart, therefore, can be applied to most narrow leaf crop plants, for instance rice, wheat, sugarcane, millet and onion, as seen in Figure 2.4 [41]. The advantages of using this method are that it is straightforward to use, non-destructive and inexpensive. To use a leaf colour chart pertaining to nitrogen estimation, the observed leaf colour only has to be compared with a standard colour in the chart, as shown in Figure 2.5 [42]. In spite of its simplicity, the result is less accurate due to differences in people's vision.

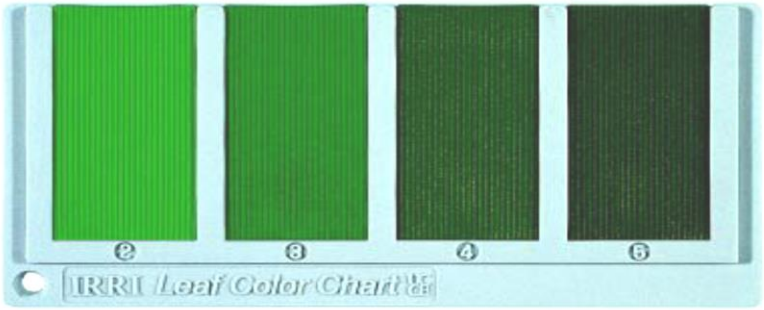

Figure 2.3. A leaf colour chart.

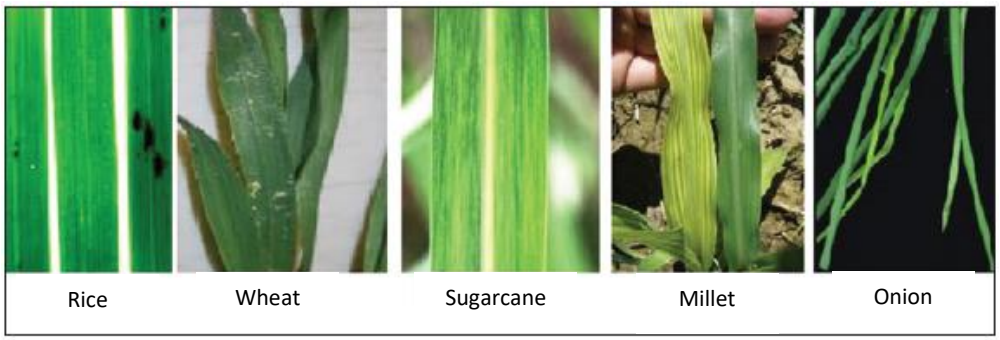

Figure 2.4. Leaves of various crops with similar shapes and sizes.

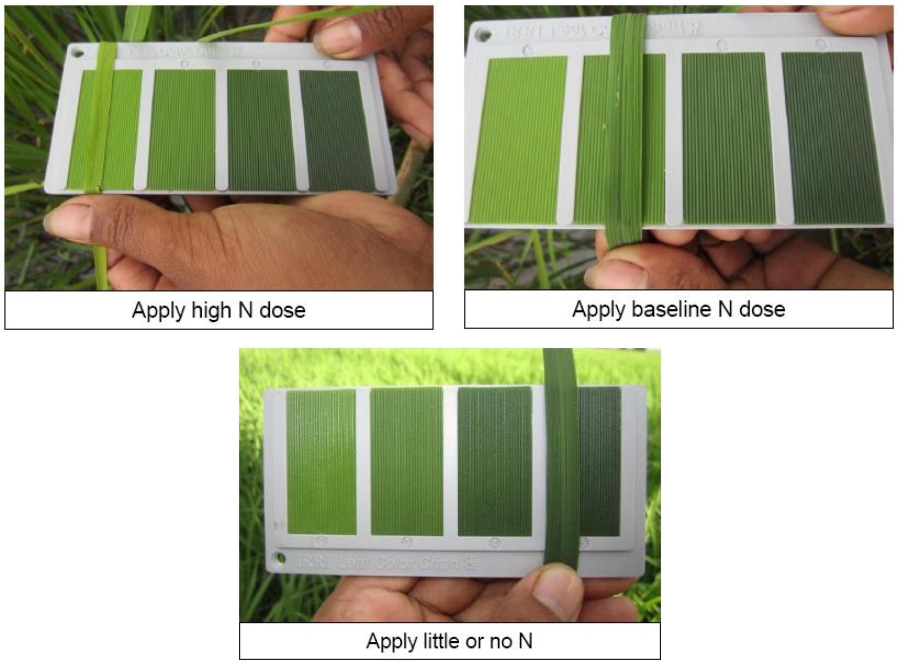

Figure 2.5. Application of leaf colour chart to determine nitrogen fertiliser dose.

e) Chlorophyll meter

It is recognised that greenness index in leaves has a strong relationship with chlorophyll content. Chlorophyll in a leaf absorbs all visible lights in various amounts. The absorbance peaks occur on absorption of blue light (400-500 nm) and red light (600-700 nm) and little absorbance in green light (550 nm) as seen in Figure 2.6. Most of the green lights are reflected from or transmitted through leaves. This is what gives chlorophyll-leaves their green colour. Furthermore, chlorophyll absorbs very little, even zero, radiation at wavelengths greater than 700 nm, termed near-infrared (NIR), which is not used in photosynthesis.

Furthermore, chlorophyll content in leaves also has a strong correlation with nitrogen amount, seeing as nitrogen is the principal component and develops chlorophyll in a leaf. Therefore, it can be claimed that nitrogen content can be detected and measured via the greenness index of the leaf. The most common and practical method applied to measure the greenness index is by

using a chlorophyll meter. The most renowned one is the SPAD-502 (Soil-Plant Analysis Development, Minolta Camera Co., Osaka, Japan). A SPAD meter is a non-destructive handy device to determine chlorophyll content in a leaf by measuring the absorbance and transmittance of lights with two different wavelengths through the leaf [43].

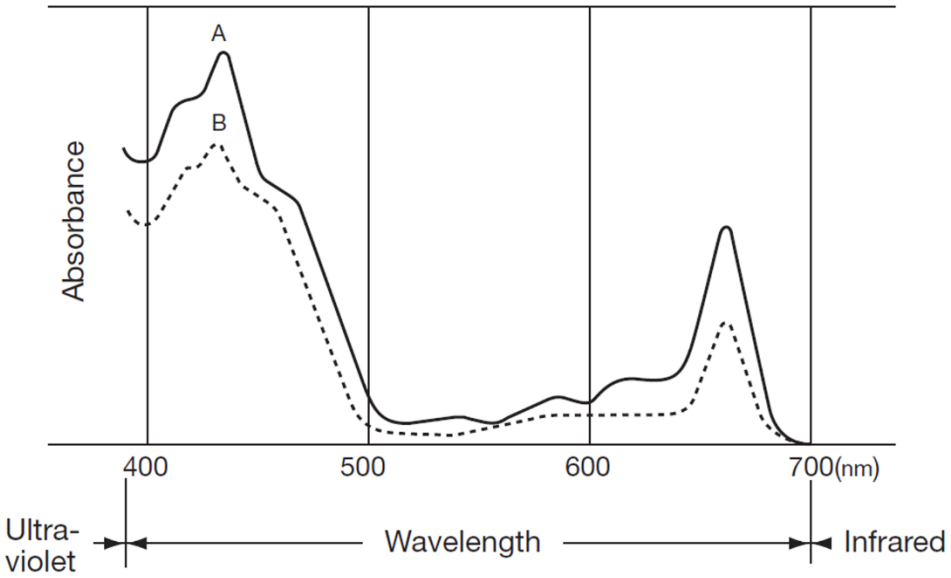

Figure 2.6. Absorbance level of green leaf on various wavelengths [44].

This device utilises two LEDs which emit lights onto the upper surface of a leaf. The two LED sources emit a red light with a peak wavelength of 650 nm (L_{650}) and an infrared light with a peak wavelength of 940 nm (L_{940}). The light from the LEDs penetrates the leaf where a portion of the light is absorbed by chlorophyll and the rest is transmitted through the leaf (Figure 2.7). The transmittance lights (L'_{650} and L'_{940}) make contact with a photodiode detector and is converted into an electrical signal. The values produced by the chlorophyll meter are nontrivial ratios and are also known as chlorophyll content index (CCI), which can be calculated as follows [45]:

$$CCI = \log \frac{L'_{940}/L_{940}}{L'_{650}/L_{650}} = \log \frac{L'_{940} \cdot L_{650}}{L'_{650} \cdot L_{940}} \tag{2.33}$$

If a light from a light source strikes an object, a number of things could happen. The light wave could be transmitted, absorbed, scattered, and/or reflected by the object. The transmitted radiant flux, thus, can be calculated as follows:

$$L' = L - L_a - L_s - L_r = L - (L_a + L_s + L_r) \tag{2.34}$$

Based on the fact of the light proportion as expressed in Eq. (2.34), therefore, Eq. (2.33) can be rewritten as follows:

$$CCI = \log \frac{L_{650} \cdot [L_{940} - (L_a + L_s + L_r)_{940}]}{L_{940} \cdot [L_{650} - (L_a + L_s + L_r)_{650}]} \tag{2.35}$$

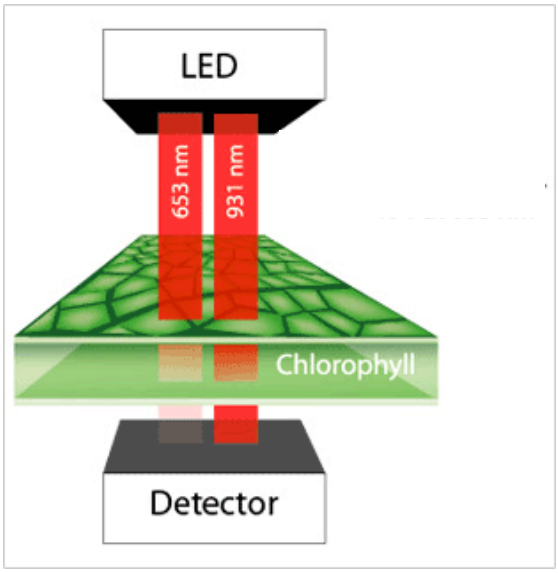

Figure 2.7. How a chlorophyll meter works [46].

After the signal processing, the absorbance is displayed and shows units that range from -9.9 to 199.9 and is known as the SPAD value. In spite of its simplicity, the result of this method is significantly influenced by leaf thickness, while the leaf area used for this measurement is exceedingly small (6 mm^2). Hence, this measurement is not suitable to use in a large field. In addition, this device is very expensive. It costs around $2,200 [47].

2.5. Image-based Nutrient Status Analysis in Plants

In general, studies on nutrient prediction can be categorised into two research groups. The first research group is with respect to nutrient deficiency prediction. Such researches are typically conducted to identify symptoms, as well as classify certain nutrient deficiency in various plants. The second research group is related to nutrient status or nutrient amount estimation. Commonly, researches in the second group aim to predict specific nutrient content

in several crops. Furthermore, Muñoz-Huerta et al. [38] summarised numerous methods to determine nitrogen status in plants, as seen in Figure 2.8.

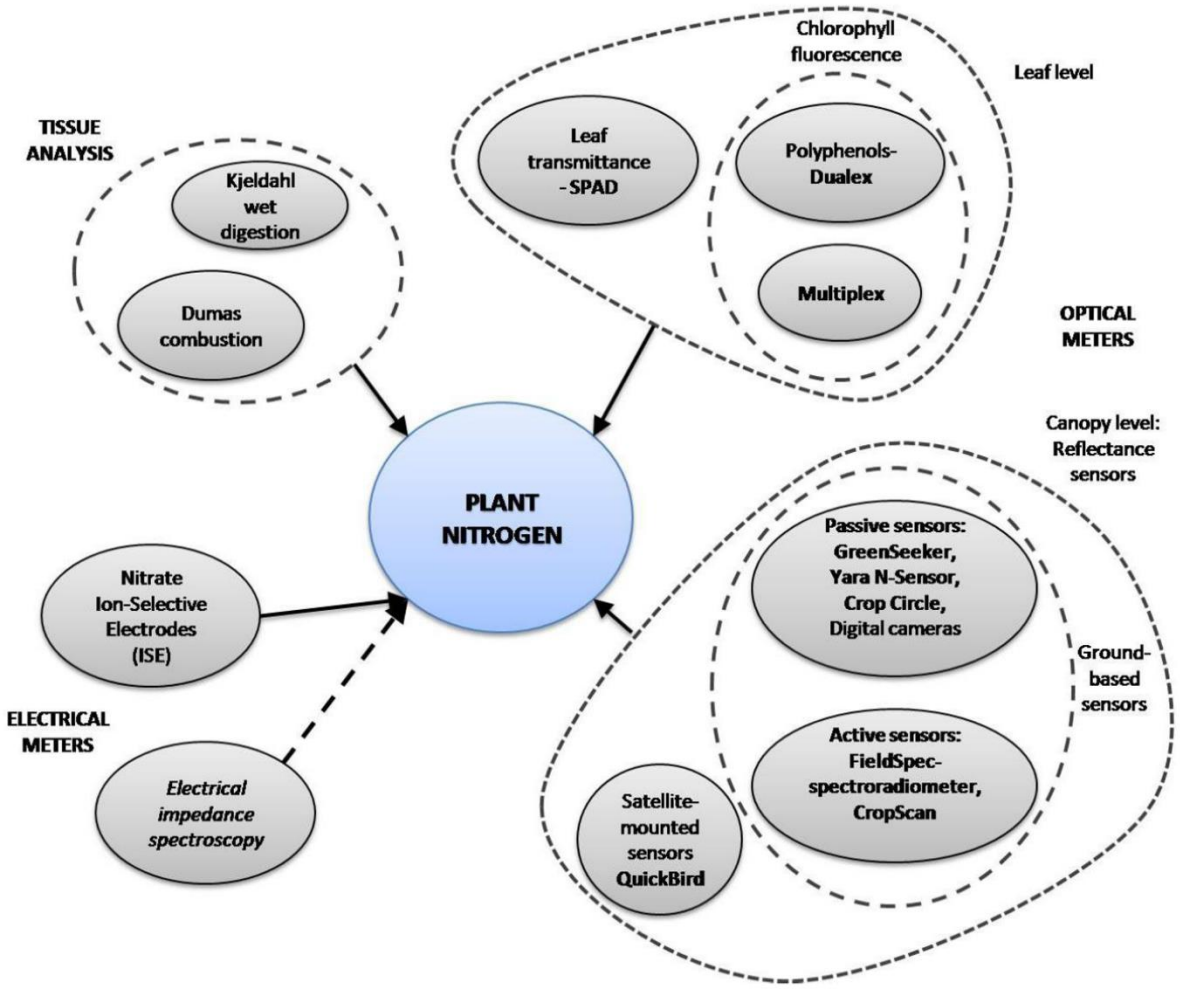

Figure 2.8. Various methods for nitrogen status determination.

Xu et al. [10] conducted research to identify nitrogen and potassium deficiency in tomato plants using images related to the colour of leaves captured in a closed sampling box, as seen in Figure 2.9. In this research, they used colour and texture features of potato leaves extracted by means of various methods, such as percent intensity histogram, percent differential histogram, Fourier transform, and wavelet packet. Furthermore, genetic algorithm (GA) was employed to choose features to obtain the most appropriate information for classifying nutrient deficiency. The experiments prove that their method can predict nutrient deficiency in a potato, with an accuracy level of 82.5%, approximately 6-10 days before experts could make a diagnosis.

1 – CCD camera
2 – Sampling box
3 - Computer

Figure 2.9. Image acquisition devices to identify nitrogen and potassium deficiency in tomato plants.

Story et al. [48] observed calcium deficiency on lettuce crops in controlled environments using machine vision, as shown in Figure 2.10. The visual plant features used in this research are top projected canopy area (TPCA) as a morphological feature; red-green-blue (RGB) and hue-saturation-luminance (HSL) values as colour features; in addition to entropy, energy, contrast and homogeneity as textural features. Based on their research, calcium deficiency on lettuce crops could be identified one day prior to detection by human vision. Moreover, they established that TPCA, energy, entropy and homogeneity were the best features with regards to detecting calcium deficiency in lettuce.

Ma et al. [49] analysed the colour of soybean leaves to diagnose nitrogen deficient and nitrogen excess soybean plants. This research applied the RGB and HSI colour model to six stages of soybean growth, which are fertilised using four levels of nitrogen fertiliser (0%, 50%, 100% and 150%). According to this study, the nitrogen content in soybean leaves can be calculated whether it has a deficiency or an excess by combining the curve trends in each stage and the value of the RGB and HSI components.

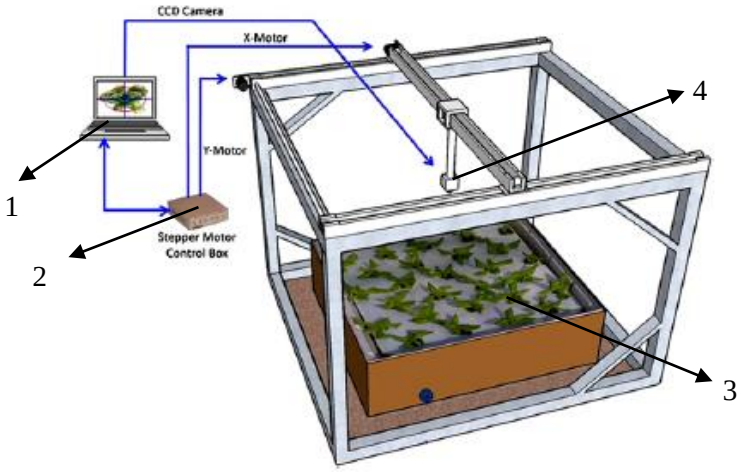

1. Personal computer
2. Stepper motor control box
3. Lettuce crops
4. CCD camera

Figure 2.10. Schematics of a machine vision for a lettuce crop monitoring system.

In research conducted by [50], image processing based algorithm was developed to represent symptoms of nitrogen, potassium and magnesium deficient oil palm leaves (Figure 2.11). The developed algorithm includes image segmentation, colour features extraction and image classification. The result reveals that the algorithm is capable of classifying three types of nutrient deficient oil palm leaves.

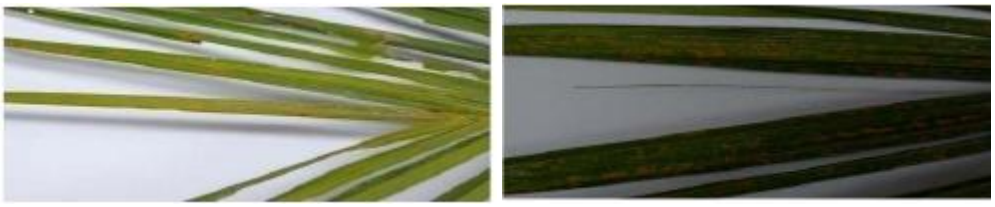

(a) (b)

(c)

Figure 2.11. Examples of nutrient-deficient oil palm leaves: (a) nitrogen, (b) potassium and (c) magnesium.

Wiwart et al. [51] analysed the colour changes of the first leaves from three legume species (faba bean, pea and yellow lupine) under nitrogen, phosphorous, potassium and magnesium deficiency conditions. Euclidean distance was applied to determine the similarity concerning

leaf colour for L*a*b* and HSI colour values. This method presents a base to develop an automated system for early detection of nutrient deficiencies in legumes.

Pagola et al. [52] developed a new technique to measure the nitrogen status of barley plants in a greenhouse using the RGB colour index analysis. In this research, a small leaf area of 1 cm^2 was captured by a digital camera, as seen in Figure 2.12. Fifteen images of barley leaves with different nutritional status from low to high level of nitrogen dose were captured. The average values of |R−B|, |G−R| and |G−B| were then calculated for all pixels in each image. Figure 2.13 shows the corresponding points for each leaf. This technique utilises principal component analysis (PCA) to calculate a correlation matrix and to obtain the eigenvalues and eigenvectors. The eigenvector associated with the highest eigenvalue corresponds to the main direction of the leaves data, as shown by the red dashed arrow in Fig. 2.13. The predicted nutrient amounts using the PCA-based greenness index (I_{PCA}) strongly correlated with the SPAD meter measurements, with a correlation coefficient of 95%.

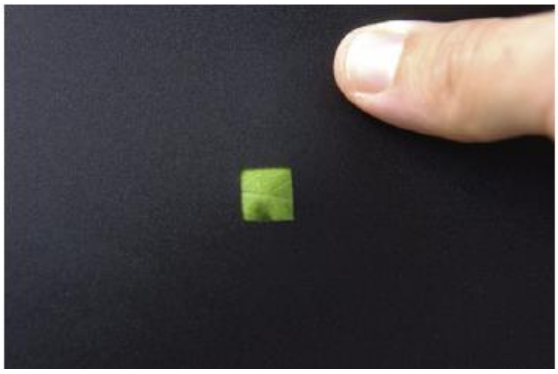

Figure 2.12. An example of a leaf image.

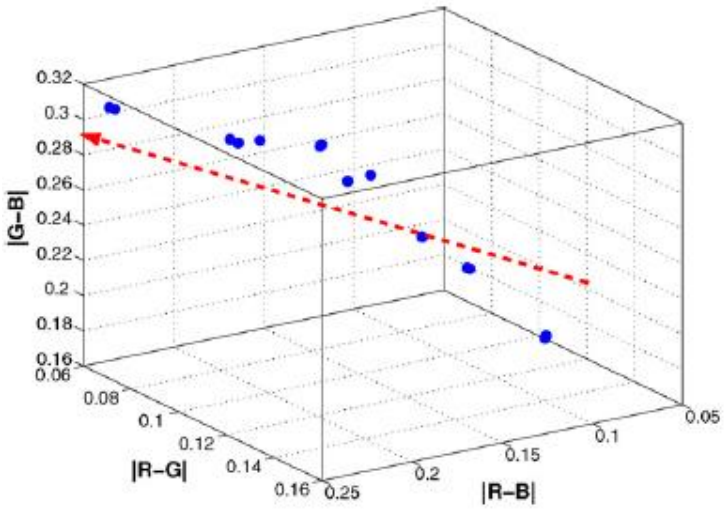

Figure 2.13. Leaf points and principal direction in PCA based on RGB colour.

Yao et al. [11] have developed a new technique for nutrient status detection. Their research proposed several tables instead of explicit linear or non-linear mathematical models. These tables consist of the data regarding leaves image features and the macronutrient percentage of a standard colour block from a given leaf sample. Nutrient status detection is subsequently performed by comparing the observed leaf features with the standard colour blocks.

Yuanfang et al. [53] studied image processing and spectral analysis based chlorophyll content monitoring maize leaves. They used colour features of RGB and HSI to establish a regression model. By using univariate regression analysis of component G, the verified regression model could be used to predict chlorophyll value with a precision level of 0.734. Furthermore, three component multiple regression statistics regarding G, I and 2G-R were also applied to estimate the amount of chlorophyll. The prediction accuracy related to this regression is up to 0.744.

Moghaddam et al. [54] investigated the use of colour image and neural network to assess nitrogen status in sugar beet leaf. The RGB colour of a leaf image is captured with a conventional digital camera and used as neural network inputs to estimate the SPAD value of sugar beet leaves. The results confirm that the developed neural network can be used to estimate SPAD value with greater accuracy compared to the linear regression model.

Wang et al. [55] developed an algorithm to estimate nitrogen status of rice crops using the image segmentation based on the value of green minus red (GMR) threshold. Canopy images of rice crops are segmented by using GMR value, and then several image features are correlated with three plant indices, i.e. above-ground biomass, nitrogen content and leaf area index. The results show that the GMR value and canopy cover will be valid indicators to estimate nitrogen content in rice crops.

A research conducted by [56] has found that dark green colour index ($DGCI$) can be utilised to assess nitrogen content in corn leaf. DGCI has a strong relationship with leaf nitrogen concentration with coefficient of determination (R^2) ranged from 0.80 to 0.89. Furthermore, $DGCI$ can be obtained by combining hue (H), saturation $(S)$and brightness (B) into one composite number, as follows:

$$DGCI = \frac{\frac{(H-60)}{60} + (1-S) + (1-B)}{3} \tag{2.33}$$

2.6. Summary

Nitrogen analysis in plants is required to provide a valuable assessment prior to the application of fertiliser, in order to provide an accurate fertilisation dose and to prevent environmental degradation. This is the concept of site-specific fertilising. This chapter presented numerous techniques pertaining to nitrogen status analysis, either destructive or non-destructive. Most of the image-based techniques were conducted in controlled conditions. In the coming chapters, three different methods that are employed to analyse nitrogen status based on crop images captured in fields will be presented.

Chapter 3

Regularised Neural Networks Fusion and Genetic Algorithm Based On-Field Nitrogen Status Estimation of Wheat Plants

3.1. Introduction

In this chapter, a novel approach of on-field nitrogen amount estimation in wheat plants is developed based on the characteristics of the plant images. The main focus of this chapter is on the utilisation of colour normalisation method using neural networks fusion and genetic algorithm to normalise wheat plant images captured under various sunlight intensities. Moreover, a Macbeth colour checker is used as colour reference to normalise the colour of the images. In the step of image segmentation and features extraction, neural network is utilised to distinguish wheat leaves as the object of interest from other images, such as soil, weeds, dried leaves, stems and stones. Twelve statistical features, i.e. first moment (mean), second moment (variance), third moment (skewness) and fourth moment (kurtosis) of each RGB colour channel, are extracted from the segmented images as the nutrient estimation predictors. These features are proposed as the nutrient predictors, instead of single colour channel from a certain colour model or combination of some colour channels, since they are more suitable to represent the colour distributions in wheat leaves. Finally, in the nutrient estimation step, a combination of committee machines and genetic algorithm from several neural networks with different hidden layer nodes is established to estimate nitrogen content.

3.2. Experimental Setup

This research work can be divided into three parts as depicted in Figure 3.1. Each part will be explained more detail in the following sections.

3.2.1. Experimental materials and design

In order to produce variations in nitrogen levels, an experiment in relation to wheat plants with various fertiliser amounts was established, as presented in Figure 3.2. This experiment was conducted at Nafferton experimental farm, Newcastle University, from April to June 2013. The treatments were set to three different fertiliser amounts, i.e. 0 (N1), 85 (N2), 170

(N3) kg/ha of NH_4NO_3 with each treatment replicated four times. Hence, there are 12 plots with each plot being 20 m × 20 m in dimension. The data collection was undertaken in three different sessions i.e. one week prior to fertilising, and two and four weeks after fertilising. Therefore, in total 36 samples were used in this research.

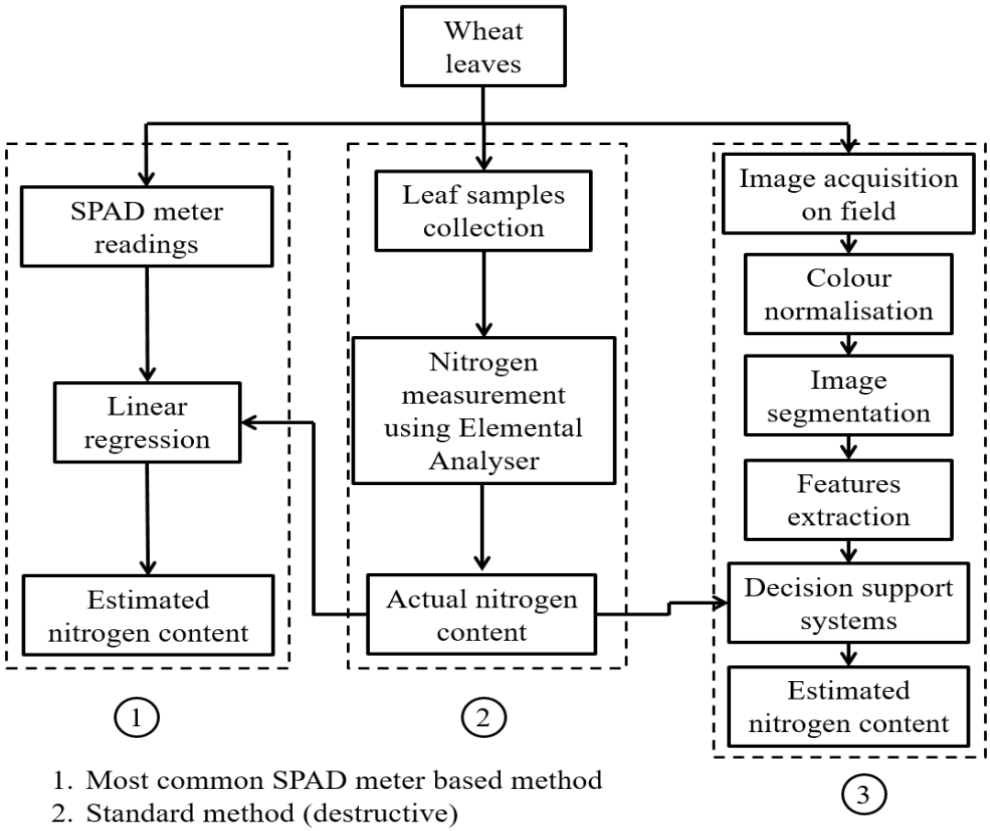

Figure 3.1. Flowchart of the research.

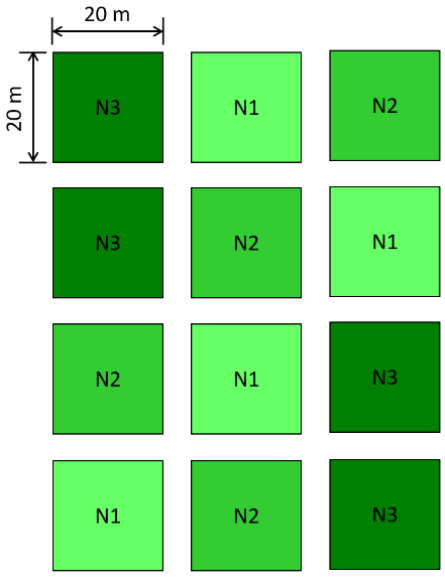

Figure 3.2. Experimental farm design to produce a variation of nitrogen levels.

3.2.2. Combustion method based nitrogen analysis

The actual nitrogen content was measured using combustion method by means of Elementar Vario Macro Cube (Figure 3.3). This device has high temperature combustion unit which can burn organic matter samples up to 1200-1800 ^{o}C. It also has the largest weighing range which is optimised for macro sample weight up to 1.5 g soil and 200 mg organic matter. In addition, the device has the largest dynamic range of element concentrations and element ratio up to 150 mg carbon or 100 mg nitrogen (or 100%), from ppm to 100%.

Prior to nutrient analysis, 50-60 leaves per plot were taken as samples. These samples were then dried in a cabinet oven dryer at a temperature of 80 ^{o}C for 2 days. Subsequently, the dried samples were ground in an electric grinder at 14,000 rpm to pulverise the samples into powder.

For the nitrogen analysis, a sample weight of approximately 100 mg was required, which was weighed into a tin foil cup. The cup was then folded and squashed into a pellet to expel the air. This analysis involved the combustion method by burning the sample up to 1800 ^{o}C with a certain amount of oxygen. The nitrogen element was analysed and a percentage figure subsequently obtained.

Figure 3.3. Elementar Vario Macro Cube for combustion method based nitrogen analysis.

3.2.3. Chlorophyll meter readings

The chlorophyll meter used in this thesis was Konica Minolta SPAD 502 Plus, which is known as SPAD meter. The SPAD meter has measurement area approximately 2 mm x 3 mm. This device measure optical density difference at two wavelengths, i.e. 650 nm and 940 nm

from 2 LEDs as the light source and silicon photodiode as the receptor. The SPAD value measured by this device represents index of relative chlorophyll content which ranging from -9.9 to 199.9.

The SPAD meter readings were conducted on 30 leaf samples in each plot. The value displayed on the SPAD meter screen signified the chlorophyll content in the leaf, which is strongly correlated with the nitrogen content.

The SPAD values of the 30 leaves on one plot were then averaged, in order to obtain the SPAD value of the plot. Therefore, there were 12 SPAD values for 12 samples in one data collection time. In total, there were 36 SPAD values used for comparison.

3.2.4. Image Acquisition

In this research, images of two objects were acquired on field with variations of sunlight intensities, i.e. Macbeth colour checker and wheat plants images. Firstly, the images of the Macbeth colour checker were captured under sunlight using a common digital still camera. The camera used in this thesis was Sony Cyber-shot DSC-W55 which has maximum resolution 7.2 megapixels. This device uses CCD sensor with focal length of 38–114 mm and maximum aperture of F2.8–5.2.

The sunlight intensity, which was measured by using a digital light meter, ranged between 7 to 82 Klux. The light meter used in this research was ISO-TECH ILM 1335 with has measurement range from 0 to 400,000 lux, sensor lead length 150 cm and sensor dimensions 100 mm × 60 mm × 27 mm. The 50 Klux was considered to be the standard (target) light intensity and the remainder as the input light intensity. In total there were 164 input images (range of 7 to 48 Klux and 52 to 82 Klux) and five target images (range of 49-51 Klux). Each image was consequently cropped twice on each patch with a cropping window of 95 × 72 pixels.

Secondly, wheat plants images were indiscriminately captured under sunlight at 30 points on each plot. Thus, related to image acquisition, there were 1,080 plants images for 12 plots during three specific times (days). The light intensity of the sun during this experiment ranged from around 8 to 80 Klux with the image data collection time being from 10 am until 2 pm. This means that the colour of the sunlight was relatively white, compared to its colour in the morning or in the evening, when it is quite reddish or yellowish. All images were captured

from the top of the plants in a distance of 10-20 cm using the digital camera. The images were recorded at a resolution of 1632 × 1224 pixels and subsequently down sampled to 448 × 336 pixels to assist with the effectiveness of the image processing.

3.3. Neural Networks Fusion and Genetic Algorithm Based Colour Normalisation

The changes in sunlight intensity will lead to different appearances in the plant images. The images, therefore, need to be equalised as if they are acquired under the same light intensity, in order to perform a more reliable comparison of the images. In this research, a 24-patch Macbeth colour checker was utilised to normalise images by using neural networks fusion and genetic algorithm. Macbeth colour checker is a square card that consists of 24 patches of colour samples which represent natural objects, chromatic, primary and greyscale colours, which are arranged in four rows (Figure 3.6). Neural networks have been used widely in various industrial applications, such as wind power plants [57], transportation [58], robotics [59], and marine [60]. Neural networks are also used in digital signal processing [61], [62] and electronic applications [63].

Figure 3.4. 24-patch Macbeth colour checker.

Colour normalisation, also known as colour constancy, is an ability to correct the colour deviations of an object due to differences in lighting conditions. According to [64], image colours are significantly affected by the direction and intensity of the light source, as well as illuminant colour. Furthermore, countless research has been conducted to overcome the

problem of colour normalisation [65], [66], [67]. The colour normalisation concept in this research differs from previous works given that the images are acquired under unconstrained daylight, as mentioned in the previous section. This poses a difficult challenge as plant images captured under various light intensities have to be corrected to a standard image that is captured under a standard light intensity.

The proposed method of neural networks fusion and genetic algorithm for image normalisation is described below. As mentioned in the previous section, each input image of Macbeth colour checker was cropped twice on each patch with cropping size of 95 × 72 pixels. The average RGB colour value of each patch of the cropped input images was then calculated. The average RGB value of each patch of the target images was obtained from five images. Thus, there were 24 datasets of input-target RGB colour from 24 patches and with each patch consisting of 328 (= 164 × 2) RGB colour samples. All the datasets were consequently combined to produce one large dataset for neural networks fusion. This new dataset, thus, consisted of 7872 (= 328 × 24) RGB colour samples.

The single neural network for each colour patch developed in this research was a multilayer perceptron (MLP), which contains one hidden layer, three nodes of input and output layers of red, green and blue colour channels. MLP is a well-established neural network that can be used for classifier [68] as well as nonlinear model prediction [69]. The cost function of the developed MLP was based on minimising the mean square error (MSE) between the targets and the network's outputs. The number of hidden layer nodes in each network was determined by applying the formula developed by [70] as follows:

$$n_h = \left(\frac{n_i + n_o}{2}\right) + \sqrt{n_p} \tag{3.1}$$

where n_i, n_h and n_o are the number of input, hidden and output layer nodes, respectively, and n_p is the number of input patterns in the training set (number of training samples).

According to Eq. (3.1), the number of hidden layer nodes for each neural network was 92 nodes ($n_i = 3$,$n_o = 3$, $n_p = 7872$). However, this method serves only as a guide and does not always provide the optimal number of hidden nodes. In this research, a new method has been proposed to optimise the MSE and impose a smooth regularisation on the weights of the hidden nodes in addition to implementing (3.1) by applying smoothness function [62]:

$$\Omega = \frac{1}{2}\int Y(\boldsymbol{X})\left\|\partial^k G(\boldsymbol{X})/\partial \boldsymbol{X}^k\right\| \boldsymbol{X}\, \partial \boldsymbol{X} \tag{3.2}$$

to develop the weighting function $\Upsilon(\boldsymbol{X})$ that ensures the above integral in Eq. 3.2 converges and subsequently determines the region of the input space over which the MLP mapping $G(\boldsymbol{X})$ is required to be smooth by making the k^{th} order derivative of $G(\boldsymbol{X})$ with respect to input $\boldsymbol{X}$ small. The larger the value of k, the smoother the mapping $G(\boldsymbol{X})$ will become. In order to achieve the objectives, the following mixture of Gaussian functions has been proposed:

$$\Upsilon(\boldsymbol{X}) = \frac{1}{Q}\sum_{k=1}^{Q}\frac{1}{(2\pi)^{N/2}|\boldsymbol{R}|^{1/2}}\exp\left[-\frac{1}{2}(\boldsymbol{X}-\boldsymbol{X}_k)^T\boldsymbol{R}^{-1}(\boldsymbol{X}-\boldsymbol{X}_k)\right] \tag{3.3}$$

so as to capture the local variation of the input space where $\{\boldsymbol{X}_k\}_{k=1}^{Q}$ are a set of input data points and that using $\boldsymbol{R} = \sigma^2\mathbf{I}$, it is required that σ be selected small such that

$$\lim_{\sigma\to\infty}\sum_{k=1}^{Q}\frac{1}{(2\pi\sigma^2)^{N/2}}\exp\left[-\frac{1}{2\sigma^2}\|\boldsymbol{X}-\boldsymbol{X}_k\|^2\right] = \delta(\boldsymbol{X}-\boldsymbol{X}_k) \tag{3.4}$$

where $\delta(\cdot)$ is the delta function. The above integral in Eq. 3.2 can be approximated as

$$\Omega \approx \frac{1}{2}\sum_{j,k} w_{jk}^2\|\boldsymbol{v}_k\|^p \tag{3.5}$$

where $\boldsymbol{v}_k = [v_{k1} \quad v_{k2} \quad \cdots \quad v_{kn_h}]$ is the k-th row of weight matrix $\boldsymbol{V}$ connecting the input to the hidden nodes, $\|\cdot\|^p$ is the p-norm. The simple algebraic form of Ω enables the direct enforcement of smoothness without the need for costly Monte-Carlo integrations. The derivatives of the weighting function Ω with respect to the parameters w_{jk} and v_{ij} have been derived as follows:

$$\frac{\partial\Omega}{\partial w_{jk}} = w_{jk}\|\boldsymbol{v}_k\|^p \tag{3.6}$$

and

$$\frac{\partial\Omega}{\partial\boldsymbol{v}_k} = \frac{p}{2}(\boldsymbol{v}_k)^{p-1}\sum_{j} w_{jk}^2 \tag{3.7}$$

The steps taken in the developed MLP neural network can be described as follows:

1) Normalise inputs (X_i)

RGB input colours should be normalised by dividing their values with the maximum value 255. Thus, $X_1 = \frac{\mathrm{R}}{255}, X_2 = \frac{\mathrm{G}}{255}, X_3 = \frac{\mathrm{B}}{255};\ 0 \leq X_i \leq 1,\ i = 1, 2, 3.$

2) Initialise all weights (v_{ij} and w_{jk})

Set weights related to hidden and output layers to small random values (between -1 to 1). Thus $v_{ij}, w_{jk} \in [-1, 1]$, $i, k = 1, 2, 3;\ j = 1, 2, 3, \ldots, n_h$ where n_h is the number of hidden unit.

3) Calculate activation function (forward propagation)

In the multilayer perceptron neural networks, outputs of one layer become inputs of the next layer.

$$Z_j = f^{(1)}\left(\theta_j^{(1)} + \sum_{i=1}^{3} X_i v_{ij}\right) \tag{3.8}$$

$$Y_k = f^{(2)}\left(\theta_k^{(2)} + \sum_{j=1}^{p} Z_j w_{jk}\right) \tag{3.9}$$

where $\theta_j^{(1)}$ is the bias on hidden unit j and $\theta_k^{(2)}$is the bias on output unit k, Z_j is the output of hidden unit j, and Y_k is the output of output unit k. In this research, sigmoid activation function with regards to the hidden layer ($f^{(1)}$) and linear function for the output layer ($f^{(2)}$) were used to gain the output signal for each layer.

4) Calculate the networks error (backward propagation)

$$\delta_k^{(2)} = (T_k - Y_k) f'^{(2)}\left(\theta_k^{(2)} + \sum\nolimits_{j=1}^{p} Z_j w_{jk}\right) \tag{3.10}$$

$$\delta_j^{(1)} = \left(\sum_{k=1}^{3} \delta_k^{(2)} w_{jk}\right) f'^{(1)}\left(\theta_j^{(1)} + \sum_{i=1}^{3} X_i v_{ij}\right) \tag{3.11}$$

where $f'(\cdot)$ is the first derivative, T_k is the target of unit k, $\delta_k^{(2)}$ is error correction for output layer weights and $\delta_j^{(1)}$ is error correction for hidden layer weights.

5) Update all weights and biases

Compute weights and biases of n-th iteration using the following formulae:

$$w_{jk}(n) = w_{jk}(n-1) + \eta_1\left(\delta_k^{(2)} Z_j + \eta_2 w_{jk} \|\boldsymbol{v}_k\|^p\right) \tag{3.12}$$

$$v_{ij}(n) = v_{ij}(n-1) + \eta_1\left(\delta_j^{(1)} X_i + \eta_2 \frac{p}{2} (\boldsymbol{v}_k)^{p-1} \sum_j w_{jk}^2\right) \tag{3.13}$$

$$\theta_k^{(2)}(n) = \theta_k^{(2)}(n-1) + \eta_1\left(\delta_k^{(2)} + \eta_2 w_{jk} \|\boldsymbol{v}_k\|^p\right) \tag{3.14}$$

$$\theta_j^{(1)}(n) = \theta_j^{(1)}(n-1) + \eta_1\left(\delta_j^{(1)} + \eta_2 \frac{p}{2} (\boldsymbol{v}_k)^{p-1} \sum_j w_{jk}^2\right) \tag{3.15}$$

where η_1 is a fixed learning rate while $\eta_2 = 1/n$ is a adaptive learning rate that reduces exponentially.

The step size η_1 was set to be a small constant. When η_1 is large, the convergence of the neural network parameters will be quicker than that when η_1 is small. However, large η_1 leads to larger fluctuation around the steady state mean square error. On the other hand, small η_1 leads to smaller fluctuation around the steady state mean square error but the convergence rate of the neural network parameters is low. Thus, there is a trade-off between accuracy and speed of convergence. In this case, an experiment with various settings of η_1 was conducted and the best performance was found when $\eta_1 = 0.0025$. As for η_2, this was set according to the decay process i.e. $\eta_2 = 0.05/n$ where n is the iteration number. In this way, the

smoothness regularisation has more impact on the neural network parameters at the start of the learning process but slowly tapers off after some time to allow convergence to the desired solution.

6) Repeating the cycle

The above processes (no. 3–5) were repeated until one of the following conditions is reached:

a) The maximum number of iteration is reached.
b) The maximum amount of time has been exceeded.
c) Performance error is less than the goal set.
d) The performance gradient falls below the minimum performance gradient.

The next step was combining all the single networks into one neural network system. The proposed neural networks fusion, as observed in Figure 3.7, was developed to generate new RGB outputs. The final output RGB values from the networks fusion was obtained as follows:

$$\begin{aligned}\mathbf{Z} &= \boldsymbol{\alpha} \cdot \mathbf{O} \\ &= [\propto_1, \propto_2, \propto_3, \cdots, \propto_{24}] \cdot [\boldsymbol{O}_1, \boldsymbol{O}_2, \boldsymbol{O}_3, \cdots, \boldsymbol{O}_{24}]^T \end{aligned} \tag{3.16}$$

where $\boldsymbol{\alpha}$ is the weight matrix of each network output, $\mathbf{O}$ is the output matrix of each neural network and $\mathbf{Z}$ is the final output matrix of the neural networks fusion. From the Eq. (3.16), it can be distinguished that matrix $\boldsymbol{\alpha}$ consists of 24 diagonal $\propto$ matrices with dimension of 3 × 3. Similar to matrix $\boldsymbol{\alpha}$, matrix $\mathbf{O}$ also has 24 matrices with a dimension of 3 × N for each matrix $\boldsymbol{O}_i$, whilst N is the number of training samples.

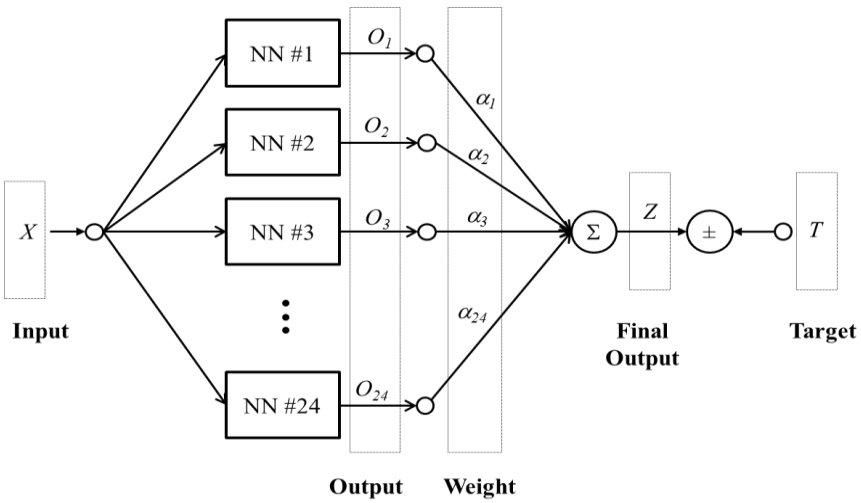

Figure 3.5. The proposed neural networks fusion using Macbeth colour checker.

In this research, a genetic algorithm was utilised to find the optimum value for each of the 24 α matrices. Genetic algorithm (GA) is an algorithm based on the Darwin principle of evolution, natural selection and biological systems. It has been extensively used for optimization in many fields, for instance, plug-in hybrid electric vehicles' (PHEVs) integration [71], plastic film manufacturing process [72], automatic path planning of unmanned aerial vehicles [73], and design of photovoltaic systems [74]. Basically, genetic algorithm encompasses a population with a certain number of individuals. Each individual in a population has the possibility of being the solution to the optimisation problem. Hence, by applying crossing over and mutation among individuals, a new generation is produced. This process is repeated several times until a new individual provides the most appropriate solution for the problem.

In this research, several methods have been conducted to determine the optimum matrix α. Based on the experiments, the developed neural networks fusion can be optimised by using a genetic algorithm with the following conditions:

1) Initial population size was 1,000 individuals
   The $\alpha = [\propto_1, \propto_2, \propto_3, \cdots, \propto_{24}]$ matrix has a dimension of 3 × 72 and every element of matrix $\propto_k$ is expressed by a 10-bit string of binary number (0s and 1s).
2) Probability of mutation was 0.05.
   The probability of mutation or mutation rate normally ranges from 0.001 to 0.01 [75], as found in researches conducted by [76], [77] which applied mutation rate values of 0.003 and 0.01, respectively. In addition, small mutation rate will be less disastrous than high one in most common problems [78]. Several experiments with various mutation rates have been conducted for the developed genetic algorithm in this step. According to the experiments, however, the mutation rate of 0.05 gave the best results.
3) The boundary of each element with regards to each matrix $\propto_k$, i.e. $a_{k,ij}$ with $i, j = 1, 2, 3$, was set as follows:

   if $i = j$ then $0 < a_{k,ij} \leq 1$

   else $a_{k,ij} = 0$

Thus, each matrix α_k was constructed as follows:

$$\propto_k = \begin{bmatrix} a_{k,11} & 0 & 0 \\ 0 & a_{k,22} & 0 \\ 0 & 0 & a_{k,33} \end{bmatrix}$$

with $k = 1, 2, 3, \ldots, 24$.

4) The fitness function was based on the mean square error between the target and the final output RGB values.

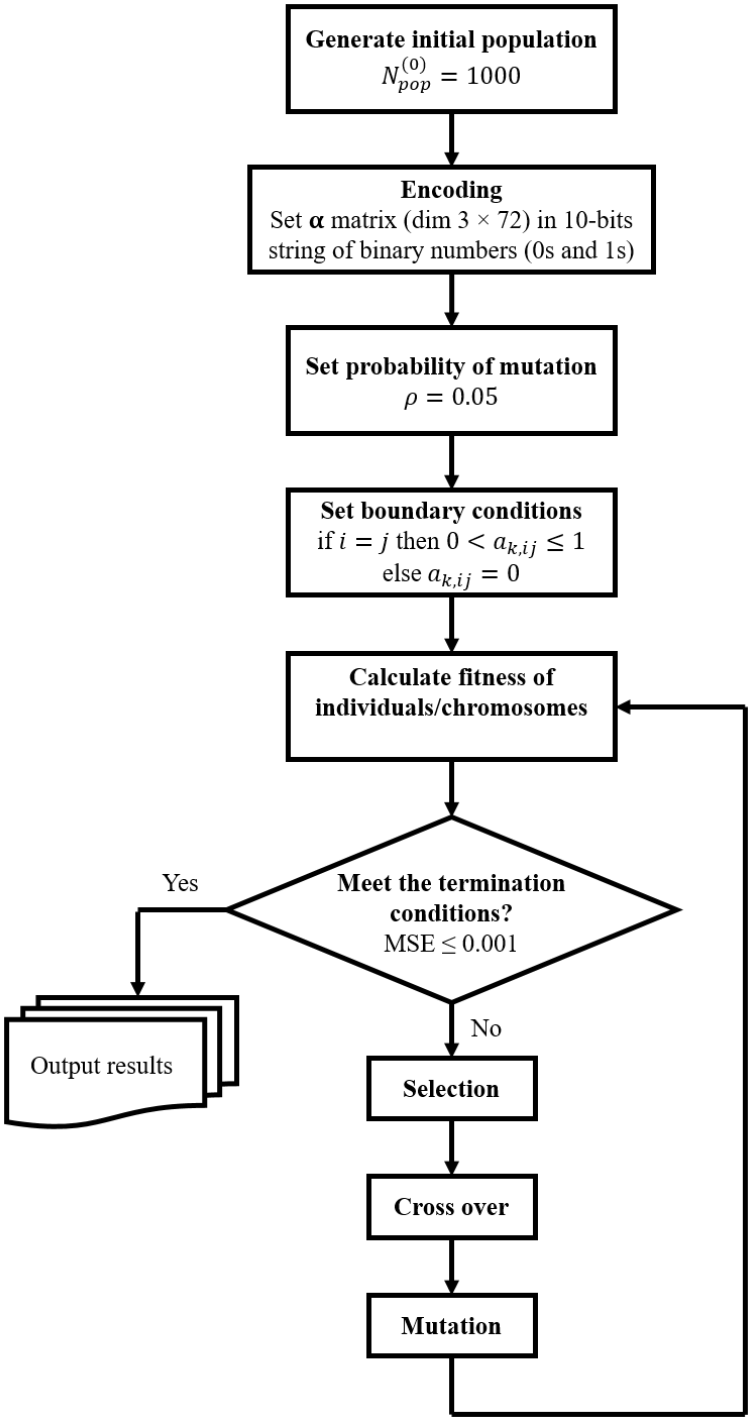

Figure 3.6. The flowchart of the developed genetic algorithm for colour normalisation.

The steps of the developed genetic algorithm for training the matrix α (Figure 3.6) can be described as follows:

1. Generate the initial population, i.e. 1,000 individuals, with 2,160 (= 10 × 3 × 72) bits length for each individual.

2. Produce the next generation by processing cross-over and mutation on each individual.

3. Compute the fitness for each individual.

4. Select the best individual with MSE lower than 0.001. The lesser the MSE, the better the prediction. However, it will be very time consuming. According to the experiments, MSE ≤ 0.001 provided best prediction with optimum training time.

Once the optimum matrix α was achieved, the next step was applying the developed neural networks fusion and matrix α to adjust the RGB colour of the wheat plants. In this research, a wheat plant image has a dimension of 448 × 336 pixels. Through the developed colour adjusting system, each pixel of a plant image acquired under various light intensities was transformed to the equivalent pixel of the image under the standard light intensity (50 Klux).

3.4. Neural Network Based Image Segmentation and Statistical Colour Features Extraction

Image segmentation plays an important role in classifying each pixel in an image either as a targeted object or a background part. Most of nutrient estimation researches are conducted in a controlled image capturing circumstance. Commonly an object, which is plant leaf, is laid down on a white paper background in a closed box with certain illumination from an artificial lighting system. In such method, the object in the captured image can easily be distinguished from its background by applying a simple threshold value. However, in this research the problem was more complicated. The images of the wheat leaves are captured directly on a field and contain leaves as the targeted object, in addition to other unwanted parts, such as soil, stones, weeds, and dried and semi-dried leaves in the background.

A multilayer, feed forward, back-propagation error neural network was used for image segmentation to distinguish the wheat leaves, as the region of interest, from other unnecessary parts. The developed neural network for this step can be explained as follows:

1. The network had three units of input layer, which indicated red, green and blue colour values (RGB) for each pixel related to the plant images with a range of 0 – 255.

2. The number of hidden units was 30.

3. The output layer had only one unit, which signified whether each pixel was a part of a leaf or not. The output value of the network was equal to 1 if the corresponding pixel was a part of a leaf, otherwise the value is 0.

4. The sigmoid activation function was used for both hidden and output layers.

A dataset was developed to perform neural network based image segmentation. The dataset was comprised of 4,800 samples of RGB colour and binary values (0 or 1) as the input and target values, respectively. Furthermore, the developed dataset was achieved from 24 plant images. On each image, 100 pixels in the leaf region and 100 pixels in other parts of the region were selected manually. The RGB colour values of the selected pixels were then used as inputs of the network.

In colour segmented images, noises should be removed prior to features extraction step. In the majority of images, weeds were also present which need to be eliminated from the segmented image, as they can influence the colour information of the wheat leaves. To resolve this problem, an algorithm to remove image noises by selecting the largest part of the leaves, which has the highest number of object pixels, was applied. This algorithm can be seen in Figure 3.8. An example of the results of image normalisation using neural networks fusion and image segmentation can be seen in Figure 3.9. As presented, the proposed colour normalisation and the neural networks based image segmentation can be used in an automated manner to normalise the images of the plants and to remove the unwanted parts from the image, as indicated by the black circles.

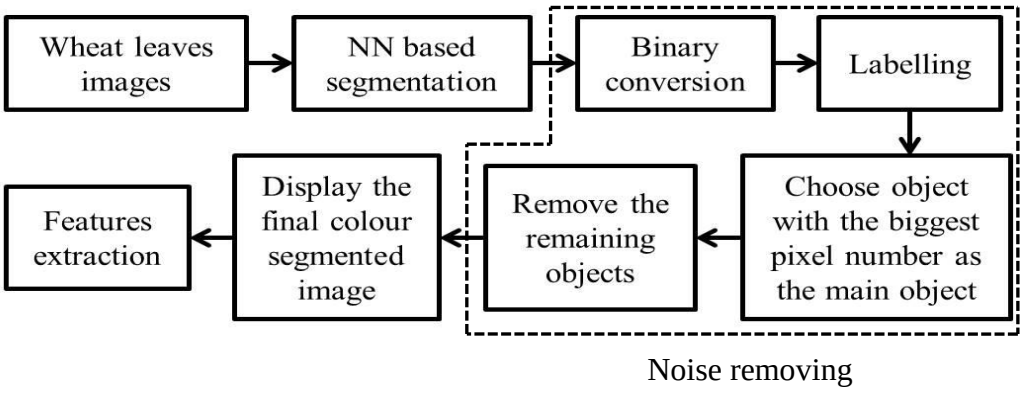

Figure 3.7. Image segmentation algorithm to remove image noises.

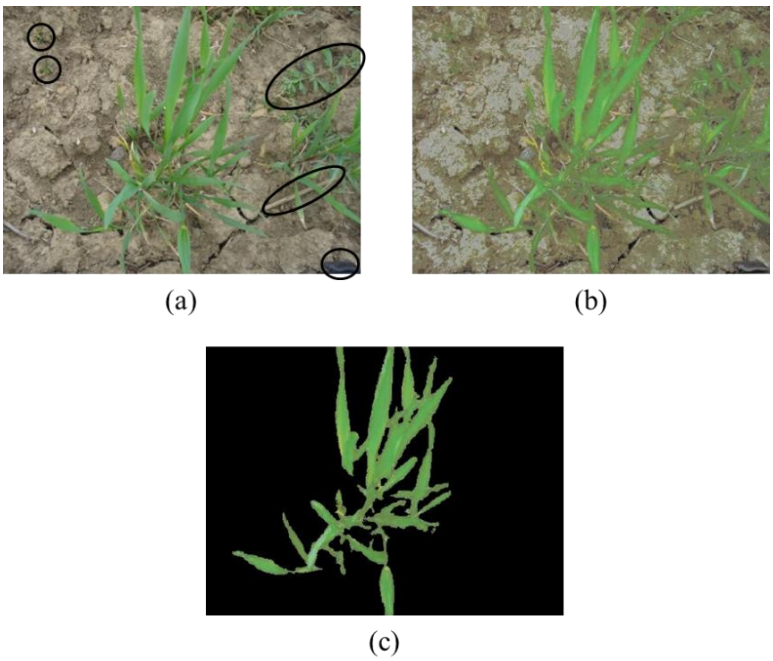

Figure 3.8. An example of the results of neural network based colour normalisation and image segmentation; (a) original image, (b) normalised image, (c) segmented image.

In the features extraction step, a number of statistical colour features pertaining to the final colour segmented images were calculated. These features were utilised for nutrient estimation in the next step. Four types of statistical features were used in this research, namely, first raw moment (mean), second central moment (variance), third central moment (skewness) and fourth central moment (kurtosis). Thus, there are 12 statistical features for three colour channels (red, green and blue) which represent the colour distributions related to the segmented images. The mean value is considered to be the central tendency of the colour distribution, while the variance measures the spread of colour distribution from the mean. Skewness determines the symmetricity of colour distribution whereas kurtosis measures the ridge colour distribution. In addition, colour moments have been extensively and successfully used in colour-based image retrieval systems, especially for a segmented image which contains only the image of object [79]. The statistical colour features can be achieved by using the following formulae:

$$mean = \bar{y}^{(c)} = \frac{1}{N_s}\sum_{i=1}^{N_s} y_i^{(c)} \tag{3.17}$$

$$variance = \sigma^{2(c)} = \frac{1}{N_s}\sum_{i=1}^{N_s}\left(y_i^{(c)} - \bar{y}^{(c)}\right)^2 \tag{3.18}$$

$$skewness = skew^{(c)} = \frac{\frac{1}{N_s}\sum_{i=1}^{N_s}\left(y_i^{(c)} - \bar{y}^{(c)}\right)^3}{\sigma^{3(c)}} \tag{3.19}$$

$$kurtosis = kurt^{(c)} = \frac{\frac{1}{N_s}\sum_{i=1}^{N_s}\left(y_i^{(c)} - \bar{y}^{(c)}\right)^4}{\sigma^{4(c)}} \tag{3.20}$$

where y_i refers to colour value of i-th pixel, c is each colour channel (red, green and blue), N_s is the number of samples (object pixels) and σ is the standard deviation.

3.5. Nitrogen Content Estimation Using Weighted Neural Networks

An MLP with back propagation error was used to determine the nitrogen amount in wheat leaves. The developed neural network consisted of 12 nodes of input layer which corresponds to the statistical colour features and one node of output layer that corresponds to the percentage related to the nitrogen amount. In this step, the number of hidden layer nodes was also determined by using Eq. (3.1).

A committee machine was employed to combine several neural networks with different hidden layer nodes, as seen in Figure 3.10. The numbers of hidden layer nodes with regards to these new neural networks were produced using the following formula:

$$n_h' = s \times n_{h0} \tag{3.21}$$

where n_h' is the new number of hidden layer nodes, n_{h0} is the initial number of hidden layer nodes (i.e. 12 nodes) and s is the multiplication factor ($s = 2, 3, \ldots, Q$), whilst Q is the number of combined neural networks.

In this case, the parameter s is also the number of neural networks used for the combination. Thus, the networks combinations attempted in this step were as illustrated in Table 3.1. Each network was repeated 100 times to eliminate the effect of the random bias numbers and initial

weights. Subsequently, a number of neural networks which provided the minimum mean square error were chosen to achieve the final estimation.

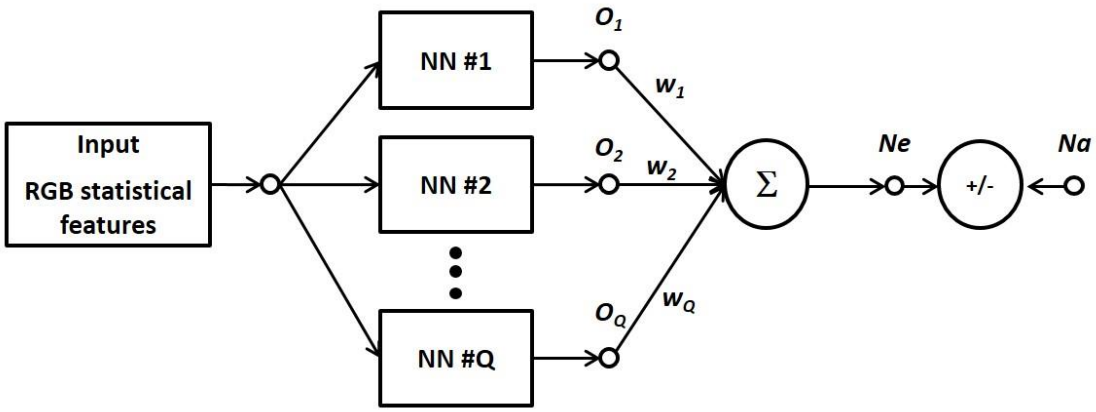

Figure 3.9. Combination of neural networks for nitrogen estimation.

Table 3.1. Neural networks combination

Number of NNs (Q)	Number of hidden layer nodes
2	12 – 24
3	12 – 24 – 36
4	12 – 24 – 36 – 48
5	12 – 24 – 36 – 48 – 60
6	12 – 24 – 36 – 48 – 60 – 72
7	12 – 24 – 36 – 48 – 60 – 72 – 84

A committee machine can produce significant improvements in the prediction given that it can minimise the effect of a random component due to data noise in the generalization performance of a single network [80], [81]. Basically, the concept of a committee machine is to combine outputs of several expert systems with the same input data, with the aim of producing a new output. Suppose that there are Q expert systems to approximate a target vector T. Each expert has output vector O_q and error e_q,

$$O_q = T + e_q$$

Thus, the sum of the squared error for the q-th expert y_q is

$$E_q = \xi\left[\left(O_q - T\right)^2\right] = \xi\left[e_q^2\right]$$

where $\xi[\cdot]$ denotes the statistical expectation.

The average error of each expert system (E_{ave}) is then

$$E_{ave} = \frac{1}{Q}\sum_{q=1}^{Q} E_q = \frac{1}{Q}\sum_{q=1}^{Q} \xi\left[e_q^2\right]$$

In other words, by using a committee machine, the output value Y can be achieved by simply averaging the output vector O_q, as follows:

$$Y = \frac{1}{Q}\sum_{q=1}^{Q} O_q$$

Thus, the squared error of the committee machine (E_{COM}) is

$$E_{COM} = \xi[(Y - T)^2]$$

$$= \xi\left[\left(\frac{1}{Q}\sum_{q=1}^{Q} O_q - T\right)^2\right] = \xi\left[\left(\frac{1}{Q}\sum_{q=1}^{Q} e_q\right)^2\right]$$

But

$$\xi\left[\left(\frac{1}{Q}\sum_{q=1}^{Q} e_q\right)^2\right] \leq \frac{1}{Q}\sum_{q=1}^{Q} \xi\left[e_q^2\right]$$

Thus, we have

$$E_{COM} \leq E_{ave}$$

The calculated error of the committee machine is always smaller than if not equal to that of the single expert. In this research, ensemble averaging was applied as the neural networks combiner to obtain improved generalization and performance. The estimated nitrogen amount of wheat leaves was calculated by using a committee machine with the simple averaging method as the combiner of Q neural networks, as follows:

$$Ne_{ave} = \frac{1}{Q}\sum_{q=1}^{Q} O_q \tag{3.22}$$

The simple averaging method as expressed in Eq. (3.22) indicates that each single neural network has the same weight to produce the new output. In this research, the possibility that each neural network has a different weight was also investigated. In this case, a weighted averaging method was applied, as expressed in the following:

$$Ne_{weigh} = \sum_{q=1}^{Q}\left(w_q \times O_q\right) \tag{3.23}$$

and

$$\sum_{q=1}^{Q} w_q = 1$$

where Ne_{weigh} is the estimated nitrogen content, w_q and O_q are the weight and the output of q-th single network, respectively.

A genetic algorithm was used to discover the optimum value of the weights in the developed committee machine. The genetic algorithm for the nitrogen estimation was developed with the following conditions:

1) Initial population size was 1,000

2) Each individual was expressed by Q × 8 bits length of binary numbers

3) Probability of mutation was 0.05

4) Each weight had a range of 0–1; $0 \leq w_i \leq 1$

5) The fitness function was to estimate the mean square error (MSE) between the actual and the estimated nitrogen content.

The level of the prediction accuracy was measured by calculating the error value of the observed/actual and predicted nitrogen content. In this research, the mean absolute percentage error (MAPE) was used for the system's performance assessment. For a comparison, several types of error were also measured, i.e. mean absolute error (MAE), mean of squared error (MSE), root mean of squared error (RMSE) and sum of squared error (SSE). The error types used in this research can be expressed as follows:

$$MAPE = \frac{100\%}{N_s}\sum_{i=1}^{N_s}\left|\frac{Na_i - Ne_i}{Na_i}\right| \tag{3.24}$$

$$MAE = \frac{1}{N_s}\sum_{i=1}^{N_s}|Na_i - Ne_i| \tag{3.25}$$

$$MSE = \frac{1}{N_s}\sum_{i=1}^{N_s}(Na_i - Ne_i)^2 \tag{3.26}$$

$$RMSE = \sqrt{\frac{1}{N_s}\sum_{i=1}^{N_s}(Na_i - Ne_i)^2} \tag{3.27}$$

$$SSE = \sum_{i=1}^{N_s}(Na_i - Ne_i)^2 \tag{3.28}$$

where n is the number of samples, Na and Ne are the actual and the estimated (using either simple (3.22) or weighted average (3.23)) nitrogen content, respectively.

3.6. Results and Discussions

3.6.1. SPAD meter based nitrogen amount prediction

The SPAD meter was widely used to determine the chlorophyll content in the leaves by measuring the absorbance of the leaf in two wavelength regions, i.e. red and infrared. After the signal processing steps, the absorbance was displayed in a units range from 0 to 199. Moreover, the chlorophyll amount was highly correlated with the nitrogen content. Furthermore, the chlorophyll content which is represented by the SPAD value, increased in proportion to the nitrogen amount.

To figure out how strong the correlation between the independent variable and the dependent variable, a statistical value, namely coefficient of determination (R^2), is applied. The coefficient of determination is a statistical feature to represent how well the data points fit the regression line. This value, which is in the range of 0 to 1, is usually used to determine how certain the independent variable (x) predicts the dependent variable (y). The coefficient of determination is obtained by squaring the coefficient of correlation (R), which is expressed as follows:

$$R = \frac{N_s \sum xy - (\sum x)(\sum y)}{\sqrt{N_s(\sum x^2) - (\sum x)^2}\sqrt{n(\sum y^2) - (\sum y)^2}} \tag{3.29}$$

where N_s is the number of samples.

Based on our experiments conducted with 36 samples of wheat leaves, the coefficient of determination (R^2) value of SPAD readings and nitrogen content is 0.7801, as seen in Figure 3.11. It means that the relationship between the SPAD and nitrogen amount was reasonably strong. By using the trend line equation, the predicted nitrogen level was calculated. The *MAPE* of this prediction was 8.48%. Figure 3.12 demonstrates the fitting plot between the actual and predicted nitrogen content. Similar research with relatively strong relationships between the SPAD and nitrogen have been reported in sugarcane (R^2 = 0.706) [8] and oilseed rape (R^2 = 0.744) [43]. The correlation between the SPAD meter readings and nitrogen percentage in leaves was strongly affected by leaf thickness. The variation in leaf thickness can influence the accuracy of SPAD meter readings, as this device works based on the leaf's capacity to absorb red and infrared lights.

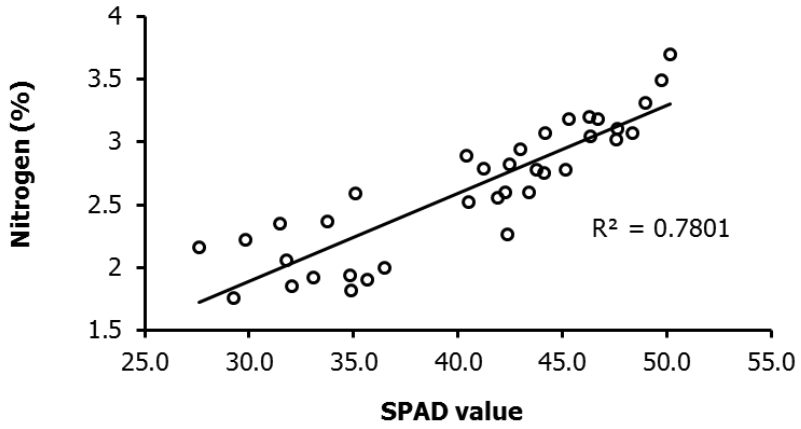

Figure 3.10. Relationship between the SPAD value and actual nitrogen content.

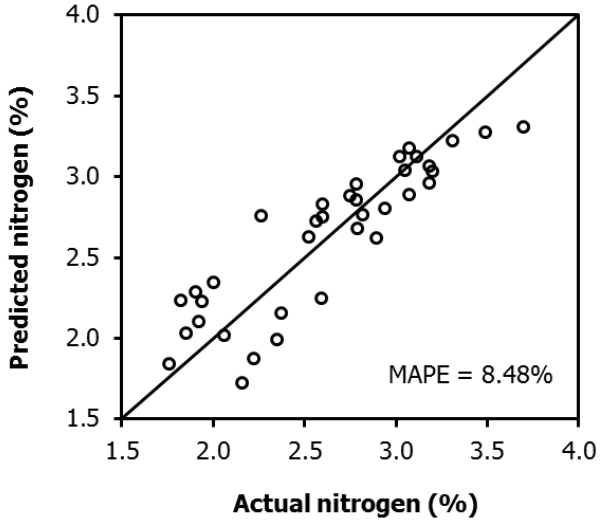

Figure 3.11. Fitting plot of the actual and predicted nitrogen content of SPAD meter based prediction.

3.6.2. Image-based nitrogen amount prediction

The proposed neural networks fusion based colour normalisation can be used to normalise plant images captured under various light intensities. After image normalisation, it can be assumed that all images are captured under the same light intensity and compared with each other.

In the colour normalisation step, the results of the proposed method were then compared with other colour normalisation methods, i.e. grey world and scale-by-max algorithms, linear

model, and one single neural network (NN) [82]. The grey world (GW) and scale-by-max (SBM) approaches are the simplest colour normalisation algorithms due to their ease and simplicity of application. In the grey world algorithm, the average of all colours in an image is considered to be neutral grey. This algorithm yields illuminant estimation by calculating the mean value of each colour channel. Hence, to normalise an image, the colour value of each pixel is scaled by:

$$K_{GW}^{i} = \frac{C}{C_{avg}^{i}} \tag{3.30}$$

with

$$C = mean\left(C_{avg}^{1}, C_{avg}^{2}, C_{avg}^{3}\right)$$

where i refers to each colour channel (red, green and blue).

In the scale-by-max approach, the illuminant estimation is acquired by determining the maximum response of each colour channel. Hence, the colour value of each pixel can be normalised by multiplying it with the following constant:

$$K_{SBM}^{i} = \frac{255}{\max(i)} \tag{3.31}$$

In the linear model, the colour values of each pixel are corrected through a transformation matrix [83]. Suppose that under an unknown lighting condition, with the transformation matrix M_{un}, the colour values of an object q_{un} is as follows:

$$q_{un} = M_{un} r \tag{3.32}$$

where r is three basic functions related to surface reflectance.

The colour values of the standard illumination q_{st}, which is in this research the light intensity of 50 Klux, can be calculated as

$$q_{st} = M_{st} r = M_{st} M_{un}^{-1} q_{un} = M_{tr} q_{un} \tag{3.34}$$

Thus

$$M_{tr} = q_{un}^{-1} q_{st} \tag{3.35}$$

where M_{tr} is the 3 × 3 transformation matrix.

Basically, the NN and the proposed methods discussed in the present chapter can be seen as a nonlinear extension of (3.34). The nonlinear model employed in this proposed method was determined by calculating the transformation matrix in (3.35) using the back-propagation neural network algorithm, consequently the M_{tr} was used to correct plant images.

In this research, the results of our proposed method are better than the other methods that have previously been mentioned, as seen in Table 3.2. Colour differences by calculating the mean Euclidean distance of the target and the output (estimated) colour value of each method were measured as the basis of comparison. The formula of the Euclidean distance can be written as follows:

$$\Delta E_{RGB} = \sqrt{(R_t - R_e)^2 + (G_t - G_e)^2 + (B_t - B_e)^2} \tag{3.36}$$

Table 3.2. Comparison of colour normalisation results

Methods	ΔE_{RGB}
Grey world	23.40
Scale-by-max	14.86
Linear model	11.06
Single neural network (NN)	5.03
The proposed method (NN fusion)	4.15

In the proposed method, by using a 24-patch Macbeth colour checker as the reference, twenty four α values as output weights for each neural network were obtained. These α matrices were then applied to correct wheat plant images by using the developed neural networks fusion method. An example of the α matrices used to produce a new output is as follows:

$$Z = \begin{bmatrix} 0.087 & 0 & 0 \\ 0 & 0.076 & 0 \\ 0 & 0 & 0.005 \end{bmatrix} \cdot O_1 + \begin{bmatrix} 0.087 & 0 & 0 \\ 0 & 0.027 & 0 \\ 0 & 0 & 0.090 \end{bmatrix} \cdot O_2 +$$

$$\begin{bmatrix} 0.033 & 0 & 0 \\ 0 & 0.071 & 0 \\ 0 & 0 & 0.099 \end{bmatrix} \cdot O_3 + \cdots + \begin{bmatrix} 0.026 & 0 & 0 \\ 0 & 0.001 & 0 \\ 0 & 0 & 0.019 \end{bmatrix} \cdot O_{24}.$$

In this research, each wheat plant image has a dimension of 448 × 336 pixels. By applying this developed colour adjusting system, each pixel of a plant image captured under various light intensities will be transformed to the equivalent pixel of the image under the standard light intensity, i.e. 50 Klux. In order to demonstrate the effectiveness of the proposed method, 30 wheat plant images which were subject to the same treatment of fertiliser dosage have been selected. Since the images were subject to the same treatment, they should have similar colour or, in other words, the colour variability should be small. As the focus of the research is on the colour of the leaves, the original and the corrected images were then segmented to obtain the leaves images as the region of interest. In the segmented images, our proposed colour normalisation can be used to reduce the variability of leaves colour which can be expressed in the standard deviation values. The standard deviations of the original leaves images are 24.76, 16.45 and 30.39 for red, green and blue colour respectively, whilst the standard deviation RGB colour values of the corrected images are 6.38, 4.07 and 7.58, respectively. This shows that the proposed method has successfully reduced the colour variability in the images by approximately four times.

After image correction using the developed neural networks fusion, the next step was image segmentation. The neural network based image segmentation method, as described in the previous section, can be applied to distinguish wheat leaves from other parts, such as weeds, soil, stones and dried leaves. This segmentation method is superior to the conventional Otsu algorithm (threshold-based segmentation). The database pertaining to the colour of leaves and non-leaves provides sufficient data to train the plant images. Therefore, the neural network can precisely classify whether a pixel belongs to the leaves or non-leaves region. A comparison of image segmentation results using Otsu algorithm and the developed neural network can be seen in Figure 3.13.

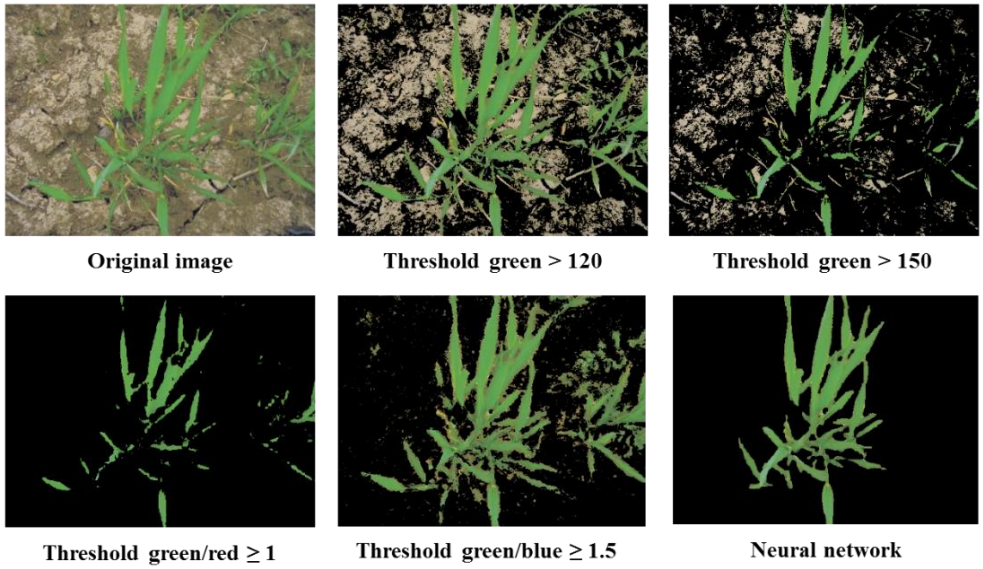

Figure 3.12. Comparison of some threshold based and the developed neural network based image segmentations.

Once all images have been segmented, twelve statistical colour features as described in previous section were subsequently extracted. These features were then utilised as predictors in the developed nitrogen estimation algorithm. In this step, several neural networks with different numbers of hidden layer nodes were combined, as tabulated previously in Table 3.1. These combinations of networks were subsequently trained to determine which offers the most appropriate results. After conducting Monte-Carlo testing of more than 100 independent trials, the combination of six neural networks resulted in the minimum generalization error of networks performance compared to other possible combinations. The first combination used in this step was simple averaging method. The estimated nitrogen amount was then calculated as follows:

$$Ne_{ave} = \frac{1}{6}\sum_{q=1}^{6} O_q \tag{3.37}$$

The best result relates to the first type of committee machine, i.e. simple average, was subsequently compared to that of the second type combiner, i.e. weighted average, which was optimized by the genetic algorithm (GA). By using this method, the weights of the output of the networks were 0.008, 0.091, 0.140, 0.219, 0.047 and 0.495 respectively for the first until the sixth neural network. The estimated nitrogen content can therefore be expressed as follows:

$$Ne_{GA} = (0.008 \times O_1) + (0.091 \times O_2) + (0.140 \times O_3) + (0.219 \times O_4)$$
$$+(0.047 \times O_5) + (0.495 \times O_6) \quad (3.38)$$

Table 3.3 illustrates the comparison of various types of error values of the discussed NN and SPAD meter methods. From that table, we can perceive that by using simple average combiner, the combination of six neural networks provides the best results compared to other network combinations. In addition, the MAPE of this combination is less than 3%. However, the weighted average combiner with GA optimization offers enhanced results. As seen in the table, the MAPE of the GA-based committee machine with six neural networks is smaller than the simple average method, i.e. 2.73%. In other words, the deviation of the estimated nitrogen using this method is approximately 2.73% of the true nitrogen percentage. For instance, if the actual nitrogen content is 3%, then the estimated nitrogen is between 2.92% and 3.08%. Thus, the error noted is relatively small.

Table 3.3. Comparison of nitrogen amount estimation errors

Methods	MAPE	MAE	MSE	RMSE	SSE
SPAD meter	8.48%	0.2042	0.0578	0.2404	1.5704
Simple averaged 2 NNs	3.68%	0.0907	0.0150	0.1224	0.5395
Simple averaged 3 NNs	3.12%	0.0780	0.0106	0.1030	0.3821
Simple averaged 4 NNs	3.04%	0.0761	0.0100	0.0999	0.3591
Simple averaged 5 NNs	3.12%	0.0774	0.0102	0.1010	0.3675
Simple averaged 6 NNs	2.93%	0.0731	0.0093	0.0967	0.3363
Simple averaged 7 NNs	3.00%	0.0757	0.0096	0.0979	0.3451
GA averaged 6 NNs	2.73%	0.0674	0.0078	0.0885	0.2819

In this research, the relationship between nitrogen content and each colour channel in addition to a number of combinations of them was also investigated. A research has established that there are significant correlations between chlorophyll content in the maize leaf and the averages of the R and G components, as well as 2G-R-B of the linear transformation [53]. The nitrogen content was also estimated using the greenness index developed by [84] (GI_{kaw}). GI_{kaw} is defined as follows:

$$GI_{kaw} = \frac{R - B}{R + B} \tag{3.39}$$

Based on the GI_{kaw} formula, [52] modified the greenness index to estimate nitrogen content in barley leaves and use the principal component analysis (PCA) to produce a new greenness index (GI_{PCA}), as follows:

$$GI_{PCA} = 0.7582|R - B| - 0.1168|R - G| + 0.6414|G - B| \tag{3.40}$$

According to the investigation, single colour features and their combinations, including I_{PCA} and I_{kaw}, are not suitable for nitrogen estimation. The estimation errors of those analyses are too high, compared to our proposed method, as seen in Table 3.4. The RGB values in those analyses are only obtained from the mean value of the observed leaves colour. This value is not sufficient to represent the colour distribution of leaves colour. In the proposed method, it was not only mean value that was utilised, but also variance, skewness and kurtosis of the observed leaves colour. The use of these statistical features is more effective to describe the colour distribution of leaves colour. As seen in the table, the proposed method is superior to all the discussed methods, as it provides an estimation error of 2.73%.

Table 3.4. Comparison of estimation errors using colour features and the proposed method

Features	MAPE (%)
R	10.49
G	13.72
B	15.87
G/R	11.21
G/B	12.15
$G - R$	12.10
$2G - R - B$	16.56
GI_{kaw}	9.84
GI_{PCA}	9.20
Proposed method	2.73

3.7. Summary

A low cost, simple and accurate nitrogen estimation of wheat leaves was conducted using the proposed method. The proposed method focused on colour constancy to normalise plant images that were subject to variation in lighting conditions, besides the application of back-propagation neural network for image segmentation and committee machines for nitrogen content estimation. The developed neural network based image segmentation could remove unnecessary components of plant images and retain the leaves as the region of interest. The genetic algorithm based committee machine to combine six neural networks with 12 statistical RGB colour features as predictors could be used to estimate nitrogen content in wheat leaves more accurately than by using simple averaged neural networks, as well as the SPAD meter and greenness index based methods from previous related works.

Chapter 4

Deep Learning Machine Fusion Based Computational Intelligence for Nitrogen Content Estimation

4.1. Introduction

In this chapter, a different approach has been developed to estimate nitrogen content in wheat leaves. An advanced neural network model, namely deep sparse extreme learning machine (DSELM), is utilised in this research for colour normalisation as well as image segmentation and nutrient prediction. Unlike other learning algorithms such as backpropagation based multi-layer perceptron, DSELM is able to exploit more important information with much faster learning speed.

Similar to the previous works explained in Chapter 3, DSELM fusion and genetic algorithm are developed to normalise wheat plant images and reduce colour variability due to different light intensities. In addition, a Macbeth colour checker is utilised as the colour reference. In the image segmentation step, DSELM is employed to differentiate wheat leaves from other unwanted surrounding parts. Four types of statistical moment features of each RGB colour channel is then extracted from segmented images. These statistical features are subsequently used as neural network's inputs to estimate nitrogen content. In this step, several combinations of DSELM with different hidden layer number are applied. Furthermore, a genetic algorithm is also utilised to optimise the combination weight of each DSELM.

4.2. Deep Sparse Extreme Learning Machine

Neural networks have been extensively used for automation in many applications, such as iron and steel industry [85], financial service [86], plastic production [87], and coal gasification [88]. Neural networks are also used in digital signal processing [89] and non-linear systems control [90], [91]. However, the training procedure of neural networks with backpropagation algorithm is easy to fall into local minima and the training speed is generally slow, especially for multi-layer perceptron. To address this problem, a deep sparse extreme learning machine algorithm was proposed to train the multi-layer perceptron. Compared with

other machine learning algorithms, DSELM is much faster in training stage and has better generalisation performance.

To achieve a high generalisation performance for colour normalisation, especially for large scales, appropriate representations are crucial. Single-Layer Feedforward Neural Network (SLFN) learning with the backpropagation algorithm is an efficient method to learn compact features. However, the information learned from SLFN is not good enough to represent the input data, especially for large dataset. Thus, multiple layer architecture of neural network is needed as the features extracted by multiple layer networks represent more abstract and accurate information than those from shallow ones. One of the most popular approaches is Deep Belief Networks (DBNs) which can be done using stacked Restricted Boltzmann Machines (RBM). It has been shown to yield good performance in various areas, however, the training speed is generally very slow for the reason that all the parameters of the entire network need to be fine-tuned multiple times to achieve the criterions. Thus, the training of DBNs is too cumbersome and time consuming. To address this problem, the Deep Sparse Extreme Learning Machine (DSELM) was proposed. Compared with DBNs, DSELM has four notably attractive features, as follows:

- The hidden nodes can be randomly generated according to any continuous probability distribution without any prior knowledge, e.g. the uniform distribution [92].
- The only parameter that needs to be determined is the output weight which can be established by searching the path back from a random space.
- Once the feature of the previous hidden layer is learned, the parameters of current hidden layer will be fixed and need not be fine-tuned [93], this is the major difference between DSELM and DBNs.
- More abstract and sparse hidden information is extracted using ℓ_1-regularisation.

The DSELM, as depicted in Figure 4.1, consists of two phases, i.e. 1) unsupervised feature mapping and 2) supervised feature regression. In the former phase, an ELM-based sparse autoencoder is used to extract sparse features of the input layer by layer with higher layers represent more abstract and accurate features than that of the previous layer. In the latter phase, an original ELM is stacked at the top of the learned deep structure to make the final decision. In the following, the overall architecture of DSELM will be introduced in details and the description of the training procedure of Sparse ELM (SELM) is also presented as the SELM is the building block which is used to construct the deep structure of DSELM.

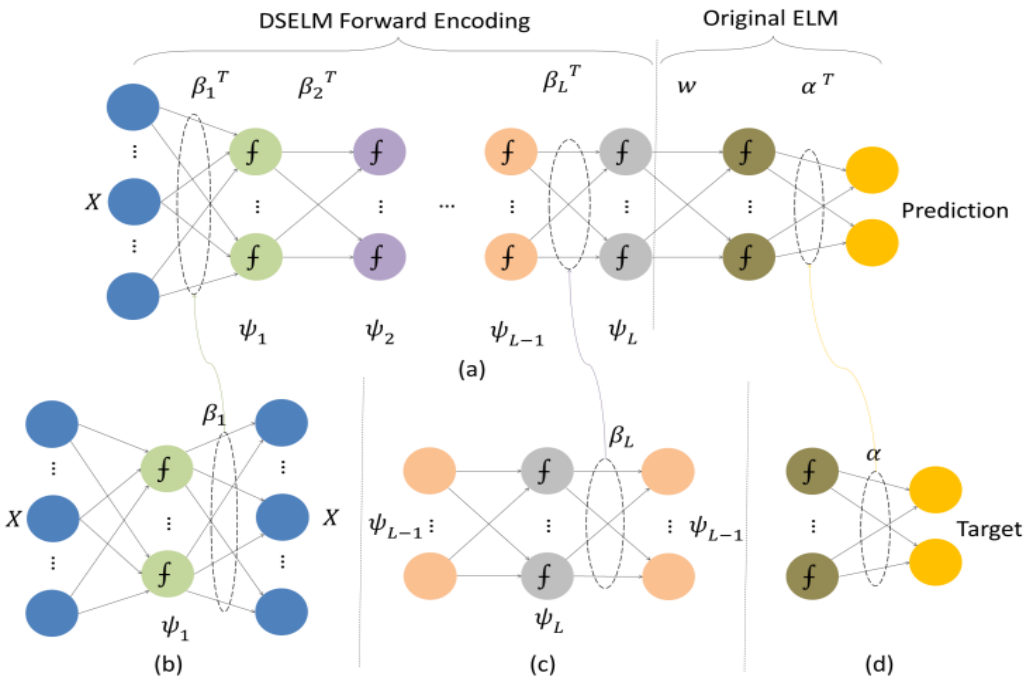

Figure 4.1. Layer wise training of Deep Sparse ELM: (a) Two phases of DSELM, i.e. deep forward learning followed by the original ELM classification. (b) Implementation of first hidden layer sparse ELM auto-encoder. (c) Training procedure of L^{th} hidden layer sparse ELM auto-encoder. (d) Analytically calculate the output weights of original ELM with labelled target using randomly initialised parameters.

In the initial ELM, given a set of N training data $(\mathrm{X}, \mathrm{T}) = \{\mathrm{x_j}, \mathrm{t_j}\}_{\mathrm{j=1}}^{\mathrm{N}}$, where $\mathrm{x_j} = [\mathrm{x_{j1}}, \mathrm{x_{j2}}, \dots, \mathrm{x_{jP}}] \in \mathbb{R}^{\mathrm{P}}$ and $\mathrm{t_j} = [\mathrm{t_{j1}}, \mathrm{t_{j2}}, \dots, \mathrm{t_{jQ}}] \in \mathbb{R}^{\mathrm{Q}}$ are the training data and the corresponding target respectively. The parameters P and Q are the dimension of input and target vector respectively. The output function f(X) of ELM with K hidden nodes fully connect the input data to the outputs is represented by

$$f(x_j) = \sum_{k=1}^{K} \psi_k(x_j w_k) \cdot \beta_k, \qquad j = 1,2, \dots N \tag{4.1}$$

where $\psi(\cdot)$ is the activation function which we used is the sigmoid function

$$\psi(x_j w_k) = \frac{1}{1 + e^{-x_j w_k}} \tag{4.2}$$

where $w_k \in \mathbb{R}^P$ is the randomly generated parameters connecting input layer and k^{th} hidden node, $\beta_k \in \mathbb{R}^Q$ is the output weight vector connecting the k^{th} hidden layer and the output layer.

The N equations in (4.1) can be written compactly as:

$$F(X) = \Psi\beta \tag{4.3}$$

where $\beta = \{\beta_k\} \in \mathbb{R}^{K\times Q}$ is the output weight matrix, Ψ is the $N \times K$ hidden feature mapping matrix with respect to input X. The elements of Ψ can be described as follows:

$$\Psi = [\psi_1(Xw_1), \psi_2(Xw_2), \dots, \psi_K(Xw_K)]$$

$$= \begin{bmatrix} [\psi_1(x_1w_1) & \cdots & \psi_K(x_1w_K) \\ \vdots & \ddots & \vdots \\ \psi_1(x_Nw_1) & \cdots & \psi_K(x_Nw_K) \end{bmatrix}_{N\times K} \tag{4.4}$$

An ELM learns the parameters in two sequential stages: 1) random feature mapping and 2) linear parameter solving. In the first stage, with randomly initialised parameters, the input data are projected into an ELM feature space using the activation function ψ (·). Huang et al. [94] have proved that ELM is able to approximate any continuous function with randomly initialised parameters. Therefore, the only parameter that needs to be calculated is output weight β. In the second stage, an ELM aims to reach the smallest training error and the smallest norm of output weights using the following equation to optimize the output weight β:

$$\underset{\beta\in\mathbb{R}^{K\times Q}}{\operatorname{argmin}} \quad \frac{1}{2}\|\beta\|_{\ell_2}^2 + \frac{C}{2}\sum_{j=1}^{N}\|e_j\|^2$$

$$\text{s.t.} \quad \Psi(x_j)\beta = t_j - e_j, \;\; j = 1,2,\dots,N \tag{4.5}$$

where the first term is ℓ_2 optimization to avoid over-fitting and obtain compact hidden information, C is a tradeoff coefficient which is chosen experimentally, $e_j = (t_j - f(x_j)) \in \mathbb{R}^Q$ is the error vector with respect to j^{th} input data. Eq.(4.5) can be rewritten as an unconstrained optimization problem:

$$\underset{\beta\in\mathbb{R}^{K\times Q}}{\operatorname{argmin}} \quad \frac{1}{2}\|\beta\|_{\ell_2}^2 + \frac{C}{2}\|\Psi\beta - T\|^2 \tag{4.6}$$

where $T = [t_1, t_2, \dots, t_N] \in \mathbb{R}^{N\times Q}$ is the target.

As ELM autoencoder is designed to encoded outputs to approximate the original inputs by minimising the reconstruction errors, therefore, the target T is set to original inputs X. In the meanwhile, due to the use of ℓ_2 regularisation, the extracted features of ELM auto-encoder may have redundancy and not sparse enough to represent the input data, therefore, a more sparse solution is needed. Compared with ℓ_2 norm, ℓ_1 regularisation is able to induce more sparsity in the optimal solution of Eq.(6). Also, ℓ_1 regularisation is less sensitive to output. Therefore, ℓ_1 penalty is applied. Eq.(4.6) can be rewritten as

$$\underset{\beta \in \mathbb{R}^{K \times Q}}{\operatorname{argmin}} \quad \|\beta\|_{\ell_1} + \|\Psi\beta - X\|^2 \tag{4.7}$$

where $\|\beta\|_{\ell_1}$ stands for the sum of the absolute values of the components of β. Eq.(4.7) can be solved by a gradient projection algorithm. Of which the most popular methods is the class of Iterative Shrinkage-Thresholding Algorithm (ISTA), where each iteration involves matrix-vector multiplication involving Ψ and Ψ^T followed by a shrinkage/soft-threshold step [95], [96]. The general step of ISTA is:

$$\beta_{i+1} = \Upsilon_t(\beta_i - 2t\Psi^T(\Psi\beta_i - X)) \tag{4.8}$$

where t is an appropriate step-size and $\Upsilon_\alpha: \mathbb{R}^n \longrightarrow \mathbb{R}^n$ is the shrinkage operator defined by

$$\Upsilon_\alpha(\beta_i) = (|\beta_i| - \alpha)_+ sgn(\beta_i) \tag{4.9}$$

One of the simplest methods for solving an unconstrained minimisation problem $\min\{p(x): x \in \mathbb{R}^n, p: \mathbb{R}^n \longrightarrow \mathbb{R}^n\}$ is the gradient algorithm which generates a sequence $\{x_i\}$ via:

$$x_0 \in \mathbb{R}^n, \qquad x_i = x_{i-1} - t_i \nabla p(x_{i-1}) \tag{4.10}$$

where t_i is an appropriate step-size. Eq.(4.10) can be viewed as a proximal regularisation of the linearized function p at x_{i-1}, thus, Eq.(4.10) can be rewritten as

$$x_i = \underset{x}{\operatorname{argmin}} \left\{ p(x_{i-1}) + \langle x - x_{i-1}, \nabla p(x_{i-1}) \rangle + \frac{1}{2t_i} \|x - x_{i-1}\|^2 \right\} \tag{4.11}$$

Rewriting Eq.(4.7) as

$$min\{p(\beta) + q(\beta), \beta \in \mathbb{R}^{K \times Q}\} \tag{4.12}$$

where $p(\beta) = \|X - \Psi\beta\|^2$ and $q(\beta) = \|\beta\|_{\ell_1}$.

Therefore, β can be calculated as

$$\beta_i = \underset{\beta}{\operatorname{argmin}} \left\{ p(\beta_{i-1}) + \langle \beta - \beta_{i-1}, \nabla p(\beta_{i-1}) \rangle + \frac{1}{2t_i} \|\beta - \beta_{i-1}\|^2 + \|\beta\|_{\ell_1} \right\} \tag{4.13}$$

The constant terms can be ignored, thus Eq.(4.13) can be written as

$$\beta_i = \underset{\beta}{\operatorname{argmin}} \left\{ \frac{1}{2t_i} \|\beta - (\beta_{i-1} - t_i \nabla p(\beta_{i-1})\|^2 + \|\beta\|_{\ell_1} \right\} \tag{4.14}$$

Let $\nabla p = 2\Psi^T(\Psi\beta - X)$ denotes the gradient of p and $L \coloneqq L(p) = 2(\Psi^T\Psi)$ is the Lipschitz constant of ∇p. Define operator $\varphi_L : \mathbb{R}^n \longrightarrow \mathbb{R}^n,\ \varphi_L(\beta) = \Upsilon_t\big(\beta_i - 2t\Psi^T(\Psi\beta_i - X)\big)$, $t = 1/L(p)$. The computation of output weight β using ISTA algorithm with constant step-size can be represented as follows:

$$\beta_i = \varphi_L(\beta_{i-1}) \tag{4.15}$$

However, ISTA algorithm shares a sublinear global rate of convergence $O(1/z)$, where z is the iteration times and it appears to be a slow method. To improve the complexity result, a Fast Iterative Shrinkage-Thresholding Algorithm (FISTA) is used [95]. FISTA keeps the simplicity of ISTA but shares complexity of $O(1/z^2)$ for minimising smooth convex problems. It computes β_i using based on the following:

$$\beta_i = \varphi_L(y_i) \tag{4.16}$$

where y_i is a new point which is a specific linear combination of previous two points $\{\beta_{i-1}, \beta_{i-2}\}$.

As the Sparse ELM is the building block of DSELM, the learned output β with respect to the input data is the first-layer weight of DSELM. After the output of the first hidden layer sparse representations are obtained, a new SELM auto-encoder is stacked at the top to learn the second layer parameters with the same procedure. In this manner, all parameters of the DSELM can be computed sequentially and all parameters can be fixed without iteratively fine-tuning. At last, an original ELM classifier is stacked at the top of the deep network to make the final decision.

4.3. Experimental Setup

This research, basically, is similar to that explained previously in Chapter 3. Research works established in the farm experimental design as well as in the combustion-based nitrogen analysis, the SPAD meter based nitrogen measurement and image data acquisition of this investigation were the same as that conducted in the previous research as described in Chapter 3.

4.4. DSELM Fusion Based Colour Normalisation

The input dataset used in this research was the same as that used in the previous method as explained in Chapter 3. A large dataset was obtained from ensemble of 24 smaller datasets which were achieved from RGB colour of 24 patches of Macbeth colour checker. In this research, the structure of the DSELM of each patch was as follows:

- three nodes of input and output layers, which represent RGB colour of input and output of the developed DSELM,
- three hidden layers, consisted of two hidden layers of SELM and one hidden layer of original ELM.

The steps taken in the DSELM fusion based colour normalisation can be described as follows:

1) Normalise inputs (X_i)

   RGB input colours should be normalised by dividing their values with the maximum value 255. Thus, $X_1 = \frac{R}{255}, X_2 = \frac{G}{255}, X_3 = \frac{B}{255}$; $X_i \in [0,1],\ i = 1,2,3.$

2) Randomly initialise the input weight w

   Set weight connecting input layers and hidden layer small random values (between -1 to 1).

3) Calculate the hidden output H

   With randomly initialised weights, the k^{th} hidden node output h_k can be calculated as:

$$h_k = \psi_k(w_k^T \cdot X)$$

where X is input data. The activation function that we use is sigmoid function.

4) Calculate the Lipschitz constant L of the gradient of smooth convex function ∇p

$$L \coloneqq L(p) = 2(\Psi^T \Psi)$$

5) Calculate the output weights β_i using SELM
   a) Take the initial value $y_1 = \boldsymbol{\beta}_0 \in \mathbb{R}^n, t_1 = 1$
   b) for i $\geqslant$ 1, compute

$$\beta_i = \varphi_L(y_i)$$

$$= \Upsilon_t\left(y_i - t\nabla p(y_i)\right)$$

$$= \underset{\beta}{\operatorname{argmin}}\left\{\frac{L}{2}\left\|\beta - \left(\beta_{i-1} - \frac{1}{L}\nabla p(\beta_{i-1})\right)\right\|^2 + \|\beta\|_{\ell_1}\right\}$$

$$t_{i+1} = \frac{1 + \sqrt{1 + 4t_i^2}}{2}$$

$$y_{i+1} = \beta_i + \left(\frac{t_i - 1}{t_{i-1}}\right)(\beta_i - \beta_{i-1})$$

6) Recompute the hidden output H with the learned output weight β instead of the randomly initialised weight w

$$H = \sigma(\beta^T \cdot X)$$

7) Stack a new SELM at the top with the input is the previous hidden layer output H.
8) Repeat the above processes (no. 2-7) until the desired deep structure is achieved.
9) Stack an original ELM which is trained with labelled data at the top of the learned deep structure to make final decisions.

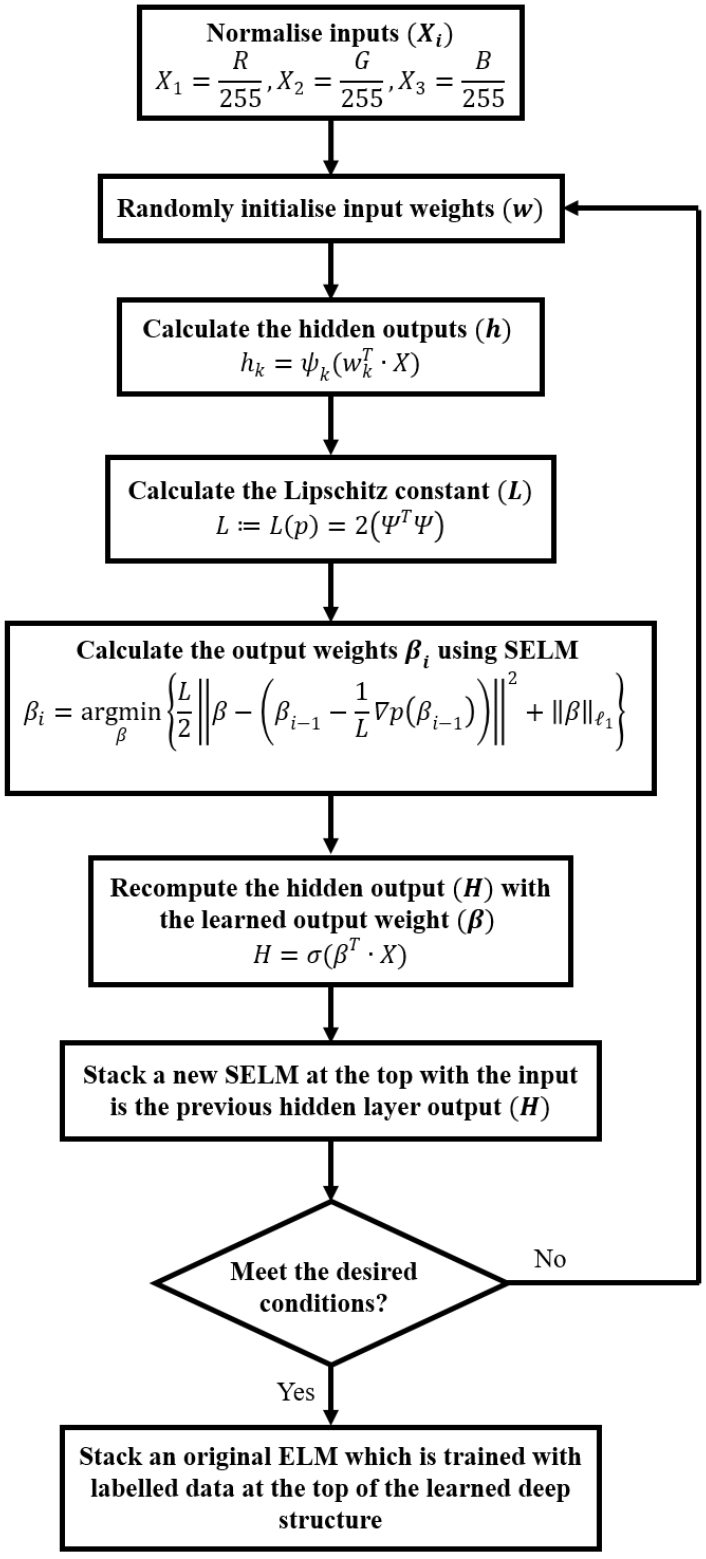

Figure 4.2. The flowchart of the developed DSELM for colour normalisation.

The next step is combining all the DSELMs into one neural network system. The proposed DSELM fusion, as shown in Figure 4.2, is developed to generate new RGB outputs. The proposed approach differs from the previous method as explained in Chapter 3 by applying

DSELM, instead of the regularised neural network. The final output RGB values from the networks fusion is obtained as follows:

$$\mathbf{Z} = \boldsymbol{\alpha} \cdot \mathbf{O}$$

$$= [\propto_1, \propto_2, \propto_3, \cdots, \propto_{24}] \cdot [O_1, O_2, O_3, \cdots, O_{24}]^{\mathrm{T}} \qquad (4.17)$$

where $\boldsymbol{\alpha}$ is the weight matrix of each network output, $\mathbf{O}$ is the output matrix of each network and $\mathbf{Z}$ is the final output matrix of the neural networks fusion.

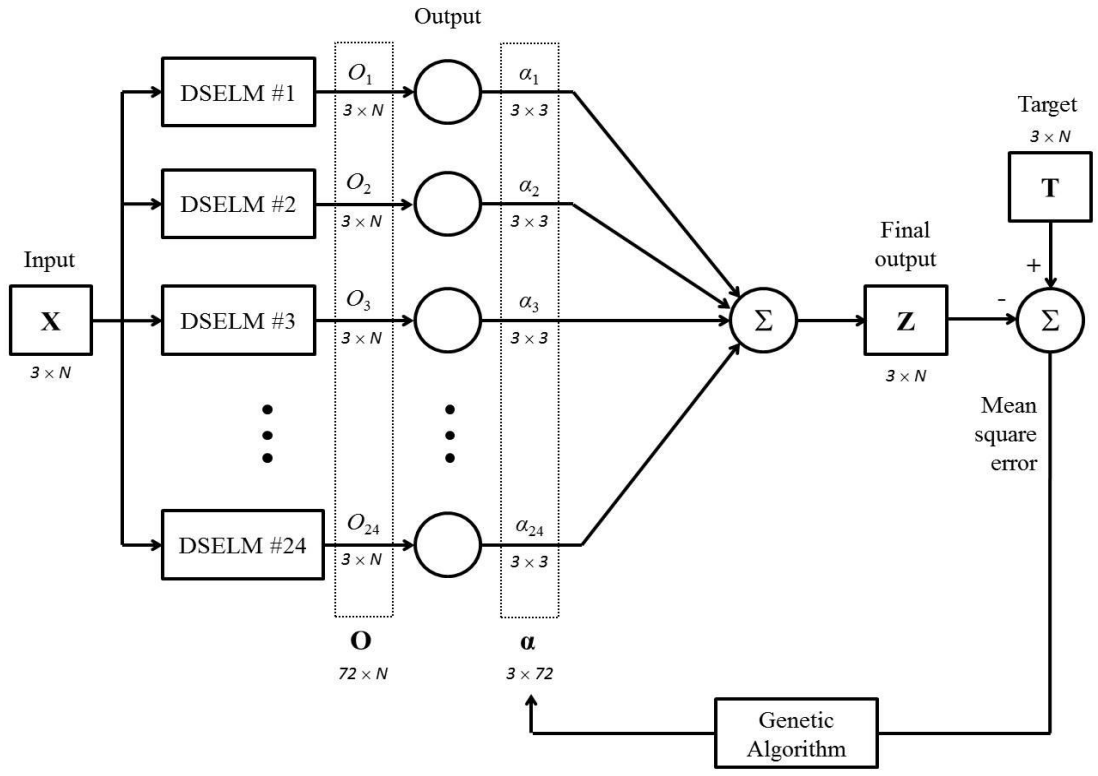

Figure 4.3. The proposed deep sparse extreme learning machines fusion using Macbeth colour checker as colour reference and genetic algorithm based optimisation for image colour normalisation.

In this research, a genetic algorithm was also utilised to find the optimum value for each of the 24 α matrices (see Figure 4.2). Based on the experiments, the proposed DSELMs fusion can be optimised by using genetic algorithm with the following conditions:

1. Initial population size was 1,000 individuals.

2. The probability of mutation was 0.05.

3. The $\alpha = [\propto_1, \propto_2, \propto_3, \cdots, \propto_{24}]$ matrix has a dimension of 3 × 72 and every element of

matrix $\propto_k$ is expressed by a 10-bit string of binary number (0s and 1s).

4. The constrain of each element in matrix $\propto_k$, i.e. $a_{k,ij}$ with $i, j = 1, 2, 3$, was set as follows:

   if $i = j$ then $a_{k,ij} \in [0,1]$

   else $a_{k,ij} = 0$

   Thus, each matrix α_k was constructed as follows:

$$\alpha_k = \begin{bmatrix} a_{k,11} & 0 & 0 \\ 0 & a_{k,22} & 0 \\ 0 & 0 & a_{k,33} \end{bmatrix}$$

   with $k = 1, 2, 3, \dots, 24$.

5. The fitness function was based on the mean square error (MSE) between the target (**T**) and the final output (**Z**) RGB values.

The steps of the developed genetic algorithm to optimise the matrix α can be explained as follows:

1) Generate the initial population, i.e. 1,000 individuals, with 2,160 (= 10 × 3 × 72) bits length for each individual.

2) Produce the next generation by processing cross-over and mutation on each individual.

3) Compute the fitness for each individual by calculating the MSE value.

4) Select the best individual with MSE lower than 0.001.

Similar to the steps undertaken in the previous method as described in Chapter 3, the next step was applying the developed DSELMs fusion and the optimised matrix α to adjust the RGB colour of the wheat plants. In this research, a wheat plant image has also a dimension of 448 × 336 pixels. The developed DSELM-based colour normalisation method was then applied to adjust each pixel of a plant image acquired under various light intensities to the equivalent pixel of the image under the standard light intensity, i.e. 50 Klux.

4.5. DSELM-based Image Segmentation and Statistical Colour Features Extraction

In this research, a DSELM was used for image segmentation to remove the non-leaf images and keep the wheat leaves as the region of interest. Basically, the developed DSELM for this step is similar to that for the colour normalisation process as explained in the previous section. The structure of the DSELM used in this step was as follows:

- Input layer has 3 nodes, which indicate red, green and blue colour values (RGB) for each pixel of plant images.
- Output layer has 1 node, which signifies whether each pixel is a part of a leaf or not. The output value of the network is equal to 1 if the corresponding pixel is a part of a leaf, otherwise the value is 0.
- The network has three hidden layers, in which the two first hidden layers are SELM and the last hidden layer is original ELM.

In this image segmentation step, we develop a dataset from 7,200 samples of RGB colour and binary values (0 or 1) as the input and target values, respectively. The dataset was acquired from 24 normalised images. On each image, 150 pixels in the leaf region and 150 pixels in other parts of the region were selected manually. The RGB colour values of the selected pixels were then used as inputs of the developed DSELM.

After image segmentation, there will be some noises in colour segmented images. These noises should be removed prior to features extraction. The algorithm of noise removing in this research was similar to that in the previous method as explained in Chapter 3. The parameters observed in this stage is not only the results of the image segmentation, but also the processing time compared to the previous method using MLP.

As for the features extraction, the steps taken in this research were the same as the method conducted in the previous research as described in Chapter 3. Four types of statistical moments of each colour RGB channel, namely mean (first moment), variance (second moment), skewness (third moment) and kurtosis (fourth moment), were extracted. These features were then employed as the inputs of DSELM for nutrient estimation, which will be explained more detail in the next section.

4.6. Nitrogen Content Estimation Using Weighted DSELM

In this section, several DSELMs were utilised to perform nutrient estimation by combining them with a committee machine, as seen in Figure 4.3. A genetic algorithm was also employed to optimize the estimation results. In this research, the experiments were limited up to 5 different DSELMs with 5 hidden layer numbers. Each network was repeated 100 times to eliminate the effect of the random bias numbers and initial weights. Subsequently, the best ensemble of DSELMs which provided the least mean square error was chosen to achieve the final estimation.

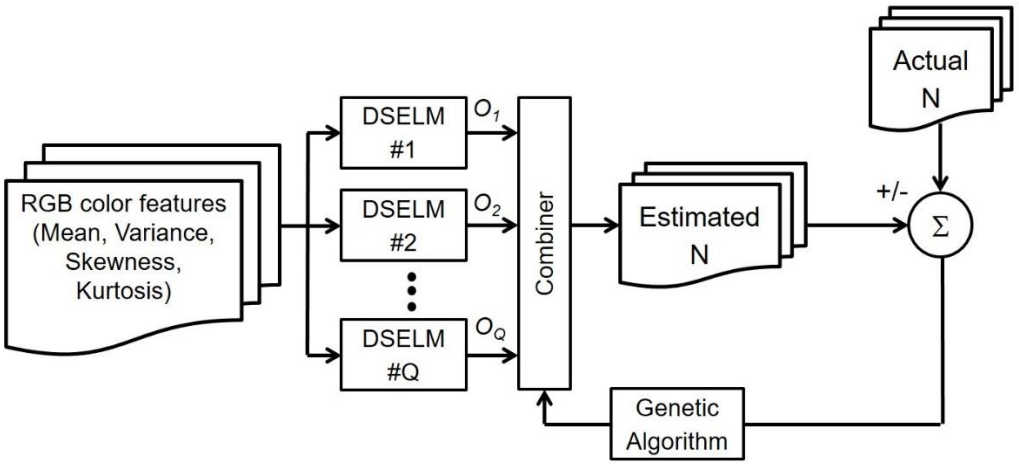

Figure 4.4. Combination of several DSELM with committee machine and GA-based optimization for nitrogen content estimation.

In this step, a committee machine with simple and weighted averaging method was employed to combine a number of DSELMs. As described in Chapter 3, a committee machine can produce more enhanced generalisation and system performance in the estimation than single neural network or expert system. Similar to the previous method in Chapter 3, the nitrogen amount of wheat leaves was estimated by using committee machines with simple averaging method and weighted averaging method, as expressed in the equation (4.18) and (4.19), respectively:

$$Y_{ave} = \frac{1}{Q}\sum_{q=1}^{Q} O_q \tag{4.18}$$

$$Y_{weigh} = \sum_{q=1}^{Q} (w_q \times O_q) \quad \text{with} \quad \sum_{q=1}^{Q} w_q = 1 \tag{4.19}$$

where Y_{weigh} is the estimated nitrogen content, w_q is the weight, and O_q is the output of q-th single network.

A genetic algorithm was utilised to discover the optimum value of the weights in the developed committee learning. The genetic algorithm for the nitrogen estimation was developed with the following conditions:

1) Initial population size was 1,000.

2) Each individual was expressed by $Q \times 8$ bits length of binary numbers.

3) Probability of mutation is 0.05.

4) Each weight ranged between 0 and 1; $w_i \in [0, 1]$.

5) The fitness function was to estimate the mean square error (MSE) between the actual and the estimated nitrogen content.

The final step of this research was measuring the accuracy level of the nutrient estimation. Similar to the previous research, this step was conducted by calculating the mean absolute percentage error (MAPE) to assess the system's performance. Several error types, namely MAE, MSE, RMSE, and SSE, were also calculated as a comparison.

4.7. Results and Discussion

4.7.1. DSELMs fusion based colour normalisation

Based on the established experiments, the proposed DSELMs fusion based colour normalisation can be used to normalise wheat plant images captured under various light intensities. In this step, the results of the developed DSELM approach were compared with other colour normalisation methods, as mentioned previously in Chapter 3, namely grey world

assumption, scale-by-max algorithm, linear regression model, and single multilayer perceptron. It was also compared to the previous proposed method as discussed in Chapter 3.

The parameters used in this comparison includes accuracy level and processing speed. The accuracy level was measured by calculating average Euclidean distance of the target and the output RGB colour of all patches while the processing speed was measured by calculating the time (in seconds) required to process colour normalisation in each method. As seen in Table IV.1, our proposed method using DSELMs fusion is superior to the aforementioned methods in both accuracy and speed. The comparison of ΔE_{RGB} of each patch by using all methods is also presented in Figure 4.4.

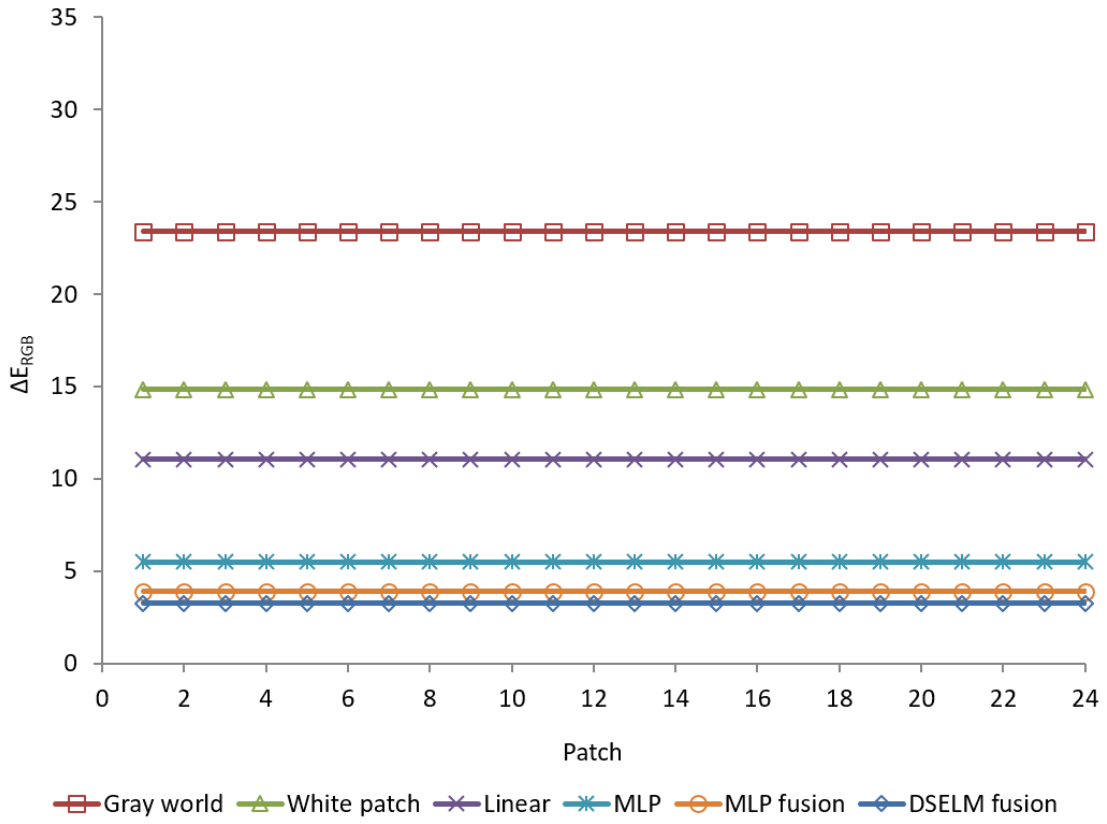

Figure 4.5. ΔE_{RGB} of each patch using all methods.

Basically, in the grey world as well as white patch and linear model algorithms, the colour normalisation process is accomplished by scaling colour value of each pixel with a certain constant. It does not require training process as that in neural networks. This is why the processing times of colour normalisation using these methods are very quick. On the other

hand, the output colours are significantly different compared to the target. These algorithms, therefore, are not suitable to normalise plants images.

In the previous proposed method, i.e. MLPs fusion, the colour normalisation processing time was considerably longer than that of single MLP since it needed to fuse the 24 MLPs. The results, however, was reasonably better, as indicated by the ΔE_{RGB} value. The challenge to produce better results and faster training process has been overcome by applying DSELMs fusion, as seen in Table IV.1. The colour normalisation error is less than that of MLPs fusion with processing speed 70 times faster.

Table 4.1. Comparison of colour normalisation results

Methods	ΔE_{RGB}	Time (s)*
Grey world assumption	23.40	0.1156
Scale-by-max algorithm	14.86	0.1251
Linear regression model	11.06	0.1468
Single MLP	5.03	1455
MLPs fusion	4.15	21861
The proposed method (DSELMs fusion)	3.86	312

* All algorithms were performed by using a desktop PC with 3.2 GHz Intel Core i5 processor and 8 GB of RAM.

In this second proposed method, a genetic algorithm was also utilised to optimise 24 α values as the output weights of each DSELM. The optimised α matrices were then applied to adjust wheat plant images by using the developed DSELMs fusion method. Following is an example of the α matrices used to correct a wheat plant image:

$$Z = \begin{bmatrix} 0.039 & 0 & 0 \\ 0 & 0.069 & 0 \\ 0 & 0 & 0.007 \end{bmatrix} \cdot O_1 + \begin{bmatrix} 0.053 & 0 & 0 \\ 0 & 0.025 & 0 \\ 0 & 0 & 0.005 \end{bmatrix} \cdot O_2 + \begin{bmatrix} 0.047 & 0 & 0 \\ 0 & 0.014 & 0 \\ 0 & 0 & 0.065 \end{bmatrix} \cdot O_3 + \cdots + \begin{bmatrix} 0.064 & 0 & 0 \\ 0 & 0.015 & 0 \\ 0 & 0 & 0.008 \end{bmatrix} \cdot O_{24}.$$

By applying the developed DSELMs fusion based colour adjusting system and the optimized α matrices, wheat crop images with a variation of light intensities were subsequently transformed to that with standard light intensity, i.e. 50 Klux. The parameter used for

measuring the effectiveness of colour normalisation was colour variability of the plant images, as established in the previous research. This parameter can be measured by calculating standard deviation of the original images and the corrected images. The smaller the standard deviation of image colours, the smaller the colour variability of the images. The colour normalisation results of this second proposed method were not significantly different to that of the first proposed method, however, it was significantly superior in the performance's speed.

4.7.2. DSELM-based image segmentation and features extraction

After colour normalisation using the developed DSELMs fusion, the next step was image segmentation. The DSELM based image segmentation can be applied to distinguish wheat leaves from other parts, such as weeds, soil, stones and dried leaves (see examples in Figure 4.5). The developed segmentation method was much better compared to the Otsu algorithm, as seen in Figure 4.6. The database pertaining to the colour of leaves and non-leaves provides sufficient data to train the plant images. Therefore, the DSELM can precisely classify whether a pixel belongs to the leaves or non-leaves region.

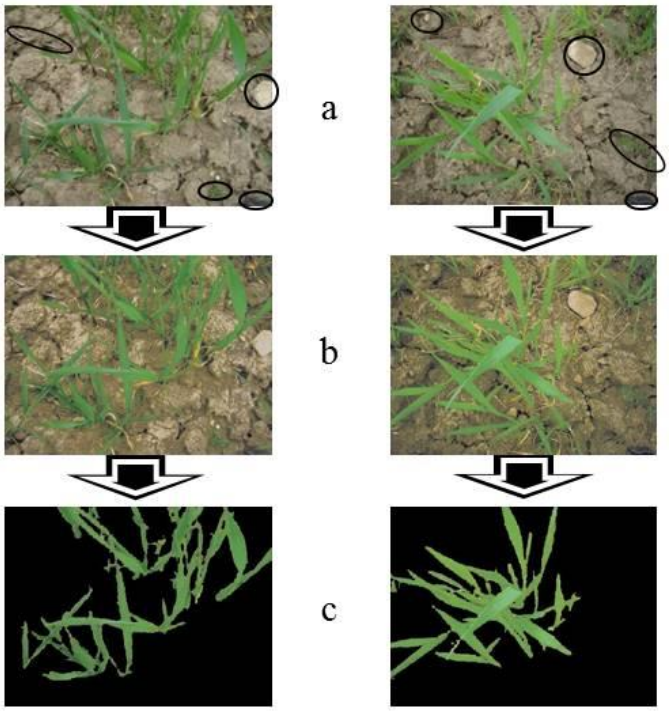

Figure 4.6. Two examples of the proposed colour normalisation and image segmentation results; (a) original images with some spots of unwanted parts, (b) normalised images, (c) segmented images.

Furthermore, the developed DSELM method can accomplish image segmentation process much faster than the conventional backpropagation MLP and the original ELM, as seen in Table IV.2. The image segmentation results using three different neural network types are all good as indicated by the accuracy level. However, the developed DSELM can perform the image segmentation 6 times faster than the MLP and slightly faster than the original ELM. Once all images have been segmented, four moment statistical features of each colour channel were then extracted to be utilised as predictors in the developed DSELM-based nitrogen estimation.

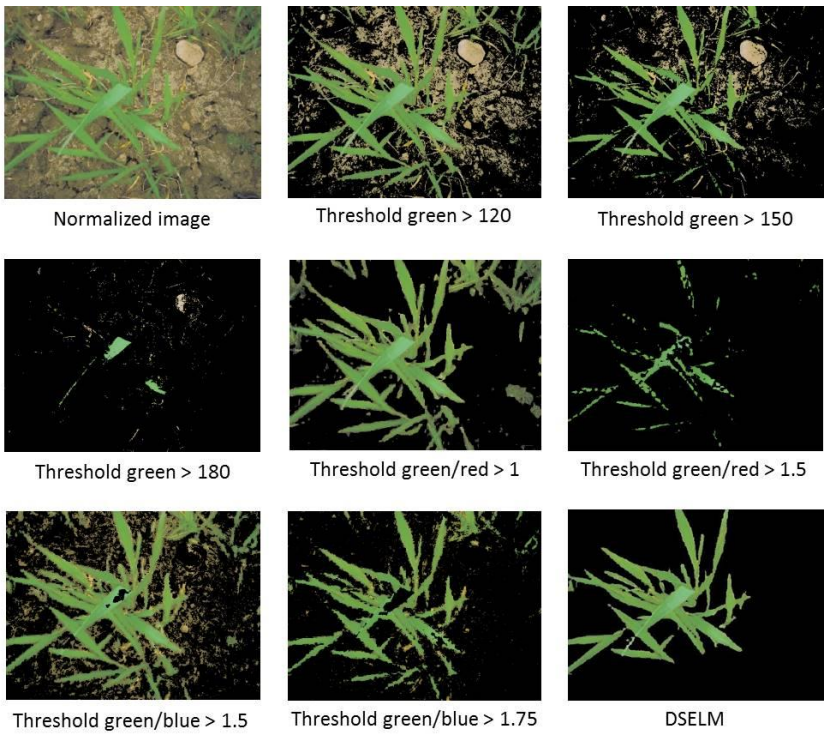

Figure 4.7. A comparison of some threshold based and the developed DSELM based image segmentations.

Table 4.2. Comparison of image segmentation results

Methods	Accuracy (%)	Time (s)*
MLP	99.8	6.349
Original ELM	100	1.154
The proposed method (DSELM)	100	0.998

* All algorithms were performed by using a desktop PC with 3.2 GHz Intel Core i5 processor and 8 GB of RAM.

4.7.3. DSELM and committee machine based image nutrient estimation

In this step, several DSELMs with various numbers of hidden layers were combined and subsequently trained to determine which gave the best results. After established several experiments, the best network's performance was achieved from the combination of four DSELMs compared to other possible combinations. The first combination method used in this step was simple average. The estimated nitrogen amount was then calculated, as follows:

$$Y_{ave} = \frac{1}{4}\sum_{q=1}^{4} O_q \tag{4.20}$$

The best result relates to the first type of committee machine, i.e. simple average, was then compared to that of the second type combiner, i.e. weighted average, which was optimised by the genetic algorithm (GA). By using this method, the optimum weights of the output of the networks system are 0.217, 0.375, 0.183, and 0.225, respectively for the first until the fourth DSELM. The estimated nitrogen content can therefore be expressed as follows:

$$Y_{GA} = (0.217 \times O_1) + (0.375 \times O_2) + (0.183 \times O_3) + (0.225 \times O_4) \tag{4.21}$$

Table IV.3 illustrates the comparison of various types of error values of the developed DSELM and SPAD meter methods. From the table, we can perceive that by using a simple average combiner, the combination of four DSELMs provides the best results compared to other combinations with simple averaging method. However, the weighted average combiner with GA optimisation offers enhanced results. As seen in the table, the MAPE of four DSELMs with weighted averaging method is smaller than that of four DSELMs with simple averaging combiner.

Similar to the works conducted in the previous steps, the processing time of nitrogen estimation was also calculated. The results of this measurement can be seen in the Table IV.4. According to the table, the method using weighted averaged 4 DSELMs run slower than other methods using simple averaging combiner since it employs genetic algorithm to optimise the weights of each DSELM. This method, however, is faster than the first proposed method using combination of six MLPs.

Table 4.3. Comparison of nitrogen amount estimation errors

Methods	MAPE	MAE	MSE	RMSE	SSE
SPAD meter	8.48%	0.2042	0.0578	0.2404	1.5704
Weighted averaged 6 NNs (first proposed method)	2.73%	0.0674	0.0078	0.0885	0.2819
1 DSELM	3.42%	0.0877	0.0125	0.0956	0.4599
Simple averaged 2 DSELMs	3.28%	0.0745	0.0277	0.0918	0.4205
Simple averaged 3 DSELMs	3.26%	0.0744	0.0275	0.0905	0.4148
Simple averaged 4 DSELMs	3.23%	0.0733	0.0273	0.0902	0.4091
Simple averaged 5 DSELMs	3.28%	0.0744	0.0276	0.0903	0.4169
Weighted averaged 4 DSELMs (second proposed method)	2.76%	0.0679	0.0081	0.0890	0.2915

Table 4.4. Comparison of nitrogen amount estimation processing speed

Methods	Time (s)
Weighted averaged 6 NNs (first proposed method)	310.46
1 DSELM	7.10
Simple averaged 2 DSELMs	12.07
Simple averaged 3 DSELMs	17.84
Simple averaged 4 DSELMs	25.13
Simple averaged 5 DSELMs	30.41
Weighted averaged 4 DSELMs (second proposed method)	52.24

4.8. Summary

A novel computational intelligent vision sensing using deep sparse extreme learning machine was proposed to acquire plant images and to estimate nutrient content in wheat leaves based on colour features of plant images captured on field with significant variations of sunlight intensities. The developed algorithm focused on the development of deep sparse extreme learning machine and genetic algorithm to overcome the problems on wide colour variability due to different lighting conditions, image segmentation to distinguish crop leaves from complex background, and optimisation of the nutrient estimation. The proposed method was

successfully demonstrated to normalise images as well as to decrease the colour deviation and to perform image segmentation considerably faster than other neural network methods. Furthermore, the combination of DSELMs with committee machine and genetic algorithm showed very promising results in estimating nitrogen content in wheat leaves compared with existing methods.

Chapter 5

Building A Globally Optimised Computational Intelligence Image Processing Algorithm for On-Site Nitrogen Status Analysis in Plants

5.1. Introduction

In this chapter, another more advance method for nitrogen status analysis based on characteristics of leaves colour has been developed. As discussed in Chapter 3 and Chapter 4, a fusion of regularised neural networks and of deep sparse extreme learning machine have been established to normalise wheat leaves images in order to reduce the colour variability due to different sunlight intensities. In those methods the colour normalisation results have been optimised locally based on the RGB vales of Macbeth colour checker as the reference.

In this chapter, another type of expert systems, namely deep learning multilayer perceptron (DL-MLP), has been employed to normalise plant images and image segmentation. Furthermore, after the Macbeth colour checker based local optimisation, the colour normalisation of the wheat plant images has also been optimised globally according to the nitrogen estimation error to produce more robust results. This chapter also discusses how well the global optimisation can fine tune the colour normalisation and the nutrient estimation results by developing similar methods without global optimisation.

5.2. Experimental Setup

Basically, the experimental research designs in this chapter, including farm and laboratory works as well as image data acquisition, are similar to that described in Chapter 3.

5.3. The proposed GA-based global optimisation for on-field nitrogen status analysis in plants

In general, this proposed method can be split into five major works (see Figure 5.1), i.e. (i) image acquisition, (ii) colour normalisation training using an ensemble of deep learning multilayer perceptron (DL-MLP), (iii) image segmentation and features extraction, (iv)

nitrogen estimation, and (v) GA-based global optimisation. The details of each particular work will be described in the following sections.

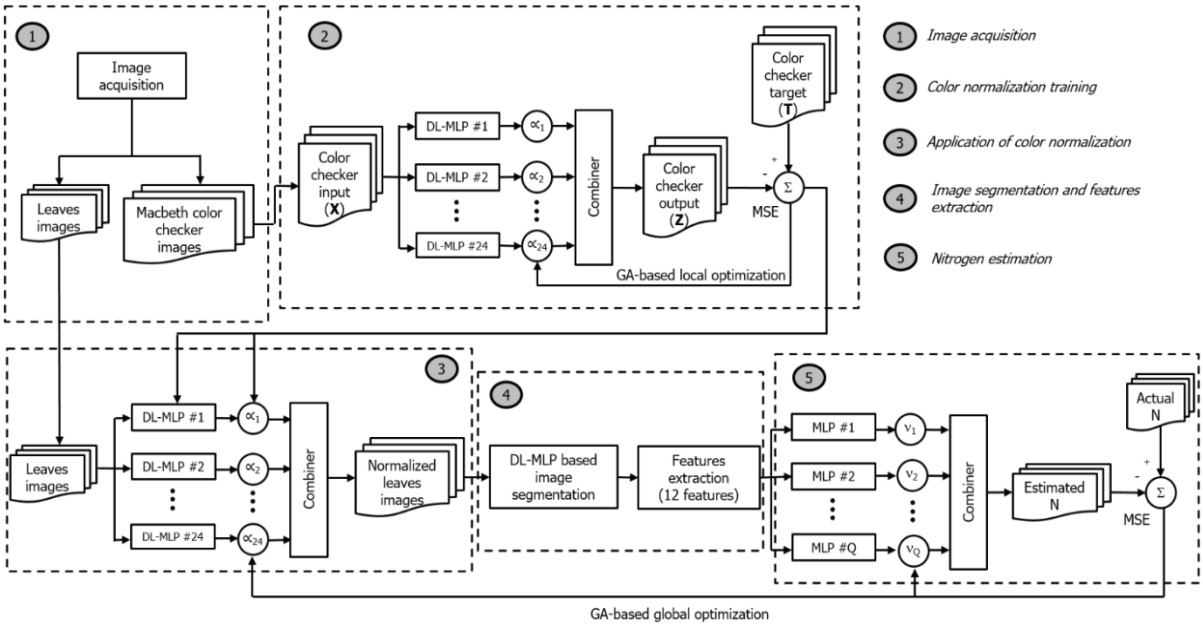

Figure 5.1. Genetically-enabled ensemble DL-MLP for on-field nitrogen status analysis in plants.

5.3.1. Image acquisition

In this research, two types of images were acquired on the field with variations of sunlight intensities, i.e. Macbeth colour checker and wheat plant images. The images of the Macbeth colour checker and wheat plant were captured under sunlight using a common digital still camera (Sony DSC-W55). Basically, the image acquisition method in this research was adopted from the method used in the previous research which is described in Chapter 3. In general, there were 7872 RGB colour samples from the Macbeth colour checker for colour normalisation and 360 wheat plant images for nutrient estimation.

5.3.2. Colour normalisation training and its application to wheat plant images

In this step, a colour normalisation was firstly performed using an ensemble deep learning multilayer perceptron (DL-MLP) and then locally optimised the results by genetic algorithm using the Macbeth colour checker datasets. The developed colour normalisation aims to reduce colour variability due to different light intensities. As shown in Figure 5.1, the RGB

information of the Macbeth colour checker was initially trained by using 24 DL-MLPs and combined by both simple and weighted averaging methods.

In order to attain a better generalization performance, a deep learning MLP is required to extract more abstract and accurate information than those from shallow ones [97]. The developed DL-MLP used in this colour normalisation, as shown in Figure 5.2, can be explained as follows. Each DL-MLP consisted of three hidden layers and three units of both input and output layers, which represented red, green and blue colour channels from the Macbeth colour checker.

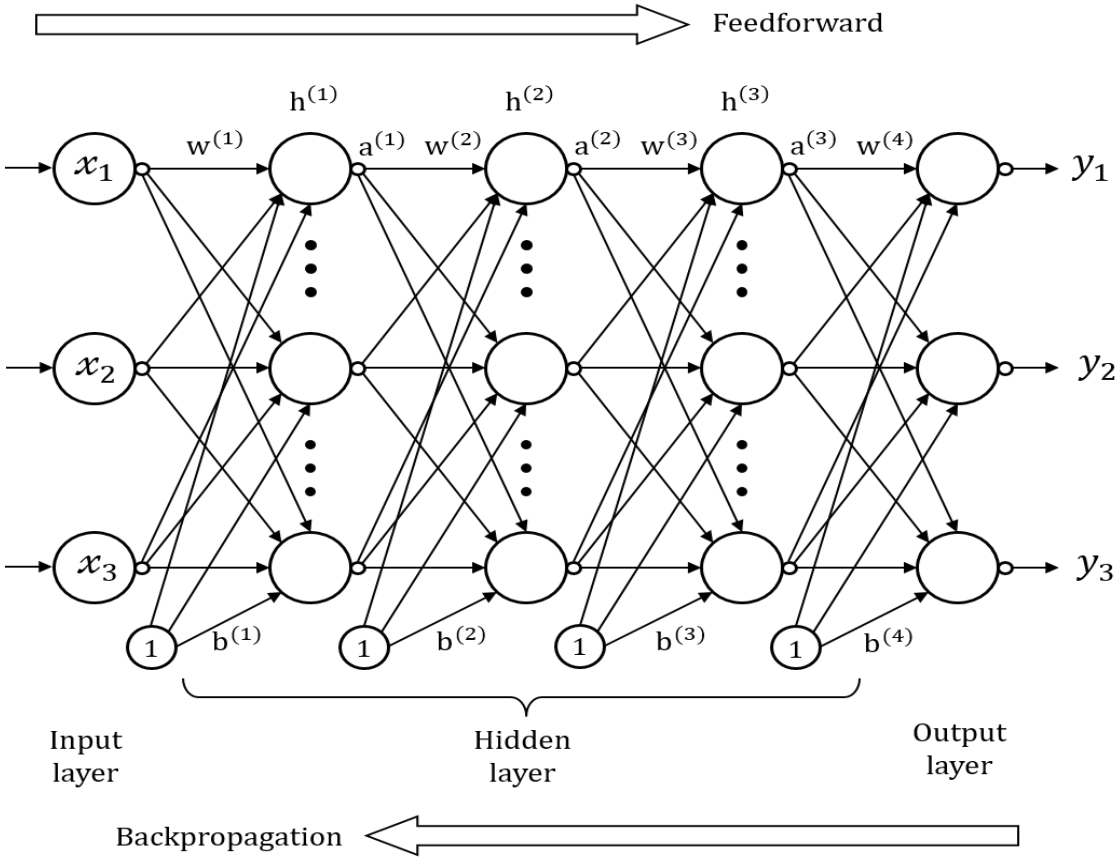

Figure 5.2. The developed DL-MLP for colour normalisation.

A DL-MLP utilizes a series of many layers (usually more than one hidden layer) of nonlinear processing units. Each consecutive layer uses the output from the previous one as input. Suppose that there is a DL-MLP with L hidden layers, the layer input activation for $k > 0$ with $\mathbf{h}^{(0)}(\mathbf{x}) = \mathbf{x}$ can be expressed as:

$$\mathbf{a}^{(k)}(\mathbf{x}) = \mathbf{b}^{(k)} + \mathbf{W}^{(k)}\mathbf{h}^{(k-1)}(\mathbf{x}) \tag{5.1}$$

The hidden layer activation (k from 1 to L) and output layer activation ($k = L + 1$), thus, can be calculated as:

$$\mathbf{h}^{(k)}(\mathbf{x}) = \mathrm{g}\left(\mathbf{a}^{(k)}(\mathbf{x})\right) \tag{5.2}$$

and

$$\mathbf{h}^{(L+1)}(\mathbf{x}) = \mathrm{o}\left(\mathbf{a}^{(L+1)}(\mathbf{x})\right) = \mathbf{f}(\mathbf{x}) \tag{5.3}$$

respectively, with $\mathrm{g}(\cdot)$ and $\mathrm{o}(\cdot)$ are the sigmoid activation function.

In the developed DL-MLP, each hidden layer was initially pre-trained in an unsupervised way using an autoencoder. Basically, an autoencoder is a feedforward neural network to transform the input into a more dense representation and rebuild the input with the learned representation [98]. An autoencoder consists of two sections, namely encoder and decoder, which can be expressed as transformations ϕ and ψ, respectively, as follows:

$$\phi: \boldsymbol{\mathcal{X}} \longrightarrow \boldsymbol{\mathcal{M}} \quad \text{(encoder)}$$

$$\psi: \boldsymbol{\mathcal{M}} \longrightarrow \boldsymbol{\mathcal{X}} \quad \text{(decoder)}$$

An autoencoder, as seen in Figure 5.3, can be considered as an MLP with one hidden layer in which the output values are equal to the inputs. Furthermore, an autoencoder uses the input $\mathbf{x} \in \mathbb{R}^d = \boldsymbol{\mathcal{X}}$ and maps it onto $\mathbf{m} \in \mathbb{R}^p = \boldsymbol{\mathcal{M}}$ such that:

$$\mathbf{m} = \varphi_1(\mathbf{W}\mathbf{x} + \mathbf{b}) \tag{5.4}$$

Subsequently, the matrix $\mathbf{m}$ is mapped onto the reconstruction matrix $\mathbf{x}'$ of the same values of $\mathbf{x}$, which can be expressed as:

$$\mathbf{x}' = \varphi_2(\mathbf{W}'\mathbf{m} + \mathbf{b}') \tag{5.5}$$

where $\varphi_1(\cdot)$ and $\varphi_2(\cdot)$ are element-wise activation function, i.e. sigmoid function. Each autoencoder is trained to minimise autoencoding errors:

$$\boldsymbol{\delta}(\mathbf{x}, \mathbf{x}') = \| \mathbf{x} - \mathbf{x}' \|^2 = \| \mathbf{x} - \varphi_2\left(\mathbf{W}'\left(\varphi_1(\mathbf{W}\mathbf{x} + \mathbf{b})\right) + \mathbf{b}'\right) \|^2 \tag{5.6}$$

After autoencoding of the first hidden layer, the pre-training process continues to the next hidden layer with the same method as previously described until the last hidden layer. Once all hidden layers are pre-trained, the next steps are then as follows:

- Add output layer
- Initialise $\mathbf{W}^{(L+1)}$ and $\mathbf{b}^{(L+1)}$ randomly as usual
- Train the whole network using supervised learning with backpropagation error algorithm, as shown in Figure 5.2. All networks' weights are then adjusted for the supervised task.

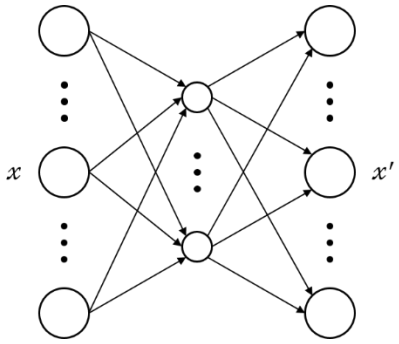

Figure 5.3. An autoencoder of the first hidden layer.

After training each DL-MLP, the next step was combining all 24 DL-MLPs into one neural network system using committee machines. By using this combination, the output value **Z** (see Figure 5.1) can be achieved by averaging the output **Y**, as follows:

$$\mathbf{Z} = \boldsymbol{\alpha} \cdot \mathbf{Y} = [\propto_1, \propto_2, \propto_3, \cdots, \propto_{24}] \cdot \begin{bmatrix} Y_1 \\ Y_2 \\ Y_3 \\ \dots \\ Y_{24} \end{bmatrix} \tag{5.7}$$

In this step, two types of combiner were used, i.e. simple and weighted averaging method. The simple averaging method indicates that each DL-MLP has the same weight, $\propto_k$, to produce the new output, **Z**. In this paper, the possibility that each DL-MLP has a different weight was also investigated. This step was conducted by local optimisation using genetic algorithm, as expressed in the following:

$$Z = \sum_{k=1}^{24} (\propto_k \times Y_k) \quad \text{with} \quad \sum_{k=1}^{24} \propto_k = 1 \tag{5.8}$$

Once the colour normalisation accomplished, the next step was applying the developed neural network and the matrix α to normalise wheat plant images. In this research, a wheat plant

image have a dimension of 448 × 336 pixels. Through this developed colour adjusting system, each pixel of a plant image which was acquired under various light intensities was transformed to the equivalent pixel of the image under the standard light intensity, i.e. 50 Klux.

5.3.3. Image segmentation and features extraction

In this step, image segmentation was conducted to remove any non-leaf images, such as soil, stones, weeds, dried and semi-dried leaves, and to keep the leaf images as the region of interest. A multilayer, feed forward, backpropagation error neural network was utilised for image segmentation to distinguish the wheat leaves from other undesired parts. In regard to the developed neural network, a dataset of 4,800 samples of RGB colour and binary values (0 or 1) as the input and target values, respectively, was established. The dataset was achieved from 24 images, in which 100 pixels in the leaf region and 100 pixels in other parts of the region were selected manually from each image.

In general, the structure of the neural network in this step is similar to the single DL-MLP used for colour normalisation as previously explained. The network had three units of input layer, which indicate red, green and blue colour values (RGB) for each pixel related to the plant images. The output layer had only one unit, which signifies whether each pixel is a part of a leaf or not. The output value of the network was equal to 1 if the corresponding pixel was a part of a leaf, otherwise, the value was 0. The developed DL-MLP utilized three hidden layers which were initially unsupervised pre-trained using autoencoder method. The sigmoid activation function was used for both hidden and output layers.

In the colour segmented images, there were several noises which should be removed before extracting image features. Furthermore, weeds were also present in the most of plant images which need to be eliminated from the segmented images, as they can affect the colour information of the wheat leaves. To unravel this problem, an image segmentation algorithm was developed to remove unwanted images by selecting the largest part of the leaves which has the highest number of object pixels (see Figure 5.4).

Once the image segmentation accomplished, several features of the segmented images were subsequently extracted. Four types of statistical colour moments of each RGB colour channel, namely mean, variance, skewness, and normalised kurtosis were extracted. These features can

represent colour distributions of an image. Additionally, the mathematical expressions of the features can be written as follows:

$$\text{mean} = \mu^{(c)} = \mathrm{E}\left(x^{(c)}\right) = \frac{1}{N_s}\sum_{i=1}^{N_s} x_i^{(c)}$$

$$\text{variance} = \text{var}^{(c)} = \mathrm{E}\left[\left(x^{(c)} - \mu^{(c)}\right)^2\right]$$

$$= \frac{1}{N_s}\sum_{i=1}^{N_s}\left(x_i^{(c)} - \mu^{(c)}\right)^2$$

$$\text{skewness} = \text{skew}^{(c)} = \frac{\mathrm{E}\left[\left(x^{(c)} - \mu^{(c)}\right)^3\right]}{\left(E\left[(x^{(c)} - \mu^{(c)})^2\right]\right)^{3/2}}$$

$$\text{normalised kurtosis} = \text{normkurt}^{(c)} = \frac{\mathrm{E}\left[\left(x^{(c)} - \mu^{(c)}\right)^4\right]}{\left(E\left[(x^{(c)} - \mu^{(c)})^2\right]\right)^2} - 3$$

where c refers to each colour channel (red, green, and blue) and N_s is the number of samples (object pixels).

5.3.4. Nitrogen content estimation

In this step, a combination of several neural networks with different hidden layer nodes using a committee machine was developed to estimate nitrogen content. Each neural network had twelve nodes of input layer which correspond to the statistical moment features of red, green, and blue colour and one node of output layer that represents the estimated nitrogen amount.

The initial number of hidden layer units was set to 12 nodes. From this initial unit number, several new neural networks with various hidden layer nodes were generated. The numbers of hidden layer nodes with regards to these new neural networks were produced using the following formula:

$$Lh_{new} = f \times Lh_{init} \tag{5.9}$$

where Lh_{new} and Lh_{init} are the number of hidden layer nodes of new and the initial neural network, respectively, and f is the multiplication factor (f = 2, 3, …, 7) and is also the

number of combined neural networks (experiments were conducted up to 7 neural networks) (see Table 5.1).

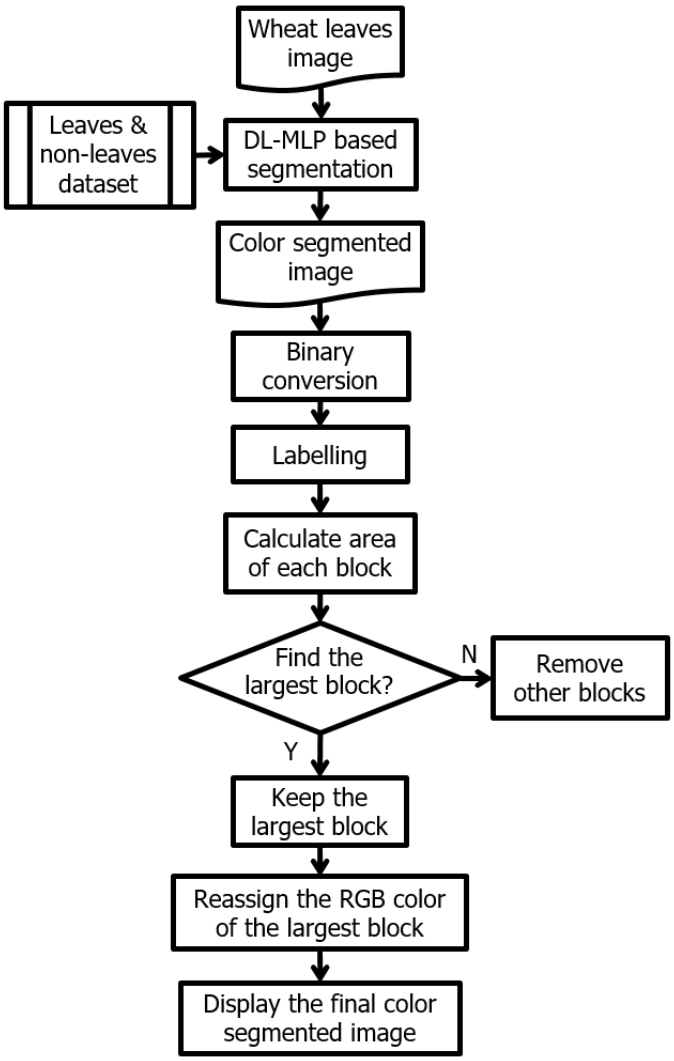

Figure 5.4. DL-MLP based image segmentation algorithm.

Table 5.1. Neural networks combinations

Number of NNs (Q)	Number of hidden layer nodes
2	12 – 24
3	12 – 24 – 36
4	12 – 24 – 36 – 48
5	12 – 24 – 36 – 48 – 60
6	12 – 24 – 36 – 48 – 60 – 72
7	12 – 24 – 36 – 48 – 60 – 72 – 84

In this research, nitrogen amount was estimated by applying a committee machine with the simple and GA-based averaging methods as the combiner of Q neural networks, as seen in Figure 5.5 and 5.6, respectively. The nitrogen percentage, therefore, can be estimated using the following formula:

$$N' = \sum_{q=1}^{Q} (\nu_q \times N_q) \quad \text{with} \quad \sum_{q=1}^{Q} \nu_q = 1 \tag{5.10}$$

where N' is the estimated nitrogen content, ν is the network weight, and N is the output of single network.

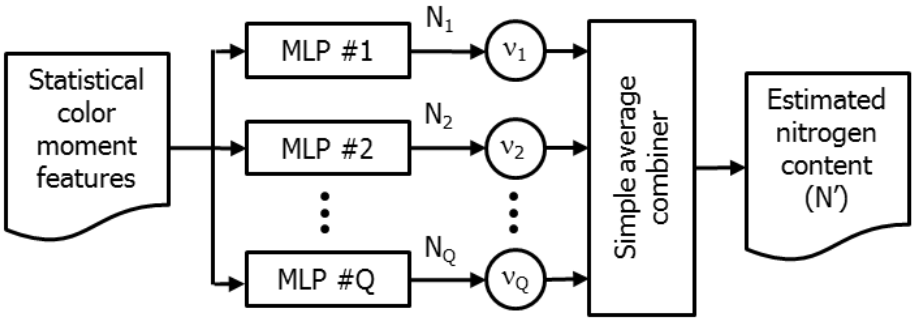

Figure 5.5. The simple average combiner method for nitrogen estimation.

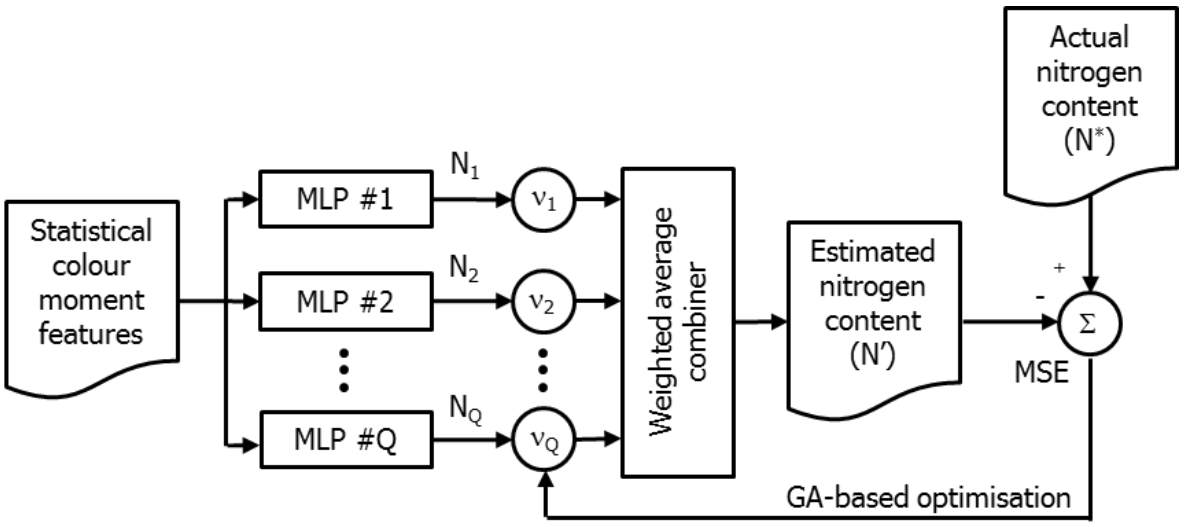

Figure 5.6. The GA-based weighted combiner method for nitrogen estimation.

5.3.5. The proposed global optimisation

The final step of this research was optimising globally the combiner weights, i.e. matrix α and matrix ν, in the colour normalisation and nitrogen estimation steps, respectively, based on the estimation error using a genetic algorithm (see Figure 5.1). Basically, a genetic algorithm encompasses a population with a certain number of individuals. Each individual in a population has a possibility of being the solution to the optimisation problem. Hence, by applying selection, crossover and mutation among individuals, a new generation is produced. This process is repeated several times until a new individual provides the most appropriate solution for the problem.

Two sequential GAs have been developed to achieve the best estimation results. The first GA was to optimise the matrix α in the colour normalisation, while the second was a GA to optimise the matrix ν in the nitrogen estimation step. Based on our experiments, the developed neural networks fusion can be optimised using genetic algorithms with the following steps:

a) Define fitness function

In this section, the fitness function of the developed genetic algorithm was to minimise the MSE between the actual (N^*) and the estimated nitrogen content (N') of S samples.

$$\underset{\propto}{\operatorname{argmin}} \ \frac{1}{S}\sum_{s}(N_s^* - N_s')^2 \qquad \text{for colour normalisation step}$$

$$\underset{\nu}{\operatorname{argmin}} \ \frac{1}{S}\sum_{s}(N_s^* - N_s')^2 \qquad \text{for nitrogen estimation step}$$

b) Determine initial population of chromosomes (N_{pop})

The population size of this genetic algorithm was initially set to 1000 chromosomes (individuals) for both steps. These chromosomes performed as the first generation.

$$N_{pop} = 1000$$

c) Encoding

Encoding is expressing each chromosome in the population by the binary strings of 0s and 1s.

In the colour normalisation step, the $\boldsymbol{\alpha} = [\propto_1, \propto_2, \propto_3, \cdots, \propto_{24}]$ matrix has a dimension of 3 × 72 and every element of the matrix $\propto_k$ was expressed by a 10-bit string of binary numbers (0s and 1s). Likewise, in the nitrogen estimation step, each chromosome (individual) referred to Q neural networks weights ($\boldsymbol{\nu} = \nu_1, \nu_2, \ldots, \nu_Q$). Each chromosome, therefore, was represented by $Q \times 10$ bit strings.

d) Boundary conditions

In the both steps, boundary conditions were defined so that each element in the matrix $\boldsymbol{\alpha}$ and matrix $\boldsymbol{\nu}$ has a positive value. In particular, the boundary of each element of matrix $\propto_k$, i.e. $a_{k,ij}$ with $i, j = 1, 2, 3$, was set as follows:

if $i = j$ then

$a_{k,ij} \in [0, 1]$

else

$a_{k,ij} = 0$

Thus, each matrix $\propto_k$ has a structure as follows:

$$\propto_k = \begin{bmatrix} a_{k,11} & 0 & 0 \\ 0 & a_{k,22} & 0 \\ 0 & 0 & a_{k,33} \end{bmatrix}$$

with $k = 1, 2, 3, \ldots, 24$.

e) Reproduce next generations by processing selection, cross-over and mutation operators

In the beginning, each chromosome in the first generation was tested by the fitness function to figure out how well it solves the optimisation problem.

According to [99], selection operator attempts to give “a pressure” to the population as the same as natural selection in the biological life. Chromosomes (individuals) with better performance, or fitter, will be kept to the next generations. Otherwise, they will be wiped out. In cross-over, two chromosomes exchange some bits of the same section one another to create two offspring, while mutation turns over bits in a chromosome (a 0 to a 1 and vice versa).

The existence of mutation depends on the probability of mutation (ρ) set in the algorithm as well as a random number given by the computer (ω). In this step, the ρ value was set to 0.05. The mutation operator was defined as follows:

$$\text{mutation} = \begin{cases} 1 \text{ (occurs) if } \rho \geq \omega \\ 0 \text{ (not occur) if } \rho < \omega \end{cases} \tag{5.11}$$

Repeat the selection, crossover, and mutation processes until the best chromosome achieved.

5.4. Results and Discussion

The objective of the developed colour normalisation was to normalise plant images captured under various light intensities and to reduce the colour variability of the images. After image normalisation, it can be assumed that all images are captured under the same light intensity. The colour difference between them was then solely affected by nutrient content in the leaves. This method, thus, can make the comparison among the plant images more reliable.

In this study, three schemes of nitrogen status analysis have been established based on the combiner type and the application of global optimisation, as seen in Table 5.2. In the first scheme, simple average combiner was used to combine several neural networks in both colour normalisation and nitrogen estimation steps. In the second scheme, the combiner weights in the colour normalisation step were optimised locally using GA while the simple averaging method was used as the combiner in the nitrogen estimation step. In the last scheme, GA was utilised to globally optimise the combiner weights in both steps.

Table 5.2. Scheme works of the nitrogen status analysis

Scheme	Colour normalisation combiner	Nitrogen estimation combiner	Global optimisation
Scheme #1	Simple average	Simple average	No
Scheme #2	GA-based weighted average (local-optimised α)	Simple average	No
Scheme #3	GA-based weighted average (global-optimised α)	GA-based weighted average (global-optimised ν)	Yes

The developed colour normalisation using 24-patch Macbeth colour checker can be applied to normalise plant images as well as to reduce colour variability due to different sunlight intensities. Figure 5.7 shows some examples of average RGB standard deviation which were taken from 30 images from three field plots. As seen in the figure, without colour normalisation, the colour variability of plant images is very high as indicated by the average standard deviation of RGB colour. It means that various sunlight intensities have considerable effects on the colour of wheat plant images. Such images cannot be used directly for nutrient estimation since they are not comparable. Theoretically, all plants from the same plot should have similar colour values since they are subject to the same fertilizer treatment. The colour of the wheat leaves is considerably influenced by the nutrient amounts in the leaves, especially nitrogen.

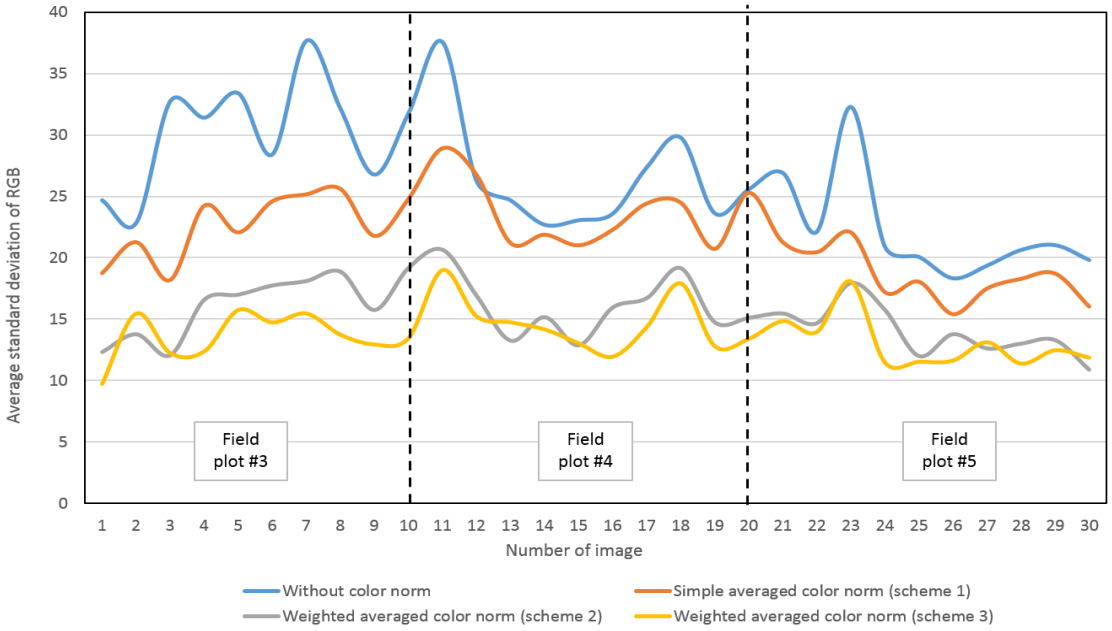

Figure 5.7. Comparison of colour normalisation results with three different schemes.

By applying the developed colour normalisation using scheme 1, i.e. simple average combiner, the standard deviation value can be decreased significantly. Furthermore, the developed GA-based weighted average combiner can reduce the colour variability more effective than the simple average method. This result indicates that each element in the matrix α has different influence factor to each MLP in the colour normalisation step. In addition, the effect of the local-optimised matrix α to reduce the colour variability of wheat plant images is not quite different compared to that of the global-optimised matrix α. In general, the global optimisation (scheme #3), however, can reduce the average standard deviation of RGB colour values slightly more than the local optimisation (scheme #2).

The proposed global optimisation can be used to estimate nitrogen content in wheat leaves more precisely than the other two developed methods and the common SPAD meter based measurement. As seen in Figure 5.8, the nitrogen estimation error using SPAD meter is 0.0578. The first developed research scheme with simple average combiner gave estimation results better than the SPAD meter based estimation. The best result based on this first scheme was obtained when using 7 MLPs in the nitrogen estimation step. On the other hand, in the second and third scheme, the best result was achieved from the combination of 6 MLPs. This finding indicates that GA-based colour normalisation gives some effects to the extracted statistical colour features which were used as the inputs in the nutrient estimation step. Furthermore, the estimation results using 6 MLPs in the third scheme was slightly better than that in the second scheme. This point denotes that each MLP in the nitrogen estimation step has different weights ($\mathbf{v}$) as resulted by the developed GA. Based on our experiments, the best estimation results can be achieved by using the following formula:

$$N' = \sum_{q=1}^{6} (v_q \times N_q)$$

$$N' = [0.427 \quad 0.055 \quad 0.114 \quad 0.094 \quad 0.023 \quad 0.287] \cdot \begin{bmatrix} N_1 \\ N_2 \\ N_3 \\ N_4 \\ N_5 \\ N_6 \end{bmatrix}$$

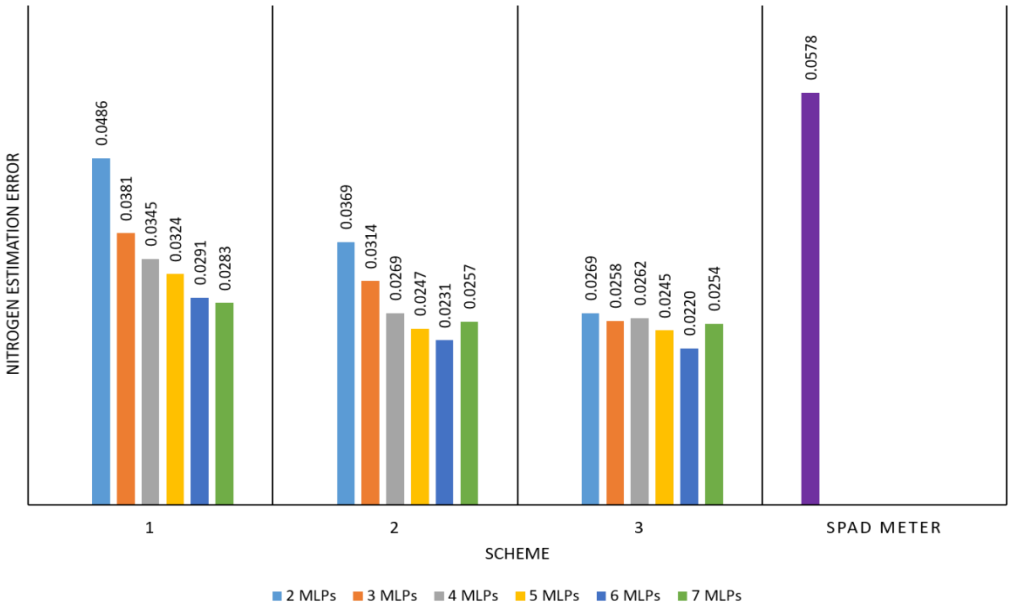

Figure 5.8. Nitrogen estimation error using three different schemes.

5.5. Summary

The variation of sunlight intensities will dominantly affect the colour of wheat plant images. Therefore, colour normalisation is required to tackle the effect of sunlight intensity by reducing the colour variability of the images. The proposed method focused on global optimisation using genetic algorithm to normalise plant images that were subject to a variation in lighting conditions and to estimate nitrogen content in wheat leaves. The global-optimised 24 neural networks fusion in the colour normalisation step and six neural networks combination in the nutrient estimation step could give the best prediction results compared to the other developed methods without global optimisation and the common SPAD meter based estimation.

Chapter 6

Conclusion and Future Works

6.1. Conclusion of the Thesis

Estimating nitrogen content of plants is commonly conducted in a controlled room with an artificial lighting system. A single leaf of a plant is usually laid down on a white paper and the image of the leaf is then analysed. Thus, it is very challenging to estimate nitrogen content of plants based on the image characteristics of the leaves which are captured on field due to the variation of sunlight intensities. It has been understood that light intensity can considerably affect the colour of an object. This fact, therefore, will influence the nitrogen estimation results.

The problem of on-field nitrogen status analysis in plants was unravelled as discussed in this thesis. The combination of neural networks, committee machines and genetic algorithm were utilised in colour normalisation, image segmentation and nitrogen estimation. In addition, the colour normalisation was performed to reduce the colour variability of wheat plant images by means of a Macbeth colour checker as the colour reference. Three novel approaches were developed to analyse the nitrogen status in plants.

In the first proposed method, as deeply described in Chapter 3, a fusion of regularised neural networks was employed to normalise plant images based on the RGB colour of the 24-patch Macbeth colour checker. Furthermore, the colour normalisation results were optimised using a genetic algorithm by revising the weights of each neural network, which were represented by the matrix $\boldsymbol{\alpha}$. The developed colour normalisation method was successfully used to normalise wheat plant images as indicated by small Euclidean distance and standard deviations of RGB colour of the images after applying the colour normalisation. This result made the plant images more comparable each other. Moreover, the results of the proposed colour normalisation were superior to that of other common methods, namely grey world, scale-by-max, linear model and single neural network. In the next step, i.e. image segmentation and features extraction, the regularised neural network was also effectively utilised to distinguish wheat leaves from other unwanted parts. This method gave improved results compared to the conventional Otsu algorithm. Afterward, four types of statistical moment features, namely mean (first moment), variance (second moment), skewness (third moment) and kurtosis

(fourth moment), of each colour channel were extracted to be applied as input parameters in the nitrogen estimation step. In this step, several neural networks with different number of hidden layer units were combined using committee machines and optimised by genetic algorithm. The experiments showed that the combination of six neural networks with the number of hidden layer nodes of 12, 24, 36, 48, 60 and 72, and the genetic algorithm based optimisation of the networks output's weights provided the best estimation results as indicated by the least mean absolute percentage error (MAPE) of the estimation, i.e. 2.73%. A significant improvement was made through the developed method compared to the common nitrogen estimation method using SPAD meter which produced MAPE of 8.48%.

In the second proposed method, a deep sparse extreme learning machine (DSELM) was implemented to replace the regularised neural network in the colour normalisation as well as in the image segmentation and nitrogen estimation step. Generally, the utilisation of DSELM in the three research steps was as effective as that of the developed regularised neural network as proposed in the first method. However, the learning speed of DSELM was extremely faster than the common backpropagation multilayer perceptron (MLP) and the regularised neural networks. As explained comprehensively in Chapter 4, the proposed DSELM based colour normalisation could be used normalise wheat plant images by reducing the colour variability due to different sunlight intensities. Despite the longer processing time compared to the non-learning based algorithms (grey world, scale-by-max and linear regression methods), the learning-based algorithms, i.e. single MLP, MLPs fusion and DSELMs fusion, provided better results in the colour normalisation. Furthermore, among the observed learning-based methods, the proposed DSELMs fusion showed the best performance in the term of colour normalisation error and processing speed. In the image segmentation step, DSELM showed its superiority to the other learning based algorithms. The accuracy level of the image segmentation results using DSELM was closely similar to that using backpropagation MLP and original ELM. However, the processing speed of the DSELM based technique was six time faster than that of the MLP method. As the same as the features extracted in the first proposed method, four types of statistical moment were also extracted as the inputs of neural network systems to estimate the nitrogen percentage. In the nitrogen estimation step, an ensemble of DSELM with different number of hidden layer was established and then optimised by genetic algorithm. The results showed that the combination of four DSELMs with 2, 3, 4, and 5 hidden layers with weighted coefficient optimised by genetic algorithm gave the best estimation with small error values and fast processing speed.

In the third proposed method, a more advanced algorithm was developed to produce a better optimisation in the nitrogen content prediction. A deep learning multilayer perceptron (DL-MLP) was employed as the expert system, instead of regularised neural network and deep sparse extreme learning machine. Furthermore, a fusion of twenty four DL-MLPs from the Macbeth colour checker and genetic algorithm based local optimisation was established successfully to normalise wheat plant images by reducing their colour variability. A DL-MLP based image segmentation was applied effectively to extract wheat leaves from the normalised plant images. After extraction of statistical colour moment features, as similar as those conducted in the two previous proposed methods, these features were then delivered to an expert system as the predictors of nitrogen amount. The developed expert system comprised a number of standard MLPs which were combined by committee machines. The difference between this method and the previous proposed methods was the utilisation of genetic algorithm to optimise globally the coefficients (weights) of each DL-MLP and standard MLP in the colour normalisation and nitrogen estimation step, respectively. In fact, the developed genetic algorithm based global optimisation could be used to fine tune the colour normalisation and nitrogen estimation in a better way. Three schemes were investigated to figure out the effectiveness of global optimisation to enhance the nitrogen estimation results. This study found that the scheme #3, which employed global optimisation, produced more improved nitrogen estimation results compared to the other schemes without global optimisation.

6.2. Recommendations for Future Works

Based on the research presented in this thesis, a number of studies can be conducted to investigate and explore more advanced ideas related to the application of computational intelligence image processing to analyse the nitrogen status in plants. The advanced studies can be enumerated as follows:

- By considering the processing speed of the deep sparse extreme learning machine (DSELM) and the effectiveness of the global optimisation, thus, a research to analyse nitrogen status by combining these two algorithms has a great potential to increase the accuracy of the estimation results as well as the time efficiency of the computational processing. The colour normalisation, image segmentation and nitrogen estimation steps can be conducted by applying DSELM as done in Chapter 4 and then optimised globally

using genetic algorithm to fine tune the colour normalisation and improve the nitrogen estimation results as done in Chapter 5.

- In the nitrogen estimation step, several networks of the same expert systems, i.e. regularised neural network (in Chapter 3), deep sparse ELM (in Chapter 4), and standard MLP (in Chapter 5), have been combined. It will be another novel approach to fuse these expert systems, or others, into one combination using committee machines, as seen in Figure 6.1.

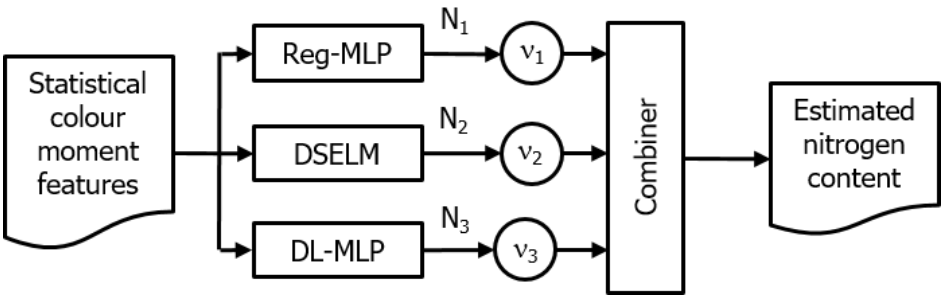

Figure 6.1. A new combination using committee machines to estimate nitrogen content.

A more advanced research that can be done is developing a smartphone based nitrogen estimation in real time. An application (app) based on smartphone operating systems, such as android, iOS, or other systems, can be built to assist people estimating nutrient content by capturing plant images using the smartphone camera. A larger database of leaves colour and nutrient amount will be required to make such research more reliable since different smartphone has different camera specifications. Due to the rapid development of information and computation technology, this advanced research will be possible to realise in the near future. This application can be very useful for farmers and agricultural practitioners.

References

[1] FAO, “Food and Agriculture: Driving action across the 2030 Agenda for Sustainable Development,” 2017.

[2] Ricepedia, “Ricepedia: The online authority on rice,” IRRI, 2014. [Online]. Available: http://ricepedia.org/index.php/indonesia.

[3] S. Banu, “Precision Agriculture: Tomorrow’s Technology for Today’s Farmer,” *Journal of Food and Process Technology,* vol. 6, no. 8, 2015.

[4] A. B. Tekin, “Variable rate fertilizer application in Turkish wheat agriculture: economic assessment,” *African Journal of Agricultural Research,* vol. 5, no. 8, pp. 647-652, 2010.

[5] R. Maheswari, K. R. Ashok and M. Prahadeeswaran, “Precision farming technology, adoption decisions and productivity of vegetables in resource-poor environments,” *Agricultural Economics Research Review,* vol. 21, pp. 415-424, 2008.

[6] R. Zinkevicius, “Influence of soil sampling for precision farming,” *Agronomy Research,* vol. 6, pp. 423-429, 2008.

[7] E. P. R. Service, “Precision agriculture and the future of farming in Europe,” STOA, Brussels, 2016.

[8] P. Auearunyawat, T. Kasetkaem, A. Wongmaneeroj, A. Nishihara and R. Keinprasit, “An automatic nitrogen estimation method in sugarcane leaves using image processing techniques,” *Proceedings of International Conference on Agricultural, Environment and Biological Sciences (ICAEBS),* pp. 39-42, 2012.

[9] X. Yao, W. Du, S. Feng and J. Zou, “Image-based plant nutrient status analysis: an overview,” *Proceedings of IEEE International Conference on Intelligent Computing and Intelligent Systems (ICIS),* pp. 460-464, 2010.

[10] G. Xu, F. Zhang, S. G. Shah, Y. Ye and H. Mao, “Use of leaf color images to identify nitrogen and potassium deficient tomatoes,” *Pattern Recognition Letters,* vol. 32, pp. 1584-1590, 2011.

[11] X. Yao, W. Luo and Z. Yuan, “An adaptive and qualitative rubber nutrient status analyzing system by digital foliar images,” *Proceedings of IEEE International Congress on Image and Signal Processing (CISP),* pp. 2492-2495, 2010.

[12] B. J. Van Alphen and J. J. Stoorvogel, “A methodology for precision nitrogen fertilization in high-input farming systems,” *Precision Agriculture,* vol. 2, pp. 319-332, 2000.

[13] E. E. Agency, “Source apportionment of nitrogen and phosphorous inputs into the aquatic environment,” *EEA Report,* no. 7, 2005.

[14] H. J. Heege, “Heterogeneity in fields: basics of analyses,” in *Precision in Crop Farming: Site Specific Concepts and Sensing Methods - Applications and Results,* Springer, 2013.

[15] S. A. Wolf and F. H. Buttel, “The political economy of precision farming,” *American Journal of Agricultural Economics,* vol. 78, no. 5, pp. 1269-1274, 1996.

[16] T. Verma, S. K. Satpathy and L. K. Sharma, “A step towards precision farming of rice crop by estimating loss caused by leaf blast disease using digital image processing and fuzzy clustering,” *International Journal of Computer Trends and Technology,* pp. 1-6, 2011.

[17] R. Casa, A. Cavalieri and B. L. Cascio, “Nitrogen fertilisation management in precision agriculture: a preliminary application example on maize,” *Italian Journal of Agronomy,* vol. 6:e5, pp. 23-27, 2011.

[18] R. Heimlich, “Precision Agriculture: information technology for improved resource use,” *Agricultural Outlook,* pp. 19-23, 1998.

[19] A. Tellaeche, X. P. Burgos-Artizzu, G. Pajares and A. Ribeiro, “A vision-based method for weeds identification through the Bayesian decision theory,” *Pattern Recognition,* vol. 41, pp. 521-530, 2008.

[20] X. P. Burgos-Artizzu, A. Ribeiro, M. Guijarro and G. Pajares, “Real-time image processing for crop/weed discrimination in maize fields,” *Computers and Electronics in Agriculture,* vol. 75, pp. 337-346, 2011.

[21] M. Montalvo, J. M. Guerrero, J. Romeo, L. Emmi, M. Guijarro and G. Pajares, "Automatic expert system for weeds/crops identification in images from maize fields," *Expert Systems with Applications,* vol. 40, pp. 75-82, 2013.

[22] J. Pan, M. Huang and Y. He, "Crop and weed image recognition by morphological operations and ANN model," *Proceedings of IEEE Instrumentation and Measurement Technology Conference (IMTC),* pp. 1-4, 2007.

[23] M. M. Mustafa, A. Hussain, K. H. Ghazali and S. Riyadi, "Implementation of Image Processing Technique in Real Time Vision System for Automatic Weeding Strategy," *Proceedings of IEEE International Symposium on Signal Processing and Information Technology,* pp. 632-635, 2007.

[24] K. H. Ghazali, S. Razali, M. M. Mustafa and A. Hussain, "Machine Vision System for Automatic Weeding Strategy in Oil Palm Plantation using Image Filtering Technique," *Proceedings of The 3rd IEEE International Conference on Information and Communication Technologies: From Theory to Applications (ICTTA),* 2008.

[25] J. K. Patil and R. Kumar, "Advances in image processing for detection of plant diseases," *Journal of Advanced Bioinformatics Applications and Research,* vol. 2, no. 2, pp. 135-141, 2011.

[26] K. Y. Huang, "Application of artificial neural network for detecting Phalaenopsis seedling diseases using color and texture features," *Computers and Electronics in Agriculture,* vol. 57, pp. 3-11, 2007.

[27] M. Zhang and Q. Meng, "Automatic citrus canker detection from leaf images captured in field," *Pattern Recognition Letters,* vol. 32, pp. 2036-2046, 2011.

[28] R. Pydipati, T. F. Burks and W. S. Lee, "Identification of citrus disease using color texture features and discriminant analysis," *Computers and Electronics in Agriculture,* vol. 52, pp. 49-59, 2006.

[29] C. Lu, H. Ren, Y. Zhang and Y. Shen, "Leaf area measurement based on image processing," *Proceedings of IEEE International Conference on Measuring Technology and Mechatronics Automation,* pp. 580-582, 2010.

[30] M. Mora, F. Avila, M. Carrasco-Benavides, G. Maldonado, J. Olguín-Cáceres and S. Fuentes, "Automated computation of leaf area index from fruit trees using improved image processing algorithms applied to canopy cover digital photograpies," *Computers and Electronics in Agriculture,* vol. 123, pp. 195-202, 2016.

[31] C. Aloisio, R. K. Mishra, C. Chang and J. English, "Next generation image guided citrus fruit picker," *Proceedings of IEEE International Conference on Technologies for Practical Robot Applications (TePRA),* pp. 37-41, 2012.

[32] C. Akin, M. Kirci, E. O. Gunes and Y. Cakir, "Detection of the pomegranate fruits on tree using image processing," *Proceedings of IEEE International Conference on Agro-Geoinformatics,* 2012.

[33] S. Arivazhagan, R. N. Shebiah, S. S. Nidhyanandhan and L. Ganesan, "Fruit recognition using color and texture features," *Journal of Emerging Trends in Computing and Information Sciences,* pp. 90-94, 2010.

[34] G. Feng and C. Qixin, "Study on color image processing based intelligent fruit sorting system," *Proceedings of the Fifth World Congress on Intelligent Control and Automation,* pp. 4802-4805, 2004.

[35] D. Lee, J. K. Archibald and G. Xiong, "Rapid color grading for fruit quality evaluation using direct color mapping," *IEEE Transactions on Automation Science and Engineering,* vol. 8, no. 2, pp. 292-302, 2011.

[36] A. Mizushima and R. Lu, "An image segmentation method for apple sorting and grading using support vector machine and Otsu's method," *Computers and Electronics in Agriculture,* vol. 94, pp. 29-37, 2013.

[37] N. Jaroonchon, K. Krisanapook and L. Phavaphutanon, "Correlation between pummelo leaf nitrogen concentrations determined by combustion method and kjeldahl method and their relationship with spad values from portable chlorophyll meter," *Kasetsart Journal (Natural Science),* vol. 44, pp. 800-807, 2010.

[38] R. F. Muñoz-Huerta, R. G. Guevara-Gonzalez, L. M. Contreras-Medina, I. Torres-Pacheco, J. Prado-Olivarez and R. V. Ocampo-Velazquez, "A review of methods for sensing the nitrogen status in plants: advantages, disadvantages and recent advances,"

Sensors, vol. 13, pp. 10823-10843, 2013.

[39] S. Huang, Y. Miao, G. Zhao, X. Ma, C. Tan, G. Bareth, U. Rascher and F. Yuan, "Estimating rice nitrogen status with satellite remote sensing in Northeast China," *Proceedings of the IEEE Second International Conference on Agro-Geoinformatics,* pp. 550-557, 2013.

[40] G. Nachimutu, V. Velu, P. Malarvizhi, S. Ramasamy and J. Bose, "Relationship between index leaf nitrogen and leaf colour chart (LCC) values in direct wet seeded rice (Oryza sativa L.)," *Asian Journal of Plant Sciences,* vol. 6, no. 3, pp. 477-483, 2007.

[41] S. J. Leghari, U. A. Leghari, M. Burriro and A. A. Soomro, "Introducing leaf color chart in agriculture of Sindh," *Journal of Plant Stress Physiology,* vol. 1, no. 1, pp. 19-22, 2015.

[42] Cambodia Harvest, "Use of Leaf Color Chart (LCC)," USAID, June 2013.

[43] H. Song, Z. Guo, Y. He, H. Fang and Z. Zhu, "Non-destructive estimation oilseed rape nitrogen status using chlorophyll meter," *Proceedings of the IEEE Fifth International Conference on Machine Learning and Cybernetics,* pp. 4252-4256, 2006.

[44] Konica Minolta, "Chlorophyll meter SPAD- 502Plus: A lightweight handheld meter for measuring the chlorophyll content of leaves without causing damage to plants," Konico Minolta Inc., 2009.

[45] J. Markwell, J. C. Osterman and J. L. Mitchell, "Calibration of the Minolta SPAD-502 leaf chlorophyll meter," *Photosynthesis Research,* vol. 46, pp. 467-472, 1995.

[46] Apogee Instruments, "Apogee Instuments Chlorophyll Content Meter Technical Information," [Online]. Available: http://www.apogeeinstruments.co.uk/apogee-instruments-chlorophyll-content-meter-technical-information. [Accessed 2016].

[47] R. Basyouni and B. Dunn, "Use of optical sensors to monitor plant nitrogen status in horticultural plants," Division of Agricultural Sciences and Natural Resources, Oklahoma State University, Oklahoma, 2016.

[48] D. Story, M. Kacira, C. Kubota, A. Akoglu and L. An, "Lettuce calcium deficiency detection with machine vision computed plant features in controlled environments,"

Computers and Electronics in Agriculture, vol. 74, pp. 238-243, 2010.

[49] L. Ma, J. Fang, Y. Chen and S. Gong, "Color analysis of leaf images of deficiencies and excess nitrogen content in soybean leaves," *Proceedings of IEEE International Conference on E-product E-service and E-entertainment (ICEEE),* pp. 1-3, 2010.

[50] M. A. Hairuddin, N. M. Tahir and S. R. S. Baki, "Representation of elaeisguineensis nutrition deficiency based on image processing approach," *Proceedings of IEEE International Conference on Computer Applications and Industrial Electronics,* pp. 607-611, 2011.

[51] M. Wiwart, G. Fordonski, K. Zuk-Golaszewska and E. Suchowilska, "Early diagnostics of macronutrient deficiencies in three legume species by color image analysis," *Computers and Electronics In Agriculture,* vol. 65, pp. 125-132, 2009.

[52] M. Pagola, R. Ortiz, I. Irigoyen, H. Bustince, E. Barrenechea, P. Aparicio-Tejo, C. Lamsfus and B. Lasa, "New method to assess barley nitrogen nutrition status based on image colour analysis comparison with SPAD-502," *Computers and Electronics In Agriculture,* vol. 65, pp. 213-218, 2009.

[53] X. Yuanfang, W. Xianmin, S. Hong, W. Haihua and Z. Yan'e, "Study of monitoring maize leaf nutrition based on image processing and spectral analysis," *Proceedings of IEEE World Automation Congress (WAC),* pp. 465-468, 2010.

[54] P. A. Moghaddam, M. H. Derafshi and M. Shayesteh, "A new method in assessing sugar beet leaf nitrogen status through color image processing and artificial neural network," *Journal of Food, Agriculture and Environment,* vol. 8, no. 2, pp. 485-489, 2010.

[55] Y. Wang, D. Wang, G. Zhang and J. Wang, "Estimating nitrogen status of rice using the image segmentation of G-R thresholding method," *Field Crops Research,* vol. 149, pp. 33-39, 2013.

[56] R. L. Rorie, L. C. Purcell, D. E. Karcher and C. A. King, "The assessment of leaf nitrogen in corn from digital images," *Crop Science,* vol. 51, pp. 2174-2180, 2011.

[57] S. Burhan and I. Cadirci, "Multi-stage wind-electric power forecast by using a combination of advanced statistical methods," *IEEE Transactions on Industrial*

Informatics, vol. 11, no. 5, pp. 1231-1242, 2015.

[58] K. Y. Chan, S. Khadem, T. S. Dillon, V. Palade, J. Singh and E. Chang, "Selection of significant on-road sensor data for short-term traffic flow forecasting using the taguchi method," *IEEE Transactions on Industrial Informatics,* vol. 8, no. 2, pp. 255-266, 2012.

[59] M. L. Corradini, V. Fossi, A. Giantomassi, G. Ippoliti, S. Longhi and G. Orlando, "Minimal resource allocating networks for discrete time sliding mode control of robotic manipulators," *IEEE Transactions on Industrial Informatics,* vol. 8, no. 4, pp. 733-745, 2012.

[60] S. Dai, C. Wang and F. Luo, "Identification and learning control of ocean surface ship using neural networks," *IEEE Transactions on Industrial Informatics,* vol. 8, no. 4, pp. 801-810, 2012.

[61] C. Wei, W. L. Woo and S. S. Dlay, "Nonlinear underdetermined blind signal separation using Bayesian neural network approach," *Digital Signal Processing,* vol. 17, no. 1, pp. 50-68, 2007.

[62] W. L. Woo and S. S. Dlay, "Regularised nonlinear blind signal separation using sparsely connected network," *IEE Proceedings: Vision, Image and Signal Processing,* vol. 152, no. 1, pp. 61-73, 2005.

[63] M. Qasim and V. Khadkikar, "Application of artificial neural networks for shunt active power filter control," *IEEE Transactions on Industrial Informatics,* vol. 10, no. 3, pp. 1765-1774, 2014.

[64] H. D. Cheng, X. Cai and R. Min, "A novel approach to color normalization using neural network," *Neural Computing and Application,* vol. 18, pp. 237-247, 2009.

[65] A. Gijsenij, T. Gevers and J. van de Weijer, "Computational color constancy: survey and experiments," *IEEE Transactions on Image Processing,* vol. 20, no. 9, pp. 2475-2489, 2011.

[66] S. Bianco, G. Ciocca, C. Cusano and R. Schettini, "Improving color constancy using indoor–outdoor image classification," *IEEE Transactions on Image Processing,* vol. 17, no. 12, pp. 2381-2392, 2008.

[67] K. Barnard, V. Cardei and B. Funt, “A comparison of computational color constancy algorithms–part I: methodology and experiments with synthesized data,” *IEEE Transactions on Image Processing,* vol. 11, no. 9, pp. 972-983, 2002.

[68] M. Cococcioni, B. Lazzerini and S. L. Volpi, “Robust diagnosis of rolling element bearings based on classification techniques,” *IEEE Transactions on Image Processing,* vol. 9, no. 4, pp. 2256-2263, 2013.

[69] Z. Yan and J. Wang, “Model predictive control of nonlinear systems with unmodeled dynamics based on feedforward and recurrent neural networks,” *IEEE Transactions on Image Processing,* vol. 8, no. 4, pp. 746-756, 2012.

[70] Ward System Group, “NeuroShell 2,” 1998. [Online]. Available: http://www.wardsystems.com/manuals/neuroshell2/index.html?idxtutorialone.htm.. [Accessed 2015].

[71] C. Chen and S. Duan, “Optimal integration of plug-in hybrid electric vehicles in microgrids,” *IEEE Transactions on Industrial Informatics,* vol. 10, no. 3, pp. 1917-1926, 2014.

[72] H. Sung-Ho, K. Reza and T. Andrew, “Modeling and control of a plastic film manufacturing web process,” *IEEE Transactions on Industrial Informatics,* vol. 7, no. 2, pp. 171-178, 2011.

[73] R. Vincent, T. Mohammed and L. Gilles, “Comparison of parallel genetic algorithm and particle swarm optimization for real-time UAV path planning,” *IEEE Transactions on Industrial Informatics,* vol. 9, no. 1, pp. 132-141, 2013.

[74] P. Charalambos, K. Eftichios, S. Vasilis, K. Tamas, S. Dezso and T. Remus, “Optimal design of photovoltaic systems using high time-resolution meteorological data,” *IEEE Transactions on Industrial Informatics,* vol. 10, no. 4, pp. 2270-2279, 2014.

[75] N. Mohamad, M. K. A. Ariffin, A. Ali, F. Mustapha and I. M. Salleh, “Development of genetic algorithm toolbox using MATLAB in cutting tool path optimization,” *Scientific Research and Essays,* vol. 8, pp. 1848-1857, 2013.

[76] A. Dacal-Nieto, E. Vasquez-Fernandez, A. Formella, F. Martin, S. Torres-Guijarro and H. Gonzalez-Jorge, “A genetic algorithm approach for feature selection in potatoes

classification by computer vision," *Proceedings of 35th Annual Conference of IEEE Industrial Electronics,* pp. 1955-1960, 2009.

[77] F. Lin, P. Huang and W. Chou, "Recurrent-fuzzy-neural-network-controlled linear induction motor servo drive using genetic algorithms," *IEEE Transactions on Industrial Electronics,* vol. 54, no. 3, pp. 1449-1461, 2007.

[78] D. A. Coley, An Introduction To Genetic Algorithm For Scientists and Engineers, Singapore: World Scientific Publishing, 1999.

[79] M. Qing-Kui, Z. Chun-Hou, W. Xiao-Feng and L. Feng-Yan, "Recognition of plant leaves using support vector machine," *Advanced Intelligent Computing Theories and Applications,* vol. 15, 2008.

[80] C. M. Bishop, Neural Networks for Pattern Recognition, Oxford University Press, 1996.

[81] C. Chen and Z. Lin, "A committee machine with empirical formulas for permeability prediction," *Computers and Geosciences,* vol. 32, pp. 485-496, 2006.

[82] C. Shengxian, D. Bangkui, S. Jiawei, L. Fan, Y. Shanrang and X. Zhiming, "A colour constancy algorithn based on neural network and application," *Proceedings of IEEE World Congress on Intelligent Control and Automation,* pp. 3100-3103, 2010.

[83] X. Xu, X. Zhang, Y. Cai, L. Zhuo and L. Shen, "Supervised color correction based on QPSO-BP neural network algorithm," *Proceedings of IEEE International Congress on Image and Signal Processing,* pp. 1-5, 2009.

[84] S. Kawashima and M. Nakatani, "An algorithm for estimating chlorophyll content in leaves using a video camera," *Annals of Botany,* vol. 81, pp. 49-54, 1998.

[85] H. Tian and Z. Mao, "An ensemble ELM based on modified Adaboost.RT algorithm for predicting the temperature of molten steel in ladle furnace," *IEEE Transactions on Automation Science and Engineering,* vol. 7, no. 1, pp. 73-80, 2010.

[86] D. Niu, Y. Sun and F. Wang, "Optimization of advertising budget allocation over time based on LS-SVMR and DE," *IEEE Transactions on Automation Science and Engineering,* vol. 11, no. 4, pp. 1076-1082, 2014.

[87] Y. Liu, F. Wang, Y. Chang and C. Li, "A SNCCDBAGG-based NN ensemble approach for quality prediction in projection molding process," *IEEE Transactions on Automation Science and Engineering,* vol. 8, no. 2, pp. 424-427, 2011.

[88] Q. Wei and D. Liu, "Adaptive dynamic programming for optimal tracking control of unknown nonlinear systems with application to goal gasification," *IEEE Transactions on Automation Science and Engineering,* vol. 11, no. 4, pp. 1020-1036, 2014.

[89] W. L. Woo and S. S. Dlay, "Neural network approach to blind signal separation of mono-nonlinearly mixed signals," *IEEE Transactions on Circuits and Systems I,* vol. 52, no. 2, pp. 1236-1247, 2005.

[90] D. Liu, D. Wang, D. Zhao, Q. Wei and N. Jin, "Neural-network-based optimal control for a class of unknown discrete-time nonlinear systems using globalized dual heuristic programming," *IEEE Transactions on Automation Science and Engineering,* vol. 9, no. 3, pp. 628-634, 2012.

[91] H. Zhang, C. Qin and Y. Luo, "Neural-network-based constrained optimal control scheme for discrete-time switched nonlinear system using dual heuristic programming," *IEEE Transactions on Automation Science and Engineering,* vol. 11, no. 3, pp. 839-849, 2014.

[92] G. B. Huang, D. H. Wang and Y. Lan, "Extreme learning machine: a survey," *International Joural Machine Learning and Cybernetics,* vol. 2, pp. 107-122, 2011.

[93] J. X. Tang, C. W. Deng and G. B. Huang, "Extreme learning machine for multilayer perceptron," *IEEE Transactions on Neural Networks and Learning Systems,* vol. 27, pp. 809-821, 2016.

[94] G. B. Huang, L. Chen and C. K. Siew, "Universal approximation using incremental constructive feedforward networks with random hidden nodes," *IEEE Transactions on Neural Network,* vol. 17, no. 4, pp. 879-892, 2006.

[95] A. Beck and M. Teboulle, "A fast iterative shrinkage-thresholding algorithm for linear inverse problems," *SIAM Journal of Imaging sciences,* vol. 2, no. 1, pp. 183-202, 2009.

[96] A. Beck and M. Teboulle, "A fast iterative shrinkage-thresholding algorithm with application to wavelet-based image deblurring," *Proceedings of IEEE International*

Conference on Acoustics, Speech and Signal Processing, pp. 693-696, 2009.

[97] Y. LeCun, Y. Bengio and Hinton G., "Deep learning," *Nature*, vol. 521, pp. 436-444, 2015.

[98] H. Wang and D. Yeung, "Towards bayesian deep learning: a framework and some existing methods," *IEEE Transactions on Knowledge and Data Engoneering*, vol. 28, no. 12, pp. 3395-3408, 2016.

[99] D. A. Coley, An Introduction To Genetic Algorithms For Scientists And Engineers, World Scientific Publishing, 1999.